1-1-2006

Continuous carbon nanofibers prepared from electrospun polyacrylonitrile precursor fibers.

Sian F. Fennessey
University of Massachusetts Amherst

CONTINUOUS CARBON NANOFIBERS PREPARED FROM ELECTROSPUN POLYACRYLONITRILE PRECURSOR FIBERS

A Dissertation Presented

by

SIAN F. FENNESSEY

Submitted to the Graduate School of the
University of Massachusetts Amherst in partial fulfillment
of the requirements for the degree of

DOCTOR OF PHILOSOPHY

MAY 2006

Polymer Science and Engineering

UMI Number: 3215896

ProQuest Information and Learning Company
300 North Zeeb Road
P.O. Box 1346
Ann Arbor, MI 48106-1346

CONTINUOUS CARBON NANOFIBERS PREPARED FROM ELECTROSPUN POLYACRYLONITRILE PRECURSOR FIBERS

A Dissertation Presented

by

SIAN F. FENNESSEY

Approved as to style and content by:

_____
Richard J. Farris, Chair

_____
Alan J. Lesser, Member

_____
Thomas J. Lardner, Member

_____
Shantikumar Nair, Consulting Member

_____
Shaw Ling Hsu, Department Head
Polymer Science and Engineering

CONTINUOUS CARBON NANOFIBERS PREPARED FROM ELECTROSPUN POLYACRYLONITRILE PRECURSOR FIBERS

A Dissertation Presented

by

SIAN F. FENNESSEY

Approved as to style and content by:

Richard J. Farris, Chair

Alan J. Lesser, Member

Thomas J. Lardner, Member

Shantikumar Nair, Consulting Member

Shaw Ling Hsu, Department Head
Polymer Science and Engineering

DEDICATED

to

Atty. & Mrs. Francis B. Fennessey

Behind every fortune is someone who has labored into the night to make it real. Behind every important discovery is a person who regularly, wearily searched for it. Behind the magnificent work of art is an artist who spent hour after hour, month after month toiling at tasks that were not so magnificent.

Take heart, your effort cannot help but payoff. The fact is that your effort is the payoff. The fortune, the discovery, and the work of art are mere tokens of the achievement. The real achievement is in the achieving. The real value is in the doing.

Sincere, focused effort makes your life rich, even as you do it. Otherwise, why would we put so much value on the artifacts, which it produces? Make the effort. The biggest reward is in doing.

- Ralph Marston

ACKNOWLEDGMENTS

It was quite a chain of events that got me to where I am standing today and there have been a lot of people who have affected me and my endeavors. I would like to thank those whom have made the greatest continual impact on my failures and eventual successes. First, I must acknowedge and thank Prof. James A. Moore, my undergraduate research advisor at Rensselaer Polytechnic Institute, for giving me my first opportunity to 'work,' or rather fool around, in a laboratory. He always encouraged me, even though sometimes it was just to encourage me to 'get moving' or to 'get organized.' He aided me in partaking in quite a few exciting opportunities, wrote countless letters of recommendation for me, advised me when I asked for guidance, and still had the time to monitor me even from afar (through quite a network of spies). He is one of the few 'grown-ups' who thinks my tales of misadventures are amusing and, for that alone, I don't think that he will ever be able to rid himself of me. I would also, like to acknowledge Herr Prof. Paul Smith and Herr Prof. Ulrich Süter of the Polymertechnologie and Makromolekulare Chemie departments, respectively, at the Eidgenossische Technische Hochschule, Zurich, Switzerland for providing me with the privilege of studying in their laboratories. In particular I would like to thank Dr. Daniel Stieger and Dr. Christoph Weder for their guidance in Prof. Smith's laboratory at the ETHZ.

I would like to, also, thank Mr. Tomas A. Vignale for being my being my best friend and my source of confidence for a great many years. Tomas always had more confidence in me than I did in myself. If it were not for Tomas' support (and the fact

that I mistakenly told my father that graduate school was free, after a lifetime of private education), I would not have attended graduate school.

Now, I must say that one of the best (consistently good) parts of studying at the University of Massachusetts Amherst was having the privledge of being a member of Prof. Richard J. Farris' group. Dr. Farris has been extremely good to me. He let me become the scientist that I wanted be and he only pushed me to be better. Dr. Farris taught me an awful lot about everything: math tricks, fibers, bearing, couplings, screws, drill bits, transmissions, motors, you name it. Dr. Farris is probably the best example of a text-book 'good' leader; he leads this students to lead themselves, to think for themselves, to analyze from as many angles, and much more. I greatly appreciate all of the opportunities that being a member of his laboratory group has provided/provides for me.

I would like to acknowledge Dr. Hak Yong Kim and his group at Chonbuk National Laboratory, South Korea and Dr. Dan Edie and Dr. Amit Naskar from the Chemical Engineering department at Clemson University, South Carolina for their aid. Both Dr. Kim and Dr. Edie provided me with a lot of guidance regarding the handling, processing, and characterization of carbon fibers and yarns. Without the lengths of yarn prepared by Dr. Kim and the use of Dr. Edie's high temperature furnace, the impact of my thesis research project would be minimal.

I would like mention the members of my thesis committee: Dr. Alan J. Lesser, Dr. Shantikumar Nair of the Mechanical Engineering department, and Dr. Thomas J. Lardner of the Civil Engineering department. Dr. Lesser and Dr. Nair have been the happiest and most energetic committee members a student could ask for. With their

egarness to learn from me, their questions and offers of advice and equipment, I have had a very difficult time constructing 'defense horror stories' to pass onto the department's underclassmen. Also, I must thank Dr. Lardner for his time and willingness to act as a 'pinch hitter' so that I could defend my thesis.

At this point I must acknowledge a few of the 'permanent' members of the PSE community whom have made my stay particularly lively: Dr. E. Bryan Coughlin and Mr. Louis Raboin. Dr. Coughlin has always made himself available to me; he has kindly lent me equipment and use of his laboroatory facilities. He has acted as a sounding board for ideas, and has spoken to recruiters on my behalf. Dr. Coughlin has been an all around good sport; he has taken all of my heckling in stride and even thrown a few good 'bruisers' back. I would like to thank Mr. Louis Raboin for just generally 'craking me up' and making endless hours of microscopy time go ever so much faster. It is not the fancy equipment that makes a science department good, rather it is the people who teach and work there. Additionally, I would like to mention Dr. Thomas P. Russell and Dr. Murugappan Muthukumar for their kindess and for the energies they put into me particularly during my first semesters at the university.

Finally, I must thank those who have made my stay in Amherst bearable, my friends. Amherst is a curious place; it is home to a large culturally diverse group of independent thinkers, a few of whom I have had the privilege of befriending. As space and time only allows me to mention a few of those individuals, I do not want to imply that the following were the only people who helped keep me entertained during the last 5+ years. In specific, I would like to thank Dr. Kristopher Lavery, Mr. Matthew Misner, and Dr. K. Amanda Leach for being a great source of entertainment and reliable

friends. Matt and Kris are, the best drinking buddies a girl could ask for! I would like to thank M. Gregoire Cardoen for always kept me well fed and happy (which is really quite an impressive feat). I consider myself very lucky to have met Dr. Pushkala Krishnamurthy, Dr. Raji Kasi, Dr. Kishore Indukuri, Dr. Waiken Wong, Miss Ilke Anac, Mr. Kevin Wier, Dr. Amiya Tripathy, Dr. Keundeuk Lee, Dr. Eui-sung Yoo and Mrs. Keumyea Lee, Mr. Alexei Popov, Dr. Ebru Catalara, Dr.M. Firat Ilker, and Dr. Javid Rzayev. Push always attempted to keep me on the straight and narrow in regards to our studies and life, although sometimes my tendency toward chaos was just to great for all of her powers. She and Raji always made me smile, no matter what. Even with all of his craziness, I consider Amiya one of my most trustworthy friends and a great confidant. He is one of the most driven people, I have ever met; after watching Amiya in action, I take my vacations much more seriously! I want to thank 'all of my Koreans' for all of the good times in and outside of the lab. I must also happily mention Dr. Arun Raman, my senior, who kept tabs on me even well after he graduated; he took his mentorship very seriously! Also, I would like to say thank those who dragged me out of the lab often: Mlle. Lucile Dieudonne, Mlle. Elodie Vidil, Sra. Tania Marques, Miss Shideh Shafie, and Miss Neshe Garfuri for more than they can imagine; it was really my pleasure. Without Mr. Benjamin Baker and Dr. Scott Wierchowski, I think that I would have happily continued living a rather sheltered life (and I am not so sure that that would have been such a terrible thing). Even though Ben and Scott are extremely unreliable, they always managed to come to my rescue when I need rescuing. I could always count on them for a great time (particularly if a free beer was involved). I would like to thank Dr. Pilar & Dr.Timothy Middlekoop for letting me join them on

their honeymoon and invite them to join me on mine, too! I would like to happily blame Dr. Renuka Sivendran for introducing me to Latin dancing and encouraging my addiction. I would like to thank Dr. Justin Hermann, Miss Gunes Solyer, Mr. John Cummings, and Mrs. Alenka and Mr. Jacob Wheeler for the evening barbeques and the beers; I am not sure that any of my future summer evenings will ever manage to be as memorable as those spent with you. I would like to mention Miss. Damla Koylu for all of her kindnesses and pleasantries. Also, I would like to apologize to Miss. Barbara Campogrosso-Sansone and Mr. Ozgur Yavuzetin for all of the communication difficulties and the bad holiday photography! Thank you to Mr. Hiroshi Nakade, Miss Manori Gunawardhana, and Mr. Dan Montville from PSE-Sian. Ultimately, I would like to acknowledge Mr. Güray Alsaç, who could make me either laugh or cry on the flip of coin but always kept me distracted from the 'real' problem at hand. Thank you, I consider myself extremely lucky to have met all of you and I look forward to the fun to come.

I would like to acknowledge my best friend Dr. Sara Lewis. Although she was always on the wrong side of the Atlantic when all hell broke loose, she always tried to take care of me. I consider her my other half and I couldn't possibly imagine how things would be had I never met her (things probably just wouldn't be quite as funny, that is for sure).

Now I would like to acknowledge the MOST important people in my life; with a Phd. or not, these guys will always take the first three places of my top ten list: my mum, dad, and brother Timmy. Thanks to my parents, I grew up thinking 'school is the most important thing. That mindset did not make me the most popular girl on the

playground by any means, but it saved me from flunking out of college during my first semester. A lot of the decisions I have made, even a few of the good ones, were based on ideas and principals my parents taught me as well as the expectations they had for me. As far as parents go, they weren't that bad; how many parents give a 17 year old a car, two sets of keys, and no curfew? Anyway, my parents have always backed me up; they have let me do everything I have wanted to do, within reason (and then some). So, thank you for coming to pick me up from the dorms almost every weekend during my first semester at RPI, dad (and doing my laundry on those weekends, mum). Thank you for taking me out to dinner before every qualifying exam, for understanding why I wanted to leave with only a Master's, and then not questioning me when I stayed to finish the Doctorate. I am at my best and my happiest when I am at home. I always have been.

To my little brother Timmy, thank you for being a better person than myself. Thank you for accepting me the way I am, even after I was so terrible to you as a child. Oh, and finally… where is your thesis, kid? Read this and weep!

ABSTRACT

MECHANICAL BEHAVIOR OF NONWOVEN ELECTROSPUN FABRICS AND YARNS

MAY 2006

SIAN F. FENNESSEY, B.S., RENSSELAER POLYTECHNIC INSTITUTE

M.S., UNIVERSITY OF MASSACHUSETTS AMHERST

Ph.D., UNIVERSITY OF MASSACHUSETTS AMHERST

Directed by: Professor Richard J. Farris

The electrospinning process of fiber production is examined in regards to the preparation of continuous Polyacrylonitrile (PAN) nanofibers with the purpose of preparing carbon nanofibers for the reinforcement of thin films and nanocomposites. The mechanical properties and reinforcing behavior of nanofibers are expected to differ significantly from their conventional counterparts; the strength of a carbon filament increases as the diameter decreases.

Discrete lengths of partially aligned and oriented electrospun PAN fibers with diameters between 0.27μm and 0.29μm (FESEM) were prepared from solution with Dimethylformamide electrospun between 10-16kV and collected onto a take-up wheel rotating between 3.5m/s and 12.3m/s. A maximum chain orientation parameter of 0.23 is determined by dichroism (FTIR) and wide angle X-ray diffraction (WAXD) for fibers collected between 8.1m/s and 9.8m/s. Twisted yarns of aligned PAN nanofibers with an average denier of 446 and twist angles between 1.1° and 16.8° are prepared. The ultimate strength and modulus of the twisted yarns increase with increasing angle of twist to a maximum of 162 $\pm$8.5 MPa and 5.9 $\pm$0.3 GPa, respectively, at an angle of

9.3°. Drawing of the untwisted yarn in batch above the T_g of the material resulted in a further increase of the ultimate strength and modulus to 253 $\pm$46 MPa and 4.8 $\pm$0.5 GPa at a draw ratio of approximately 1:2; the ultimate strength of commercially prepared precursor fiber is 512MPa with post-treatment. A high temperature oxidation process is optimized and carbon nano fibers are prepared. The carbonized yarns are observed to exhibit graphitic structure by Raman scattering and wide angle X-ray diffraction (WAXD), although the mechanical properties are weak.

Continuous lengths of electrospun PAN yarn, provided through a collaboration, are characterized and evaluated for the production of carbon nanofiber yarn. The yarn is continuously processed and converted into carbon. Although, the yarn exhibits graphitic strucuture, the strength of the carbonized nanofiber yarn is only approximately 5% that of commercial carbon fiber prepared from the same precursor material. The poor mechanical properties are due to a loss of preferred orientation during an extended stabilization step.

TABLE OF CONTENTS

Page

LIST OF TABLES

Table Page

LIST OF FIGURES

Figure Page

LIST OF SCHEMES

Scheme Page

CHAPTER 1

CARBON FIBER REINFORCERS

1.1 Introduction

The utilization of materials for the preparation and production of fibers and textiles began at the beginning of civilization and extended until the twentieth century when steam driven machinery revolutionized the mechanical operations of spinning and weaving. In 1846 with an accidental discovery by Christian Friedrich Schoenbein, a chemistry professor at the University of Basel, man-made materials and fibers were realized. He observed that cotton may be converted into a soluble, plastic substance in a mixture of nitric and sulfuric acid; in 1884, Hilaire de Chardonnet extruded this solution into fine filaments. In the 1920s as viscose and acetate rayon became commercially important items, polymer science emerged and provided the opportunity to produce new synthetic fibers directly from the polymerization of monomers. Polyamides (nylons), polyesters, polyacrylics, polyvinyls, polyolefins, and polyurethanes were all developed as synthetic fibers between the 1940s and 1950s. By the 1960s, a large body of knowledge on structure-property relationships for synthetic fibers existed and 'tailor-made' specialty fibers were starting to be designed by/from graft and block copolymers, surface treatments, polyblends, two-component fiber spinning, and cross-section modification. Also at this time, fiber science and engineering evolved to expand the application of fiber use to outside of the classical textile industry. Currently applications involving fibers include uses in: the

reinforcement of thermoplastics for structural applications, optical fibers for light telephony, and in medicine and hygiene[1].

1.2 Carbon Fiber

1.2.1 Introduction

Carbon fibers were first produced by Edison in the late 19th century[2]; after initial trials using bamboo fibers, Edison found that regenerated cellulose (rayon) could be converted into carbon filaments for use in incandescent lamps. In the 1960s Union Carbide Corporation used rayon to produce the first commercial carbon fiber[1]. Today, carbon fibers are used as high strength and modulus-reinforcing materials in the fabrication of high performance composites.

The need for carbon fiber reinforced structural materials originated shortly after World War II as military aircraft manufacturers in the United States found that the existing materials were limiting the performance of their designs[3]. Initially boron fibers were developed to reinforce plastics[4]; boron fibers were strong, stiff, and relatively lightweight in comparison to the existing materials. Boron fibers had numerous drawbacks; their large diameter (100-150μm) made them difficult to handle and the loop strength of the fiber is low, so that only monofilaments could be used. The fibers suffered from shell-core effects (creating thermal mismatch difficulties) and they were quite expensive. Since the 1950s many varieties of reinforcing fibers have been developed, including glass and organic fibers. The low cost and relatively high-strength of glass fibers permitted the evolution of techniques for the fabrication of composites

with a variety of shapes and contours[5]. The use of glass fiber is limited by its higher density and other mechanical deficiencies (i.e. low specific stiffness), so organic fibers were developed for applications where very high specific strength and impact resistance is required.

The specific strength and stiffness of carbon fibers is superior to all other reinforcing materials except poly(p-phenylene-2,6-benzobisoxazole) (PBO) (Figure 1.1). Carbon fibers surpass all other high performance fibers in temperature applications[6] (Figure 1.1 and 1.2, and Table 1.1); the stability and retention of properties at high temperatures is a primary requirement of reinforcing fibers.

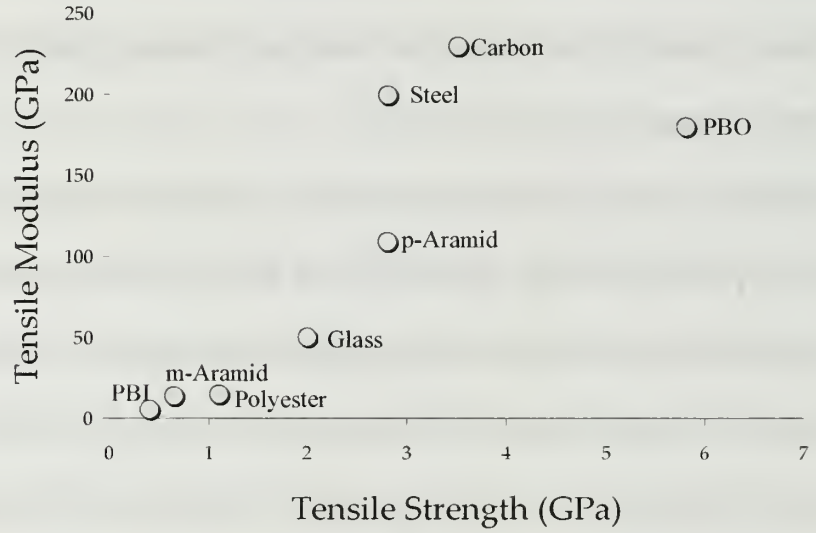

Figure 1.1: Mechanical properties of reinforcing fibers at room temperature[7]

Table 1.1: Comparison of properties of high performance fibers[7, 28]

	Tensile Strength (GPa)	*Tensile Modulus (GPa)*	*Elongation at Break (%)*	*Density (g/ml)*	*Heat Resistance* (°C)*
Glass	2-4	50-80	4.8	2.55	838
PBO	5.8	180-270	3.5-2.5	1.54-1.56	650
p-Aramid	2.8	109	2.4	1.45	550
m-Aramid	0.65	14	22	1.38	400
Steel Fiber	2.8	200	1.4	7.8	
Carbon Fiber[28]	3.5-5.8	220-290	1.5	1.76-1.80	
PBI	0.4	5.6	30	1.4	550
Polyester	1.1	15	25	1.38	260

*Melting or Decomposition

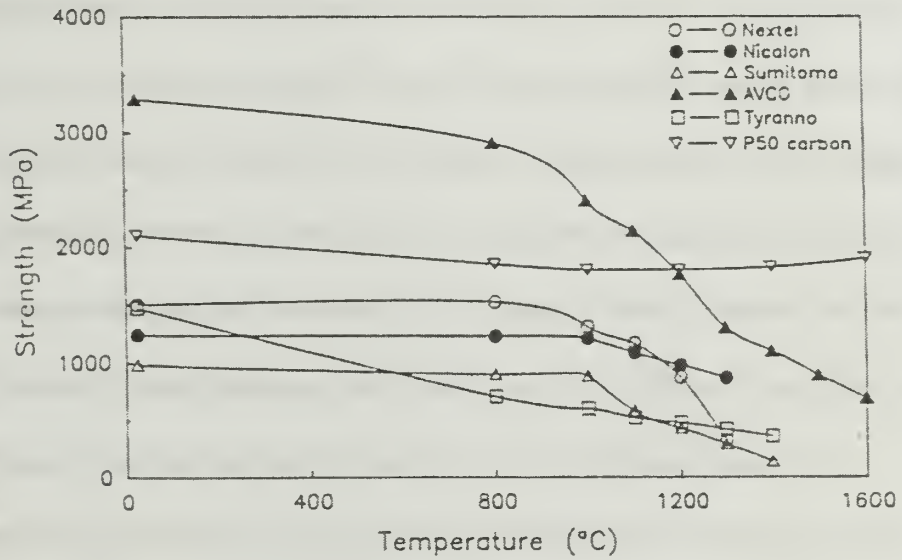

Figure 1.2: The effect of elevated temperatures on the tensile strength of various commercial reinforcing fibers[2, 6]. 3M Company's Nextel fiber is a ceramic reinforcing fiber consisting of Al_2O_3, SiO_2, and B_2O_3, while Tyranno and Nicalon fiber (diameter of approximately 15μm) are both commercial SiC fiber products of Ube Industries and Nippon Carbon, respectively, both of Japan. Sumitomo refers to glas fiber produced by Sumitomo Corporation of America. AVCO are SiC filaments (with a diamter of about 140μm) prepared by chemical vapor deposition by Avco Specialty Materials/Textron. PSO/Carbon refers to a thermoplastic matrix of polysulfone reinforced with carbon fiber.

1.2.2 Origin of Carbon Fiber Strength and Stiffness

The unique properties of carbon fiber are directly attributed to the highly anisotropic nature of the graphite crystal. The graphite crystal is composed of stacks of multiple sheet-like layers of carbon atoms separated by a distance of 0.335nm. The graphite structure is extremely strong in the crystallographic *a* direction; in the plane of the sheet, the carbon atoms are covalently bonded and have a bond strength of $400kJ/mol$ due to sp^2 hybridization. A theoretical tensile modulus and strength of 1060GPa and 106GPa, respectively, should be possible for graphite loaded in the crystallographic *a* direction. Normal to the basal plane, the crystallographic *c* direction, the carbon layers are held by weak Van der Waals forces and the tensile modulus of graphite loaded in this direction is quite low, 36.5GPa. Despite the high elastic constant in the direction parallel to the graphene layers, the mechanical properties of carbon fibers are limited by the low transverse properties of the graphite structure[1, 10] (but they are still greatly superior to organic fibers such as polyethylene, Kevlar®, and PBO).

If it were possible to produce a hypothetical carbon fiber from infinitely large polyaromatic layers of elemental carbon arranged in the ideal graphite structure, it would be weakest in compression. The low shear resistance of crystalline graphite allows it to be easily bent despite its high strength in the crystallographic *c* direction. Research has focused on finding ways to overcome the natural shear sensitivity of the graphite structure. One of the most promising approaches involves modifying the molecular structure of the carbon fiber as a means of inhibiting shear failure. It has been found that small sized polyaromatic layers, containing disclinations deviating from the perfect preferred orientation, leads to improved tensile and compressive properties

in carbon fibers. The molecular orientation of the fiber is more or less parallel to the fiber axis in the turbostratic structure and the axial properties of the fiber are still a reflection of the covalent bonding parallel to the basal planes. The turbostratic structure offers a compromise between properties that reflect the molecular orientation (i.e. modulus and thermal conductivity) and mechanical properties that are affected by the size of the graphitic layers (i.e. tensile and compressive strength).

1.2.3 Precursor Materials and Pyrolysis

Although many different precursor materials can be used to produce carbon fibers, only three are considered suitable for commercial processes: rayon, pitch and Polyacrylonitrile. The processing routes necessary to produce carbon fibers from these precursor materials are not the same for each precursor and differences between these, as well as, the precursor yield (Table 1.2) largely determine the economics of each of the competing processes. The essential features of the processes are similar and involve (a) a stabilizing treatment to prevent the precursor fibers melting or fusing together, (b) a carbonizing heat treatment to drive off the majority of non-carbon elements, and (c) an optional high temperature treatment 'graphitization' to improve the mechanical properties of the fiber. The term 'graphite' is strictly a misnomer and has been used in the literature to describe the turbostratic structure of high modulus carbon fiber.

The precursor fibers are often pretreated to ensure that they decompose before melting and the decomposition always results in a weight loss ranging from 50-90% depending upon the precursor. The diameter of the fiber decreases during decomposition, but the external morphology is always retained[8].

Table 1.2: Carbon yield for various carbon precursors

Precursor	Process Yield*
Rayon	20-30%
Polyacrylonitrile (PAN)	45-50%
Pitch	75-90%

*Kilogram of carbon fiber per kilogram of precursor fiber[10]

1.2.3.1 Rayon

Cellulosic precursor fibers are of considerable historic significance, although they are no longer an important source of carbon fibers. Cellulose is a naturally occurring polymer and often exists in a fibrous form. Cotton was one of the first fibers carbonized due to its rare property of degrading before melting, although it is unsuitable for the manufacture of high performance carbon fibers. Cotton is highly crystalline and has a low degree of orientation along the axis of the fiber, but it is not available in continuous fiber tows. To overcome these difficulties continuous rayon fibers are produced by wet spinning of cellulose extracted from wood pulp.

The repeat unit of rayon is β-D(+)-glucose (Scheme 1.1); the three hydroxyl groups in the repeat unit take part in intermolecular hydrogen bonding, giving a cross-linked effect and stopping the fibers from melting upon heating. Intermolecular hydrogen bonding is partly responsible for the insolubility, crystallinity and suitability of the polymer for fiber formation. The hydroxyl groups are removed before the polymer is dissolved and respun; the fiber is then subjected to a three-stage pyrolysis consisting of a low temperature decomposition (<400°C), carbonizaton (<1500°C), and a stress graphitization (>2500°C)[9].

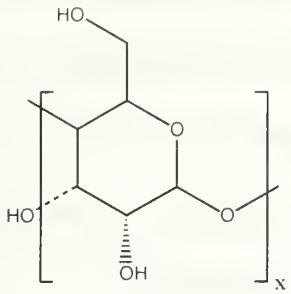

Scheme 1.1: The repeat unit of rayon is β-D (+)-glucose

The low temperature decomposition is carried out at a low rate of temperature increase in an oxidative, or inert atmosphere, and is accompanied by an inevitable theoretical 55.5% weight loss (Scheme 1.2). A 70-90% weight loss is often realized,

$$(C_6H_{10}O_5)_n \rightarrow 6nC + 5nH_2O$$

Scheme 1.2: Decomposition of rayon

though, due to chain splitting and the driving off of carbon in the form of low molecular weight compounds (i.e. carbon monoxide). Many different reactions occur during the pyrolysis. The process is complex and has not been fully resolved, although, it has been found that one reaction in particular is responsible for a large part of the additional weight loss, the production of levoglucosan[10]. Levoglucosan is produced in the early stages of pyrolysis from an intermediate stage of dehydration (Scheme 1.3) and it breaks down into volatile fragments during later stages of pyrolysis.

High performance graphite fibers may be produced from this system, although the yield is low, therefore a reactive atmosphere and flame retardants are used to reduce the availability of the primary hydroxyl group; the primary hydroxyl group is necessary to the production of levoglucosan. The efficiency of a reactive atmosphere in improving the processing rate and carbon yield is limited by the rate of diffusion of the

reactive species into the interior of the fiber (a slow process). An increase in temperature will increase the rate of diffusion but may lead to excessive degradation of the fiber structure. Impregnation of the fibers with flame-retardants results in an increase in the amount of carbon formed, and allows for the decomposition of cellulose at a faster rate and lower temperature[11].

Rayon fibers suffer major molecular breakdown after being heated to a temperature of 400°C; the modulus of the fibers passes through a minimum[9,12]. The residue consists of low molecular weight furan derivatives that form a graphitic structure by condensation reactions involving the removal of hydrogen at higher temperatures. Graphitized layers are formed in the orientation and direction of the original cellulose chain and the adjacent chains then condense to form six-member carbon structures[10]. The modulus increases and the resistivity of the fibers decreases with temperature up to 1400°C [11]. The ultimate orientation of carbon fiber is not adequate after carbonization, so graphitization at temperatures above 2800°C is carried out for a fraction of a second under stress.

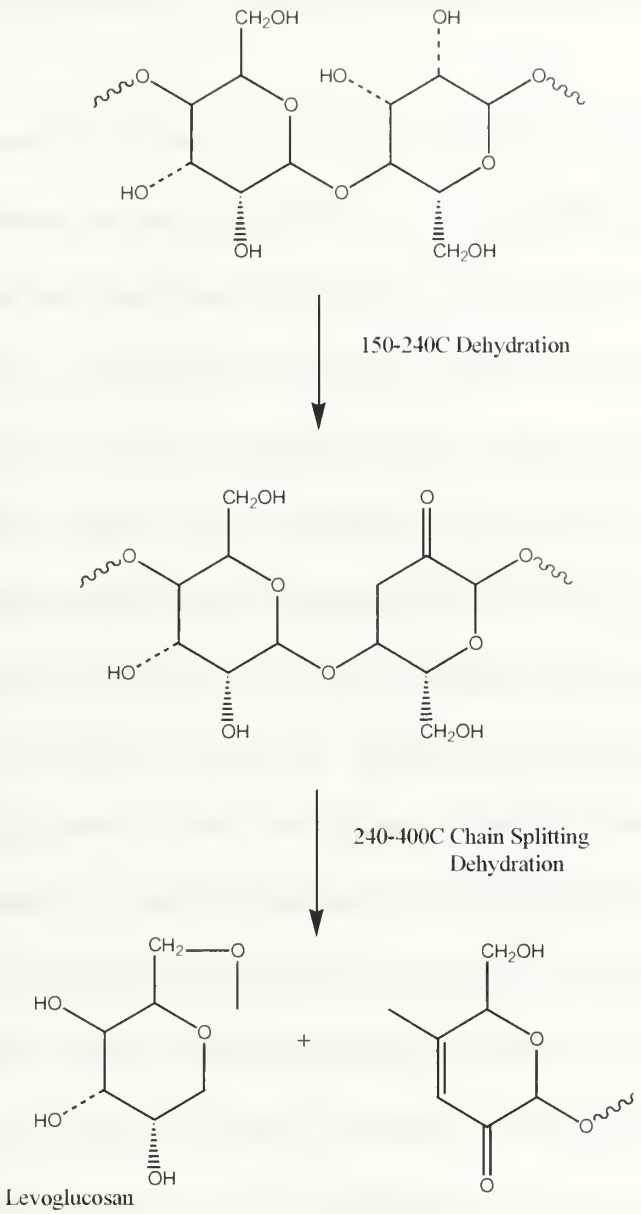

Scheme 1.3: Formulation of levoglucosan

1.2.3.2 Pitch

Pitch is a low-cost material commonly obtained from petroleum asphalt, coal tar and PVC. Pitches are made up of numerous organic compounds with aggregates of condensed benzene ring systems separated by and carrying alkyl chains (average

molecular weights are between 400 and 600). The composition of a pitch depends upon its source.

Pitches are thermoplastic and require some kind of thermosetting to maintain the filament shape during pyrolysis. Ordinarily pitches are extruded into a fibrous form, thermoset between 250-400°C (generally in an oxidative atmosphere) and then carbonized between 1000°C and 2500°C. The suitability of a pitch for the production of carbon fibers is determined by its ability to be spun and converted to a nonfusible state so that the fibers can be carbonized without melting. All of these properties are dependent upon the chemical composition and molecular weight distribution of the pitch. The molecular weight affects the viscosity of the melt and determines the temperature and speed of spinning. The viscosity of the melt is adjusted with the addition of various additives. Additionally, pitch is commonly impregnated into braided, or woven, carbon fiber structures (preforms) and carbonized to prepare carbon-carbon composites; several impregnation and carbonization cycles are usually required.

PVC and a number of other pitch materials produce isotropic carbon fibers with poor mechanical properties, unless hot stretched at a high temperature[13]. Since the hot stretching process for the production of pitch carbon fibers is difficult and costly, other varieties of pitch materials that form anisotropic pitch fibers have been explored. Mesophase pitch is prepared by thermal treatment of small polynuclear aromatics, or from the byproducts of thermal cracking of petroleum fractions or crude. During prolonged heating, the molecules undergo dehydrogenative reactions and form large molecules that aggregate into a liquid crystalline phase with a nematic order, the mesophase. The mesophase has a higher surface tension than the lower molecular

weight isotropic phase from which it grows, and forms small liquid droplets that grow in size. Once the anisotropic phase grows to approximately 45%, phase inversion occurs and the anisotropic phase becomes the continuous phase. Fibers with a high degree of orientation can be spun from mesophase pitch and converted into high strength and modulus graphite fibers.

Mesophase pitches are also thermoplastic and must be oxidized (stabilized) in order to preserve their preferred orientation during the carbonization process. Since the pitches have a high softening temperature, they may be oxidized at a higher temperature than fibers from ordinary pitches where diffusion and oxidation occurs at a faster rate. Stabilization of mesophase pitch fibers requires only a few minutes, in comparison to a few hours for ordinary pitch fibers, and stabilized fibers are ready for carbonization and graphitization without the need for high temperature stretching[10].

1.2.3.3 Polyacrylonitirile (PAN)

Polyacrylonitrile (PAN) is a linear polymer containing approximately 68% carbon (Scheme 1.4). Acrylonitrile is emulsion polymerized in an aqueous medium by free radical or negative initiators. PAN is also polymerized in a solvent used for wet spinning; in order to eliminate the need for a dissolution step (of the intermediate polymer powder) in fiber production. The highly polar character of the nitrile group causes strong dipole-dipole forces, which act as cross-links. Due to these strong interactions, PAN is insoluble except in highly ionizing solvents and it has a high melting point, which makes it a suitable carbon precursor material. Also, these strong dipole-dipole interactions prevent rearrangements necessary for the development of

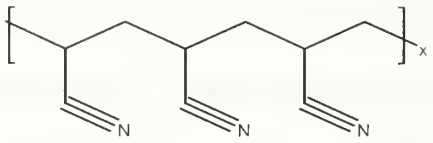

Scheme1.4: Polyacrylonitrile

crystallinity and cause shrinkage of the fiber during heat treatment (entropic and chemical shrinkage occurs). Shrinkage is a disadvantage to carbon fiber manufacture because it disturbs the orientation of the fiber and produces carbon fibers with poor mechanical properties[14]. If shrinkage is prevented, by stretching during stabilization (high temperature oxidation), carbon fibers with improved mechanical properties can be prepared[15].

A copolymer of 85% acrylonitrile and a maximum of 15% comonomer is wet spun to prepare carbon precursor fibers. Generally, a good textile fiber consists of a system of highly ordered and amorphous zones; the crystalline regions provide fiber's tensile strength, rigidity, and stability of shape. The amorphous regions provide the fiber with elasticity and segment mobility. Drawn PAN homopolymer has excellent tensile properties (tensile strength of 512MPa[16]) but the properties dependent upon the amorphous phase are poor due to a high degree of ordering and intermolecular nitrile interactions. The introduction a few percent of comonomer enhances the internal mobility of the polymer segments by interrupting the sequences of acrylonitrile molecules and therefore reducing the number of interactions with neighboring sequences. The comonomer affects the solubility, oxygen permeation, melting point depression, and acts as a site of initial cyclization (influencing the rate of degradation of PAN)[17].

PAN precursor fibers are heated to 200-300°C in an oxidizing atmosphere while under tension, to avoid shrinkage and extension. During this stabilization step, the thermoplastic PAN is converted into a nonplastic ladder compound. The oxidized fibers are carbonized to approximately 1000°C without tension and then heated to any temperature up to 3000°C depending upon the required Young's modulus of the final carbon fiber.

1.2.4 Polyacrylonitrile Precursor Fibers

Of the three precursors, Polyacrylonitrile (PAN) is the most suitable to develop the carbon structure needed to produce high strength fibers and most carbon fibers manufactured commercially, today, are PAN based. Carbon fibers prepared from PAN are more expensive than rayon but the carbon yield of PAN is approximately double that of rayon. High Performance carbon fibers are prepared in greater yield from oxidized PAN fibers due to their preferential aromatic character, which prevents the backbone carbon chain from extensive splitting during pyrolysis.

1.2.4.1 Stretching

The better the degree of molecular orientation in the PAN precursor fiber, the better the mechanical properties, in particular the modulus, of the resultant carbon fiber[18]. PAN precursor fiber suffers from entropic shrinkage at low temperatures, once the glass transition temperature (T_g) is reached, where kinetic conditions are provided for the molecules to relax strain acquired by stretching during spinning. The precursor fiber is drawn prior to stabilization (up to 14 times in steam at 100°C)[19, 20], while it is

still a thermoplastic polymer, to generate the preferred orientation. During the later stages of stabilization, shrinkage due to chemical reaction occurs and can disrupt the orientation of the molecular chains. Fiber shrinkage and a decrease in the modulus of the final carbon fiber results, therefore, mechanical means are employed to control the natural shrinkage during the stabilization process[1, 15, 21].

1.2.4.2 Stabilization

The stabilization step converts the precursor from a linear polymer to a highly condensed, thermally stable structure. The principle feature of the overall reaction is an exothermic cyclization of the nitrile groups. The temperature at which the cyclization takes place depends upon the comonomer content of the precursor, the stretch applied to the fiber before and during stabilization, and the surrounding atmosphere during the stabilization. If the precursor fiber is heated too rapidly to the cyclization temperature, the cyclization is spontaneous and a large amount of heat is generated. A rapid release of heat can cause a loss of molecular orientation and melting of the fiber, which will have a detrimental effect on the mechanical properties of the final carbon fiber. To ensure optimal properties of the final carbon fiber, cyclization is conducted so to promote a slow release of heat to minimize loss of orientation and fragmentation of the polymer[22]. Oxidation, the incorporation of oxygen containing groups into the polymer chain, occurs concurrently with the cyclization reaction. Oxygen containing groups promote cross-linking reactions in the early stages of carbonization. While the cyclization reaction is temperature dependent, the oxidation reaction is diffusion

controlled. Oxidation depends upon the diameter and composition of the precursor fiber, and the temperature and concentration of oxygen in the reacting atmosphere.

Low temperature stabilization is time consuming; stabilization temperature has a significant effect on the mechanical properties and manufacturing cost of carbon fibers. The thermal process occurs in two distinct temperature ranges; between 100-200°C coloration occurs due to the polymerization of the nitrile groups and oxidation[23]. Cross-linking becomes extensive and small amounts of volatiles are formed. At temperatures greater than 240°C, thermally stable material is produced and volatile substances are evolved by chain scission and decomposition reactions.

The polymerization depends upon the presence of a structural defect leading to a species capable of initiating the cyclization. A growing chain attacks a pendant nitrile group and an imine radical is formed, which can either propagate further or terminate (Scheme 1.5). The imine structure can be hydrolyzed to form a ketone. The same ketone defect can also be introduced thermally at 150°C by an autoxidation process involving attack at the backbone methylene group (Scheme 1.6). The enolate form of this cyano-ketone is believed to be the major initiating species (Scheme 1.7).

The dihydronaphthyridine rings are susceptible to oxidation under the conditions of cyclization. To a lesser degree, initiation may be accomplished by other functionalities present as by- or decomposition products. Above 240°C, the reaction is that of aromatization and the elimination of ammonia (Scheme 1.8)[24].

The chemical composition of the stabilized precursor fiber has a dramatic influence on the mechanical properties of the final carbon fiber. The oxygen content required for optimum fiber properties varies for different PAN copolymers; in general,

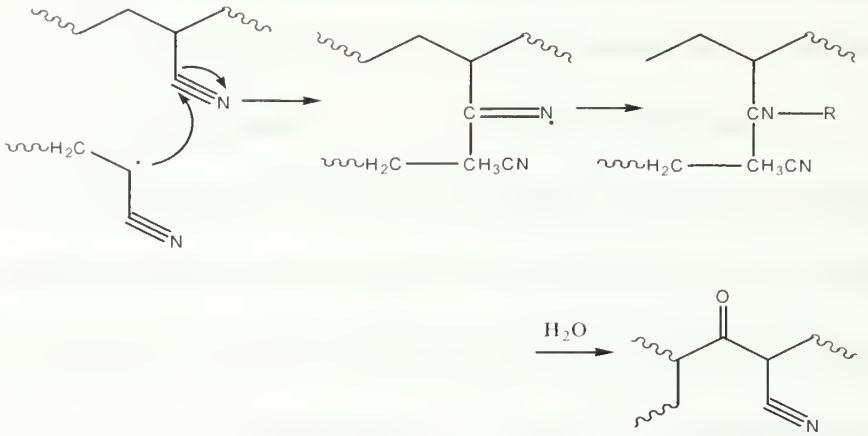

Scheme 1.5: Generation of a ketone defect by mis-addition of the growing chain

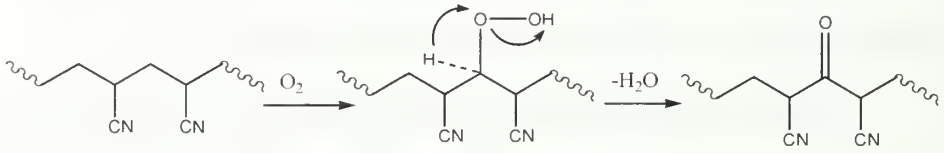

Scheme 1.6: Generation of a ketone defect by an autoxidaton process

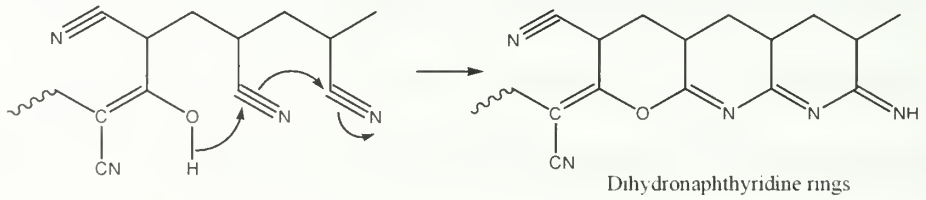

Scheme 1.7: Mechanism for the formation of a dihydronaphthyridine rings

the oxygen content increases by 8% to 11%. The evolution of CO_2 from decarboxylation reactions and HCN from the reaction of uncyclized nitrile groups, cause the carbon content of the PAN fiber to decrease from 68% to 65% during stabilization. Evolution of HCN and H_2O cause the hydrogen content of the fiber to decrease. Overall, the fiber experiences a 5% to 8% weight loss during stabilization.

(a)

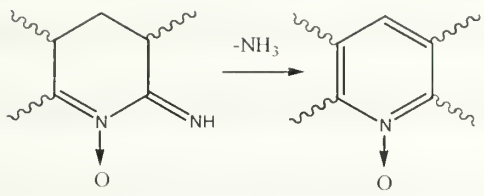

(b)

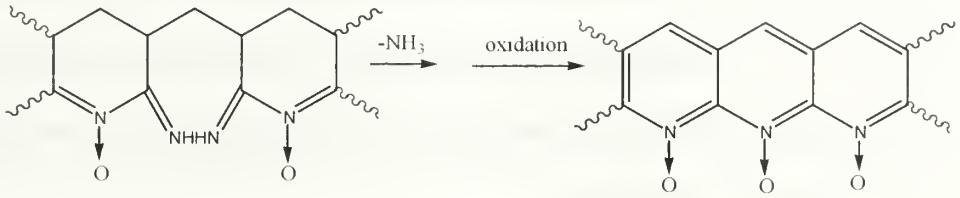

Scheme 1.8: (a) Aromatization and (b) combination of 'dead-ends' to eliminate ammonia

1.2.4.3 Carbonization

The carbonization step, high temperature treatment, eliminates most of the non-carbon elements from the fiber and converts the stabilized precursor into a carbon fiber. Carbonization is conducted in an inert atmosphere at temperatures ranging from 1000°C to 2500°C. During this stage, a thermally stable pyridinic structure forms and subsequently collapses into a turbostratic stacked ring structure.

Chemical reactions involving cross-linking, reorganization, and the coalescence of cyclized sections to evolve H_2O, NH_3, HCN, CO, CO_2, and CH_4 and low molecular weight nitriles occur between 300°C to 600°C. The hydroxyl groups present in the oxidized fiber initiate cross-linking condensation reactions that aid in the reorganization and coalescence of the cyclized sections (Scheme 1.9). During the low temperature stage of carbonization, the foundation of the carbon building block is set-up. Cross-linking fixes the structure of the polymer while the remaining linear segments either

become cyclized, or undergo chain scission and are evolved as gaseous by-products. The cyclized structures undergo dyhydrogenation and link producing a graphite-like structure of three hexagons in the lateral direction bounded by nitrogen atoms[8, 25]. Intermolecular cross-linking takes place and H_2, HCN, and H_2O are evolved between 600°C and 1000°C[26]. The carbon content of the fiber increases to 92%, nitrogen decreases to 7%, and hydrogen is less than 0.3%. The PAN based carbon attains a tensile strength of 3GPa and a modulus of 250GPa (comparable to that of PBO fibers) between 1200°C and 1400°C[1].

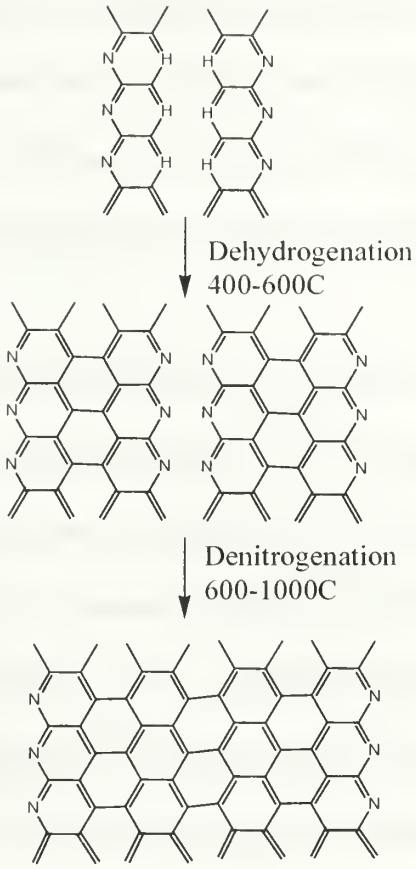

Scheme 1.9: Carbon fiber preparation from PAN[10]

1.2.4.4 Graphitization

The carbonized fiber has lost most of its non-carbon impurities and has a graphite-like structure. High temperature heat treatment greater than 2500°C does not cause weight-loss in the fiber, but improves the ordering and orientation of the crystallites in the direction of the fiber axis. The modulus of the carbon fiber can be directly related to the final heat treatment temperature.

1.2.5 Fiber Processing

Manufacturing of a composite structure starts with the incorporation of a large number of fibers into a thin layer of matrix to form a lamina (ply). Techniques of

reinforcing a matrix with carbon fiber usually involve the fabrication of carbon fiber fabrics, preforms, staple yarns, or slurries to ease handling and processing. Woven fabrics provide the most convenient way to handle continuous carbon fibers and the impregnation of a fabric with resin is easily performed by immersing the fabric in a resin bath.

In contrast, continuous unidirectional composites are commonly prepared from the winding of continuous tows of fibers, hand lay-up of unidirectional tapes or woven fabric, or by pultrusion. Various shaped anisotropic prepregs are prepared by the winding of a continuous tow of fibers immersed in a resin bath onto a rotating mandrel and by hand laid unidirectional tapes, or woven fabrics (fabrics with a larger number of yarns in one direction than in the perpendicular direction), that are impregnated with resin. Another method of forming unidirectional fiber composite parts with a constant cross section is pultrusion. In pultrusion, fibers are drawn from spools, passed through a resin bath for impregnation, and gathered together to form a particular shape before entering a heated die. Anisotropic fabric preforms provide a way to fabricate composite materials of near net shapes and to build structures with a reduced amount of external fasteners; the interface between a fastener and a composite is the weak point in the structure.

Braiding is a method used to fabricate continuous fiber composites; it is particularly suitable to fabricate seamless composite tubing. Braided fabric layers, interlacing structures consisting of at least two sets of yarns (not necessarily orthogonal), may be interconnected so that yarns traverse from one layer into at least one continuous layer and form a three dimensional braid.

Three and two-dimensional isotropic preforms can be prepared from short carbon fibers. The preparation of the preform involves filtering or pressing the slurry of short fibers, binder, and a vehicle, drying, and heat treatment. The slurry method is particularly important for preforms with less then 25 vol.% carbon fiber[27]. All of the weaving processes used to prepare carbon fiber fabrics or braids require that the fibers be coated with sizing before weaving due to the brittleness of the fibers and that complicated weaving equipment be used.

1.2.6 Application

A potential for weight savings with fiber-reinforced composites exists in many engineering fields. Major structural application areas for carbon fiber-reinforced composites include: aircraft, space, automotive, and sporting goods. Weight reduction is critical for aircrafts in order to increase payloads and speed of travel. The Airbus A320, A330 and A340 series of aircraft use carbon fiber, either alone or in hybridization with Kevlar® fiber, in the nacelles, fairing, flaps, and empennage. Boeing aircrafts use carbon fibers in floor panels, interiors, and door springs, and commuter and business aircrafts use carbon fiber in primary and secondary structures. In addition, it is possible to tailor the dynamic frequencies of helicopter and engine rotor blades within operating parameters with composites. Fiber-reinforced composites offer manufacturing flexibility in blade applications (composite blades can be molded into complex air foil shapes at little additional manufacturing cost). In the early 1990's General Electric formed a joint venture with Snecma for design and production of carbon fiber fan blades for the GE-90 engine. The critical flopping and twisting

frequency of the blade can be controlled and tuned not just by the method of mass distribution but also by varying the concentration, distribution, and orientation of fibers along the blade chord length.

The unique environment of outer space places rigorous demands on the materials used for construction of satellites. Severe temperature changes can cause ordinary materials to warp, expand, or contract depending on temperature. Carbon fiber-reinforced laminates are designed to produce a coefficient of thermal expansion close to zero. The low specific gravity, higher strength, and higher stiffness to weight ratio have lead to the use of carbon fiber-reinforced materials for the support structure for mirrors and lenses in the space telescope and building trusses for optical benches, solar array panels, and antenna reflectors[28].

The automotive market has started to use carbon fiber in a variety of applications: compressed Natural Gas (CNG) tanks, friction reduction applications, and car interiors. The CNG tanks manufactured using carbon fiber emit less pollution and maintain equivalent MPG to conventional gas tanks, and meet current government crash standards. High-end consumer autos feature carbon fiber in the dashboard instruments and seats. High performance race vehicles use carbon fibers in the construction of chassis, bodies, suspensions, brakes, and helmets.

Carbon fiber-reinforced polymers are used in sporting good applications due to weight reduction, vibration damping, and design flexibility. Weight reduction has lead to higher speeds and quick maneuvering in bicycles and canoes, and has allowed for the placement of additional weight in golf club heads, allowing for a faster swing and longer drive. Callaway, Taylor Made, Ping, and Titleist all have carbon fiber golf

shafts in their product offerings. The use of carbon fiber-reinforced composites in tennis and racquetball racquets provide fast damping of vibration and reduces the shock transmitted to the player's arm[29,30].

1.3 Fiber Reinforcement

1.3.1 Introduction

High performance composites usually result from embedding high-strength, high-stiffness fibers of one material into a surrounding matrix of another material. While the fibers are the principal load carrying members, the matrix maintains them in the desired location and orientation, acts as a load transfer medium, and protects them from the environment. The strength and modulus of a composite material result from the homogeneous dispersion of fibers throughout the matrix, good interfacial adhesion and load-transfer between the matrix and the fiber, and a high aspect ratio (l/d) of the fiber[31,32]. Fiber-reinforced composite materials offer a combination of strength and modulus that are either comparable or better than traditional metallic materials. The strength to weight and modulus to weight ratios of composite materials are superior to metallic materials, in addition to their fracture strength to weight ratio. Fiber reinforced materials are a major class of structural materials and are replacing metallic materials in many weight critical designs.

1.3.2 Longitudinal Tensile Loading

1.3.2.1 Continuous Parallel Fibers

Fiber-reinforced composites are microscopically inhomogeneous and non-isotropic (usually orthotropic). The mechanics of fiber-reinforced composites are studied in two levels: the micromechanics level examines the interaction of the constituent materials on the microscopic scale, and the macromechanics level examines the response of the composite material to mechanical and thermal loads on a macroscopic scale. Basic assumptions are made when describing the response of fiber-reinforced lamina to tensile and compressive loading: (a) fibers are uniformly distributed throughout the matrix, (b) perfect bonding exists between fibers and matrix (Equation 1.1), (c) matrix is free of voids, (d) applied loads are either parallel or normal to the fiber direction, (e) lamina is initially in a stress free state, and (f) both the fibers and matrix behave as linear elastic materials (Equation 1.2 and 1.3).

$$\varepsilon_f = \varepsilon_m = \varepsilon_c \tag{1.1}$$

$$\sigma_f = E_f \varepsilon_f = E_f \varepsilon_c \tag{1.2}$$

$$\sigma_m = E_m \varepsilon_m = E_m \varepsilon_c \tag{1.3}$$

Where ε_f, ε_m, and ε_c are the longitudinal strains in the fibers, matrix and composite, respectively. In a composite of continuous parallel fibers where the modulus of the fiber E_f is greater than that of the matrix E_m, the stress in the fiber σ_f is always greater that the matrix stress σ_m. The total tensile force P applied on the composite lamina is shared by the fibers P_f and the matrix P_m (Equation 1.4). The

longitudinal modulus E_L, or rule of mixtures, shows that the composite modulus is an intermediate between the fiber and matrix modulus (Equation 1.5).

$$P = P_f + P_m \tag{1.4}$$

$$E_L = E_f \upsilon_f + E_m (1 - \upsilon_f) \tag{1.5}$$

Where υ_f is the volume fraction of the fibers in the composite ($\upsilon_f = A_f / A_c$ where A_f and A_c are the net cross sectional area of the fibers and the matrix, respectively). 0.2 volume fraction of fibers carries more than 70% of the composite load; the composite load and the fiber load fraction can be increased by increasing the fiber volume fraction. The practical limit for cylindrical fibers is 80%; the matrix will not be able to wet the fibers above this limit.

1.3.2.2 Discontinuous Parallel Fibers

The tensile load applied to a discontinuous fiber lamina is transferred to the fibers by a shearing mechanism between the fibers and the matrix. Since the matrix has a lower modulus, the average longitudinal strain in the matrix is higher than that in the adjacent fibers. The difference in longitudinal strains creates a shear stress distribution across the fiber/matrix interface. The stress in the fiber is not uniform; it is zero at the ends and builds up nearly linearly to the maximum value $\sigma_{f\,(max)}$ at the central portion of the fiber (Equation 1.6)

$$\sigma_{f\,(\max)} = \frac{2\tau_f l_t}{d_f} \tag{1.6}$$

Where τ_f is the interfacial shear stress, l_t is the load transfer length (the minimum fiber length in which the maximum fiber stress is achieved), and d_f is the fiber

diameter. The critical fiber length l_c is the minimum fiber length required for the maximum fiber stress to be equal to the ultimate fiber strength at its midsection (Equation 1.7).

$$l_c = \sigma_{f(\max)} \frac{d_f}{2\tau_f} \qquad (1.7)$$

For effective fiber reinforcement, the fiber length selected must be greater that the critical fiber length. The critical fiber length may be controlled by adjusting the fiber diameter and strength, or the interfacial shear stress through the use of a matrix-compatible coupling agent[21].

1.3 Effect of Aspect Ratio (*l/d*)

Theoretical calculations using either equations by Halpin-Tsai equations[32, 33, 34] (Equation 1.8, 1.9, and 1.10) or Christensen's[35] equation are used to predict the modulus of a composite and the effect of short to continuous fiber as reinforcing materials in a composites. The Halpin-Tsai equations are a simplification of the analysis originally done by Hill.

$$\frac{E_c}{E_m} = \frac{1 + \xi\eta\upsilon_f}{1 + \eta\upsilon_f} \qquad (1.8)$$

$$\eta = \left(\frac{E_f}{E_m} - 1\right) \Big/ \left(\frac{E_f}{E_m} + \xi\right) \qquad (1.9)$$

$$\xi = 2\frac{l}{d_f} + 40\upsilon_f^{10} \qquad \text{for } E_{11} \qquad (1.10)$$

Where l/d_f is the aspect ratio and ξ is a geometrical factor. ξ is a measurement of reinforcement geometry, packing geometry, and loading conditions. The Halpin-Tsai

equations show that the modulus depends upon the fiber aspect ratio, the volume fraction of the fibers, the fiber to matrix modulus ratio, and the average fiber orientation distribution. As ξ nears the limit of infinity, the effect of continuous fiber reinforcement materials on the modulus of a composite are predicted. The Halpin-Tsai relationships have been used to predict composite modulus using the rule of mixtures; the rule of mixture approximation includes a degree of error due to the dropping of an additional term, which is present in Christensen's equation. Christensen's equation predicts the effective modulus of a composite containing finite length fibers, and is reduced when considering the special cases where $(E_f/E_m)\chi^2 \ln(2/\chi) >> 1$ for finite length fibers (Equation 1.11) and $(E_f/E_m)\chi^2 \ln(2/\chi) << 1$ long continuous fibers (Equation 1.12)

$$\frac{E_c}{E_m} = 1 + v_f \left(\frac{1/2(1+v_m)}{\kappa^2 \{\ln(2/\chi) - (5-4v_m)/4(1-v_m)\}} \right) \qquad (1.11)$$

$$\frac{E_c}{E_m} = 1 + v_f \left(\frac{E_f}{E_m} - 1 + \frac{2(v_f - v_m)^2}{1 + v_m + (E_m/E_f)(1+v_f)(1-2v_f)} \right) \qquad (1.12)$$

Where χ is the aspect ratio (d_f/l), and v_m and v_f is poisson's ratio of the matrix and the fiber, respectively. Equation 1.11 and 1.12 are reduced to $E_c/E_m = 1 + cA$, where A describes the reinforcement effect, or the change in modulus of the composite due to the addition of the fiber. The reinforcement effect of short fibers on a composite is greatly affected by the length of the fiber through the χ^2 term in the denominator of Equation 1.11; the smaller the fiber aspect ratio (the greater length than diameter), the greater the ability of the fiber to reinforce the matrix. A continuous fiber will enhance the modulus

of a composite much more then a short fiber, according to Figure 1.3 where v_f and v_m are assumed to be 0.25 and 0.35, respectively. Continuous fibers ($\chi = 0$) reinforce the composite as the ratio of the fiber to matrix modulus is increased. As the length of the reinforcing fiber decreases (aspect ratio χ increases), the reinforcement effect on the composite initially increases and then reaches a plateau regardless of the mechanical properties of the reinforcer. Composites containing short fibers, particles, or whiskers are only expected to produce moderate improvements over non-reinforced polymer materials. According to Equation 1.11 and 1.12, the potential of a reinforcer to enhance the modulus and strength of a composite is limited by its aspect ratio regardless of the reinforcer's properties. Therefore, according to this argument, a continuous carbon nanofiber is expected to better reinforce a matrix than a commercial carbon fiber[36] or nanotube. The predicted modulus of a carbon nanotube is expected to be as high as 1TPa[37], although nanotubes are not able to reinforce a composite fully due to their finite length. If carbon nanotubes could be dispersed homogeneously without incurring defects on the nanotubes, the stiffness of the material would be increased but the strength likely would not. A plot similar to that shown in Figure 1.3 for carbon nanotubes would show an initial increase in the reinforcement effect and then a plateau, above which the nanotubes have limited ability to reinforce the matrix. Continuous nanofibers have a lower aspect ratio (d/l) than nanotubes and according to the predictions of Christensen, provide reinforced composites with moduli that will surpass those of nanotubes.

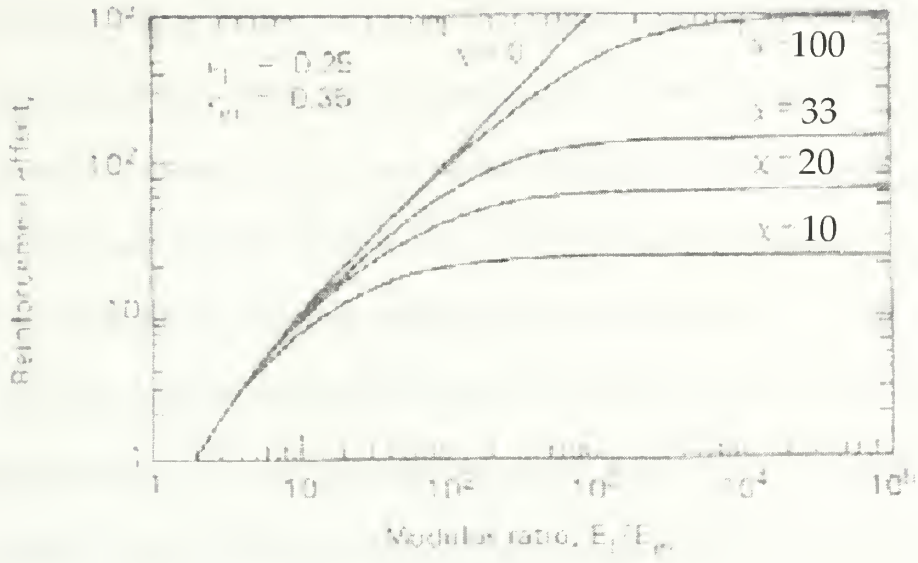

Figure 1.3 The Reinforcement Effect versus the Modulus Ratio (E_f/ E_m) for various aspect ratios (*l*/*d*)[38]

1.4 Fiber Spinning Technique of Electrospinning

1.4.1 Introduction and History

Electrospinning was first patented in 1902[39] as an apparatus for electrically disbursing fluids. In this patent, a design is given for the collection and reeling of fibers prepared from solution with the application of a voltage. Since then, several patents have been published describing a variety of products prepared by electrospinning, including: a method of preparing patterned and textured nonwoven material[40a], tubular structures[39b, 39d, 39e], and synthetic vascular grafts[39c].

Electrospinning, a fiber spinning technique that relies on electrostatic forces to produce fibers in the nanometer to micron diameter range, has been extensively explored as a simple method to prepare fibers from polymer solutions or melts[41]. In a typical process, an electrical potential is applied between a droplet of polymer solution.

or melt, held at the end of a capillary tube and a grounded target. When the applied electric field overcomes the surface tension of the droplet, a charged jet of polymer solution is ejected. The trajectory of the charged jet is controlled by the electric field. The jet exhibits bending instabilities due to repulsive forces between the charges carried with the jet. The jet extends through spiraling loops, as the loops increase in diameter the jet grows longer and thinner[42] until it solidifies or collects on the target. The fiber morphology is controlled by the experimental design and is dependent upon solution conductivity, solution concentration, polymer molecular weight, viscosity, and applied voltage[43].

1.4.1 Development and Applications

In the past several decades, this technique has been used to generate narrow fibers from a broad range of polymers including engineering plastics, biopolymers[44], conducting polymers[45], and polymer blends and recently it has been used to prepare nanofibers made from ceramics and composite materials[46]. The main feature of the electrospinning process is that it is a simple means to prepare continuous fibers with unusually large surface to volume ratios and pore structure surfaces[47]. Due to the chaotic oscillation of the electrospinning jet, a characteristic feature of the electospinning process, randomly oriented and isotropic structures in the form of nonwoven nanofiber mats or webs are often generated due to a lack of control over the forces driving fiber orientation and crystallization. These mats are of great interest for applications including composite reinforcement[48], membrane-based separation, sensing[49], and tissue engineering. Recent efforts have been made to control the spatial

orientation of electrospun fibers for use with 1D device fabrication, which require well aligned and highly ordered architectures through redesign of the collection apparatus[50]. Molecular orientation has been observed in electrospun fibers collected onto a parallel plate and a rotating drum collection apparatus, although the orientation has not been quantified[51]. Progress in understanding the electrospinning technique has allowed for recent engineering efforts in processes used to collect electrospun fibers for various applications, however, very limited work has addressed the mechanical properties of electrospun fiber mats[52].

1.5. Proposed Research

1.5.1 Introduction

The market for carbon fibers is dominated by fibers made from Polyacrylonitrile due to their combination of good mechanical properties, particularly tensile strength, and reasonable cost. The high strength and modulus of carbon fibers make them useful in the reinforcement of polymers, metals, carbons, and ceramics, despite the fibers' brittle nature. Carbon fibers prepared from Polyacrylonitrile (PAN) precursor fibers by conventional techniques have a minimum diameter between 5-7μm. The bulk of production cost incurred during carbon fiber production is due to long heating times required to stabilize and carbonize the precursor fiber, in addition to engineering costs to maintain tension on fibers during stabilization. During stabilization, cyclization and oxidation reactions occur concurrently; the rate of oxidation is diffusion controlled and depends upon the diameter and chemical composition of the fiber in addition to the

temperature and atmosphere. A decrease in the fiber diameter of the precursor fiber would result in a decreased stabilization time[1]. If mechanically useful PAN fibers could be produced by electrospinning, they could be carbonized 1000 times faster than conventional fibers and therefore be a lower cost, high-output means of producing sub-micron carbon fibers. Also, the fibers prepared by electrospinning have diameters so small that skin-core effects caused by differential stabilization are eliminated.

Carbon fibers fail at critical flaws; reducing the fiber diameter lowers the probability of encountering a critical flaw in a given test length. The strength of a carbon filament typically increases as the diameter decreases[1, 36]. Carbon fibers produced from electrospun precursor nanofibers would be on a similar size scale as vapor grown carbon (CCVD) filaments, which have diameters between 1μm and 100μm. The final CCVD product consists of primarily discontinuous filaments with lengths ranging from a few millimeters to a few hundred millimeters, while electrospun fibers are continuous. The mechanical properties and reinforcing behavior of continuous nanofibers are expected to differ significantly from their finite length, conventional counterparts. Composites containing continuous fibers perform better than those prepared containing short fibers, particles, or whiskers since the reinforcement effect of a fiber is dependent upon its length to diameter ratio, according to the Halpin-Tsai equations[30, 31, 32]and Christensen's equation[33] of composite modulus prediction. There is a greater possibility of increasing the modulus and strength of a composite by using a continuous fiber as reinforcement, rather than a high modulus short fiber.

Carbon nanofibers have been produced from electrospun precursor fibers and characterized physically and structurally[53, 56], although limited study of their mechanical properties has been made[49b] and no molecular orientation study of the precursor fiber prior to carbonization has been completed.

1.5.2 Summary

The project is focused on the fiber spinning technique of electrospinning and its application for the production of continuous nanofibers for reinforcement of composite materials. Efforts are directed towards the fabrication and post treatment of Polyacrylonitrile precursor carbon fibers, and determining the mechanical properties of their yarns. The goal of the research is to mechanically evaluate these high aspect ratio (l/d) carbon nanofibers and compare them to commercially produced fibers. The eventual outcome of the project is to determine the reinforcement effect of continuous carbon nanofibers in thin films.

1.6 References

(1) Fitzer, E.; Manocha, L.M. Carbon Reinforcements and Carbon/Carbon Composites. Springer-Verlag, New York (1998), Ch. 1.

(2) Fitzer, E. *Carbon.* **1989**, *27*, 621.

(3) McKee, D.W.; Mimeault, V.J. 'Surface Properties of Carbon Fibers.' In: Walker, P.L.; Thrower, P.A. Chemistry and Physics of Carbon.Vol. 8 Marcel Dekker, Inc., New York (1973), Ch. 2.

(4) (a) Talley, C.P. *J. Appl. Phys.* **1959**, *30*, 1114. (b) Wawnes, F.E. 'Boron Filaments.' In: Brautman, L.; Kersch, R. (Eds) Modern Composite Materials. Addison-Wesley, (1967).

(5) Lubin, G. (Ed) Handbook of Composites. Van Nostrand Reinhold Co., New York (1982).

(6) Hillig, W.B. *Proceedings of International Conference on Reinforced Materials and Composite Technologies.* Weisbaden, Germany (1988).

(7) www.toyobo.co.jp

(8) Jain, M.K.; Balasubramanian, M.; Desai, P.; Abhiraman, A.S. *J. Mater. Sci.* **1987**, *22*, 301.

(9) Goodhew, P.J.; Clarke, A.J.; Bailey, J.E. *Mater. Sci. and Eng.* **1975**, *17*, 3.

(10) Tang, M.M.; Bacon, R. *Carbon.* **1964**, *2*, 211.

(11) Donnet, J.; Bansal, R.C. Carbon Fibers. Marcel Dekker, Inc., New York (1984), Ch. 1.

(12) Ross, T.E. *Textile Res.* **1968**, *38*, 906.

(13) (a) Otani, S.; Yokoyama, A.; Nukui, A. *Appl. Polymer Symposia.* **1969**, *9*, 325. (b) Hawthorne, H.M.; Baker, C.; Bentall, R.H.; Linger, K.R. *Nature* **1970**, *227*, 946.

(14) Shindo, A. *Yogyo-Kyokai-Shi* **1961**, *69*, 195.

(15) Watt, W.; Phillips, L.N.; Johnson, W. *Engineer (London)* **1966**, *221*, 815.

(16) Moncrieff, R.W. Man-Made Fibres, 6th Ed. John Wiley & Sons, New York (1975)

(17) Henrici-Olive, G.; Olive, S. 'The Chemistry of Carbon Fiber Formation from Polyacrylonitrile.' In: Advances in Polymer Science: Industrial Developments. Springer Verlag, Berlin (1983).

(18) Bahl, O.; Mathur, R.; Kundra, K. *Fibre Sci. Tech.* **1981**, *15*, 147. (b) Chari, S.; Bahl, O.; Mathur, R. *Fibre Sci. Tech.* **1981**, *15*, 153.

(19) (a) Dorey, G. *Phys. Technol.* **1980**, *11*, 56. (b) Bajaj, P.; Sreekumar, T.V.; Sen, K. *J. Appl. Polym. Sci.* **2002**, *86*, 773.

(20) Damodaran, S.; Desai, P.; Abhiraman, A.S. *J. Text. Inst.* **1990**,*81*, 384.

(21) Ko, T. *Mater. Chem. & Phys.* **1994**, *38*, 289.

(22) Wang, P.H.; Yue, Z.R.; Li, R.Y.; Liu, J. *J. Appl. Polym. Sci.* **1995**, *56*, 289.

(23) (a) Peebles, L.H. *J. Polym. Sci. Part A-1* **1967**, *5*, 2637. (b) Peebles, L.H.; Brandrup, J. *Makromol. Chem.* **1966**, *98*, 189.

(24) (a) Overberger, C.G.; Moore, J.A. *Adv. Polymer Sci.* **1970**, *7*, 113. (b) Xue, T.J.; MeKinney, M.A.; Wilke, C.A. *Polym. Degrad. & Stab.* **1997**, *58*, 193.

(25) Kasatochkin, V.I.; Kargin V.A. *Doklady Phys.Chem.* **1970**, *191*, 303.

(26) Tsai, J.S. *J. Mater. Sci. Letters* **1996**, *15*, 835.

(27) Chung, D. Carbon Fiber Composites. Boston, Butterworth-Heinemann **1994**.

(28) Connell, S.J.; Abusafieh, A. *SAMPE J.* **2002**, *38*, 46.

(29) www.hexcelfibers.com

(30) Mallick, P.K. Fiber-reinforced Compostites: Materials, Manufacturing, and Design. 2nd Ed. Marcel Dekker, Inc., New York (1993).

(29) Schwartz, M.M. Composite Materials: Properties, Nondestructive Testing, and Repair. Prentice Hall Inc., New Jersey (1996), Ch 1.

(32) Kardos, J. L. High Performance Polymers. Baer, E. and A. Moet, Eds. Hanser Publishers, New York (1991), Ch 6.

(33) Halpin, J.C. and J.L. Kardos. *Polym. Eng. & Sci.* **16** (15), 344-352 (1976).

(34) Halpin, J.C. Revised Primer on Composite Materials: Analysis. Technomic Publishing Co., Pennsylvania, 1984, Ch. 6.

(35) Christensen, R.M. Mechanics of Composite Materials. John Wiley & Sons, New York, 1979. Ch. 3.

(36) (a) Chung, D.D. *Carbon* **2001**, *39*, 1119. (b) Jones, B.F.; Duncan, R.G. *J. Mater. Sci.* **1971**, *6*, 289.

(37) Schadler, L.S.; Giannaris, S.C. and P.M. Ajayan. *Appl. Phys. Lett.* **1998**, *73*, 3842.

(38) Russel, W.B. *Z. Angew. Math. Phys.* **1973**, *24*, 581.

(39) Cooley, J.F. U.S. Patent 692,631, Feb 4. 1902.

(40) (a) Simons, H.L. U.S. Patent 3,280,229, Oct 18, 1966. (b) Bornat, A. U.S. Patent 4,323,525, Apr 6, 1982. (c) How, T.V. U.S. Patent 4,689,186, Aug 25, 1987. (d) Berry, J.P. U.S. Patent 5,024,789, Jun 18, 1991.

(41) Larrondo, L. and R.S. Manley. *J. Polym. Sci.* **1981**, *19*, 921.

(42) (a) Reneker, D. H.; Yarin, A.L.; Fong, H. and S. Koombhongse. *J. Appl. Phys.* **2000**, *87*, 4531. (b) Shin, Y. M; Hohman, M.M.; Brenner, M.P.; Rutledge, G.C. *Polymer* **2001**, *42*, 9955.

(43) (a) Fong, H.; Chun, I.; Reneker, D.H. *Polymer* **1999**, *40*, 4585. (b) Deitzel, J.M.; Harris, K.D. and N.C. Beck Tan. *Polymer* **2000**, *42*, 261-272.

(44) (a) Matthews, J.; Wnek, G.; Simpson, D.; Bowlin, G.. *Biomacromolecules* **2002**, *3*, 232. (b) Kenawy, E.; Abdel-Fattah, Y. R. *Macromol. Biosci* **2002**, *2*, 261. (c) Haung, L.; Nagapudi, K.; Apkarian, R.P.; Chaikof, E.L. *J. Biomater. Sci. Polymer Edn.* **2001**, *12*, 979.

(45) MacDiarmid, A.G.; Jones, W.E.; Norris, I.D.; Gao, J.; Johnson, A.T.; Pinto, N.J.; Hone, J.; Han, B.; Ko, F.K.; Okuzaki, H.; Llaguno, M. *Synth. Met.* **2001**, *119*, 27.

(46) (a) Fong, H.; Liu, W.; Wang, C.; Vaia, R.A. *Polymer* **2002**, *43*, 775. (b) Dror, Y.; Salalha, W.; Khalfin, R.L.; Cohen, Y.; Yarin, A.L.; Zussman, E. *Langmuir* **2003**, *19*, 7012. (c) Kumar, S.; Doshi, H.; Srinivasarao, M.; Park, J.O.; Schiraldi, D.A. *Polymer* **2002**, *43*, 1701. (d) Yang, Q.B.; Li, D.M.; Hong, Y.L.; Li, Z.Y.; Wang, C.; Qiu, S.L.; Wei, Y. *Synth. Met.* **2003**, *137*, 973.

(47) Megelski, S.; Stephens, J.S.; Chase, D.B.; Rabolt, J.F. *Macromolecules* **2002**, *35*, 8456.

(48) Kim, J. and D. H. Reneker. *Polym. Comp.* **1999**, *20*, 124.

(49) (a) Madhugiri, S.; Dalton, A.; Gutierrez, J.; Ferraris, J.P.; Dalkus, K.J. *J. Am. Chem. Soc.* **2003**, *125*, 14531. (b) Pedicini, A.; Farris, R.J. *J. Polym. Sci.: Part A* **2004**, *42*, 752.

(50) (a) Theron, A.; Zussman, E.; Yarin, A.L. *Nanotechnology* **2001**, *12*, 384. (b) Li, D.; Xia, Y. *Nano Lett.* **2003**, *3*, 555. (c) Zussman, E.; Theron, A.; Yarin, A.L. *Appl. Phys. Lett.* **2003**, *82*, 973.

(51) (a) Lee, S.; Yoon, J.; Suh, M. *Macromol. Res.* **2002**, *10*, 282. (b) Dersch, R.; Liu, T.; Schaper, A.K.; Greiner, A.; Wendorff, J.H. *J. Polym. Sci.: Part A* **2003**, *41*, 545.

(52) (a) Lee, K.; Kim, H.; Ryu, Y.; Kim, K.; Choi, S. J. Polym. Sci.: Part B 2003, 41, 1256. (b) Yang, K.S.; Edie, D.D.; Lim, D.Y.; Kim, Y.M.; Choi, Y.O. Carbon 2003, 41, 2039. (c) Pedicini, A.; Farris, R.J. Polymer 2003, 44, 6857.

(53) (a) Chun, I.; Reneker, D.H.; Fong, H.; Fang, X.; Deitzel, J.; Beck Tan, N.; Kearns, K. Adv. Mater. 1999, 1, 36. (b) Kim, C.; Yang, K.S. Appl. Phys. Lett. 2003, 83, 1216. (c) Wang, Y.; Santiago-Aviles, J.J.; Furlan, R.; Ramos, I. IEEE Trans. Nano. 2003, 2, 2003. (d) Park, S.H.; Kim, C.; Choi, Y.O.; Yang, K.S. Carbon 2003, 41, 2653. (e) Yang, K.S.; Edie, D.D.; Lim, D.Y.; Kim, Y.M.; Choi, Y.O. Carbon 2003, 4, 2039.

CHAPTER 2

ELECTROSPINNING TECHNIQUE

2.1. Introduction

Polymeric fibers with diameters in the submicron or nanometer range may be optimal candidates for various applications due to their high surface to volume ratio and their potential for mechanical properties. Nanofibers have a large surface area available for functionalization for sensing type applications, or adhesion in structural and reinforcement type applications, for example. Polymer nanofibers are expected to have mechanical properties different from those of their conventional counterparts.

Several techniques have been used to prepare polymer nanofibers in recent years, including: drawing[1], template synthesis[2], phase separation[3], self-assembly[4], and electrospinning. The drawing process, similar to dry spinning in the fiber industry, produces long single nanofibers through large deformations. Only viscoelastic materials that are cohesive enough to support the stresses developed during the pulling may undergo drawing, therefore limiting the process. Template synthesis uses a nanoporous membrane as a template to make nanofibers of solid (fibril) or hollow (tubular) shape. Nanofibrils, or tubules, of various raw materials may be fabricated, although single nanofibers cannot be prepared by template synthesis. Phase separation consists of a series of dissolution, gelation, extraction, freezing, and drying steps to produce a nanoporous foam that is used to prepare fibers; the process to transfer the solid polymer into nanoporous foam is quite time consuming. In self-assembly, individual components of a multicomponent system organize themselves into patterns

and shapes with the application of energy, or a force (typically heat, pressure, or electric field), and time. Unfortunately, it is a time-consuming to prepare continuous polymer nanofibers by the self-assembly technique. In comparison, electrospinning is a quick, straightforward, simple, cost effective method to produce novel fibers through the use of columbic forces. The electrospinning technique allows for the preparation of reproducible, continuous fibers with diameters in the micron to 10s of nanometer size range from polymer solutions and melts at room temperature in a matter of seconds. The electrospinning process overlaps with contemporary textile fiber technology and appears to be the only method that can be further developed for mass production of continuous nanofibers from various polymers. Presently, several research groups are looking at the use of electrospun nanofiberous materials for applications in filtration, templating[5] and patterning[6], sensors[7], protective clothing[8], wound dressings[9] (and biomedical applications), drug delivery systems[10], as scaffolding materials to generate new tissue[11], and in composites[12].

2.2 History

The utilization of electrostatic forces to deform materials in the liquid state goes back many centuries; throughout the 20th century, there have been a number of studies focused on electrohydrodynamic atomization[13]. Electrospinning is an extension of this technology applied to higher viscosity fluids. The electrospinning process was first patented in 1902[14] and since then has been employed to produce a variety of polymeric ultrafine fibers in recent years from mostly from solution and some from melt; electrospinning is recognized as an efficient technique.

Although the term 'electrospinning,' derived from 'electrostatic spinning,' was used relatively recently (in around 1994), the fundamental idea dates back more than 60 years. Between 1934 and 1944, Formhals published a series of patents[15] describing an experimental setup for the production of polymer filaments using electrostatic forces. A polymer solution is introduced into an electric field; an electrode is placed into the solution and an electrode bearing electrical charges of opposite polarity is attached onto a collector. With sufficient potential, the solution is ejected out of a metal spinneret, the solvent evaporates, and fibers are collected onto a collector; polymer filaments are formed from solution. The potential difference, used by Formhals, depended upon the properties of the spinning solution (i.e. molecular weight and viscosity). His collection distance was short; the fibers he collected tended to stick to one-another and the collection device due to incomplete solvent evaporation. In 1966, Simons patented an apparatus for the production of patterned, ultra thin, low weight, non-woven fabrics using electrical spinning[16]. A positive electrode was immersed into a polymer solution and a negative electrode was attached to a belt where non-woven fabric was collected. He found that fibers from low viscosity solutions tend to be short and fine, while those from more viscous solutions are relatively continuous. In 1971, Baumgarten prepared an apparatus to electrospin acrylic fibers with diameters in the range of 50nm to 1.1μm[17]. The spinning dope was suspended from a stainless steel capillary tube; the size of the droplet was maintained constant by adjusting the feed rate of an infusion pump. A high voltage dc current was connected to the capillary tube and fibers were collected onto a grounded metal screen.

Since the 1980's, the electrospinning process has regained more attention due in part to the surge of interest in nanotechnology, as ultrafine fibers and fibrous structures of various polymers with diameters in the micron and submicron range can be easily fabricated. To date, it is generally believed that nearly one hundred different polymers, mostly dissolved in solvents, have been successfully spun into ultrafine fibers using this technique. Although the electrospinning process has shown promising potential and has existed for several decades in the literature, the process has remained essentially unchanged and its understanding is still limited[18].

2.3 Electrospinning Process

2.3.1 Fundamental Theory

The electrospinning apparatus consists basically of three components: a polymer reservoir, a high voltage power supply, and a grounded collection device or target (Scheme 2.1). The polymer reservoir consists of either a polymer in solution, or in the melt; a pendent drop of polymer solution is held at the end of a capillary tube through the use of a syringe pump (used to maintain constant back pressure).

Scheme 2.1: Diagram of a typical solution electrospinning apparatus consisting of a syringe containing solution mounted on a syringe pump, a high voltage source and a stationary, grounded target

An electrode, connected to a high voltage power supply, is attached to the syringe tip and a voltage is applied. An electrical charge develops at the fluid's free surface and interacts with the external electric field resulting in the emission of a fluid jet that thins as it accelerates downfield. The surface of the pendant droplet distorts to form a conical protrusion and a straight jet is ejected from the surface of the drop as a consequence of electrical forces; the conical protrusion is often called a Taylor cone[13h]. Farther downfield, the jet experiences a whipping instability that leads to bending and stretching of the jet; loops of increasing size are observed as the instability grows[19].

The electrically charged jet travels straight for a few centimeters; at the end of this straight segment, a diaphanous conical shape is observed with its vertex at the end of the straight segment[19,20]. Within this conical envelope, the jet's path becomes complex due to the growth of electrically driven bending instabilities. Instabilities are triggered by perturbations of the lateral position and velocity of the jet. The repulsive forces between the charges carried with the jet cause every segment of the jet to lengthen continuously along a changing path until the jet solidifies. The jet bends and develops a series of lateral excursions that grow into spiraling loops. Each loop grows larger in diameter as the jet grows long and becomes thin. The cycles of bending instability repeat in a self-similar manner until the solvent evaporates and the remaining polymer fiber resists further elongation by the columbic forces of the charge that is still present in the jet. The jet follows a whipping trajectory towards the grounded target and an entangled web of fibers is collected[21].

2.3.2 Electrospinning Parameters

The ability to transform a polymer solution or melt into a fiber by the electrospinning technique is controlled by several parameters, including: solution or melt properties (viscosity and surface tension), governing variables (applied voltage and current, solution flow rate, and the distance between the capillary tip and the grounded target), and ambient parameters (humidity, and air velocity in the electrospinning chamber). Manipulation of these variables will determine the morphology of the resultant material; electrospraying techniques form droplets and films, while 'beads-on-a string' and fibers with diameters in the range of a micron to submicron typically result from the electrospinning technique. Fiber formation is the least energetically favorable shape of the various possible geometries; researchers commonly observe the 'beads-on-a-string' type morphology due to incomplete contraction of the fiber into individual droplets (Figure 2.1).

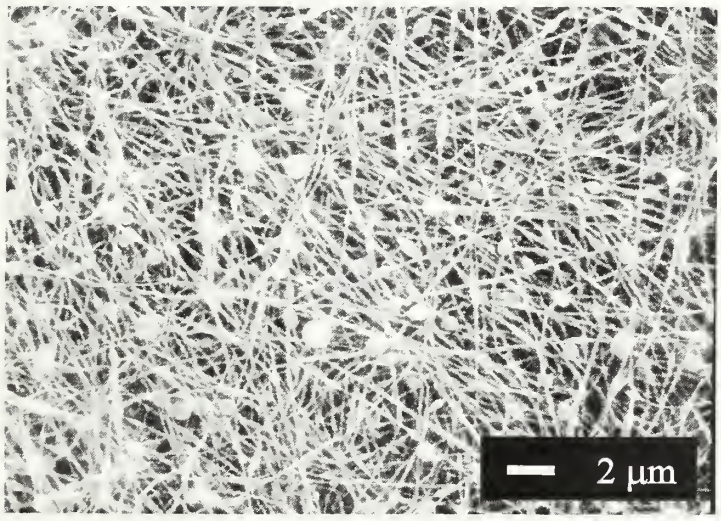

Figure 2.1: Scanning electron microscopy (SEM) image of Polyacrylonitrile (PAN) fibers electrospun from 10wt% PAN solution with dimethylformamide (DMF) at 8kV onto a stationary target exhibiting 'beaded fiber' morphology

Researchers have investigated the spin-ability of several different polymers by monitoring the effects of polymer molecular weight and solution (and entanglement) concentration, viscosity, surface tension, and conductivity. If the molecular weight of a polymer is not significantly greater than the critical molecular weight required to form entanglements in the melt, then droplet formation is favored over that of fibers (and electrospraying is favored over electrospinning). The molecular weight affects the ability of the chains to form entanglements; it is difficult for low molecular weight chains to form entanglements. As the zero shear rate viscosity, η_o, increases, larger fibers are generated by electrospinning; an increase in η_o indicates a larger number of entanglement couplings. As the number of entanglements and η_o increase, the morphology of the collected material changes from polymer droplets, to beaded nanofibers, and finally to defect-free nanofibers[22]. Attempts to electrospin from solutions with low viscosity have resulted in the collection of electrospun fibers in geometries other than two-dimensional fiber mat or film[23]. As a rule of thumb, a molecular weight of approximately 10,000g/mol is necessary to prepare fibers by electrospinning.

Solution concentration affects the diameter of electrospun fibers; researchers have shown that the diameter of electrospun fibers have a ~0.3 power law dependence upon solution concentration (with linear and branched PET-co-PEI fibers[14] and segmented polyurethaneurea copolymers[24]). In order to generate fibers with equivalent fiber diameters from a polymer with two different molecular weights, the solution concentration must be increased as the entanglement concentration of the polymer is

increased. As the percent solid in solution is increased, the resultant fiber diameter is also increased[25].

The solution surface tension is a function of solvent composition[26]. The surface tension and initial volume charge density dictate the strength of the voltage that should be applied in order to eject a jet from the pendent droplet. It has been shown that by reducing the surface tension of a polymer solution, fibers without beads can be obtained[27] (although, this is not considered a rule). It has been proposed that surface tension acts as a restoring force in regards to the path of the electrospinning jet; when the surface tension dominates over surface charge repulsion (within the jet) the path of the jet follows the centerline of the electric field. The jet experiences bending instabilities when charge repulsion within the jet dominates over the surface tension[20].

The conductivity of the solution affects the spinning, or jet, current. As the conductivity of the solution is increased (i.e. through the addition of salt), the number of charge carriers is increased and the mass flow of material through the electric field is increased; the electrospinning jet velocity is affected by changes in solution conductivity. Increasing the conductivity of a solution through the addition of salt has not been shown to increase the electrospun fiber diameter[26].

The electrospinning technique of fiber production is dependent upon Columbic forces. The application of voltage to the polymer reservoir leads to a competition between the supply of solution at the capillary tip and its withdrawal into the induced electric field. Application of an electric field leads to a change in the shape and volume of the pendant drop as the jet ejects. As the voltage is gradually increased, the diameter of the generated fiber decreases[28]. Once the voltage is increased so that the rate at

which solution is removed from the capillary tip exceeds the rate of delivery of solution, the Taylor cone is not maintained. The shift in mass balance does not only result in a disturbance of the conical shape, but generates an unstable jet. The unstable jet produces fibers with increased bead density.

The electric current due to the ionic conduction of charge in the polymer solution is usually assumed to be small, or negligible, in electrospinning[17]. The only mechanism of charge transport is the flow of polymer from the capillary tip to the target; an increase in electrospinning current reflects an increase in the mass flow rate from the capillary tip to the grounded target (when all other variables are held constant) [20]. Changes in the solution flow rate (pump speed) of solution into the induced electric field affect the generated fibers' diameter and morphology; the formation of beads along the fiber is observed at high flow rates. Changes in the working distance (gap) between the capillary tip and the grounded target do not affect the fiber size significantly, although, a large reduction in the working distance has been shown to result in the inhomogeneous distribution of elongated beads along the fibers[28].

Solution properties and the governing variables control the fiber morphology while the spinning environment play a great role in dictating the surface morphology of the fiber and fiber collection. Humidity directly affects the surface morphology of electrospun fibers; porous surface features have been observed in polymers electrospun from solution in the presence of humidity[28]. As the relative humidity of the environment increases to greater than 30%, pore formation is observed. Increasing humidity results in an increase in the number of pores on the fiber surface, the pore diameter, and the pore size distribution. An increase in molecular weight, while

maintaining all other variables constant, results in the formation of nonuniform pores (in shape and size) on the surface of the fiber. Humidity does not influence the fiber shape or diameter[29].

Departures from circular symmetry (around the axis fiber) have occasionally been reported; the geometrical shapes created by the fluid jet are often preserved in the shape of the solid fibers created by electrospinning. Jets without circular symmetry around the axis have been observed[30]; jets with ribbon-like geometries[31] and jets and fibers containing branches[32, 33] have been observed. 'Flat ribbon' fibers with flat or 'dogbone' cross-sections have been observed[34]; as the solvent escapes from the fiber, the skin collapses under atmospheric pressure forming a ribbon-like shape. Fibers collected by the electrospinning process, generally, still contain a high percentage of solvent in their core. As the solvent is removed, the outer skin tends to collapse inward to form fibers with a rough or wrinkled surface (depending upon the resultant internal structure). It is also common to observe 'deflated' beads after removal of residual solvent from the material.

2.4 Polyacrylonitrile Nanofibers

Polyacrylonitrile (PAN) nanofibers were prepared by electrospinning previously and the effect of processing parameters on the diameter of the resultant fiber was investigated[35]. Study has been limited to the effect of applied voltage, velocity of rotating collector, and the distance between the charged spinneret and the grounded target on the resultant fibers. Additionally, carbon nanofibers have been produced from electrospun Polyacrylonitrile (PAN) precursor fibers and characterized physically and

structurally[36]; the surface topography, crystalline structure, and conductivity were examined. A limited study of the mechanical properties of carbon nanofibers has been made[36c] (from electrospun poly (amic acid) precursor fibers) and no molecular orientation study of the precursor fiber prior to carbonization has been completed.

In the present work, the electrospinning process of fiber production is evaluated in regards to the preparation of PAN nanofibers with the ultimate purpose of preparing continuous carbon nanofibers for the reinforcement of thin films and nanocomposites. The effect of solution concentration and applied voltage on the generated fiber diameter is examined. The change in velocity and fiber diameter across the electrospinning jet is studied and the results obtained are considered in regards to the preparation of carbon precursor nanofibers.

2.5 Experimental

2.5.1 Materials

Polyacrylonitrile copolymer (PAN) is received from an industrial source and dimethylformamide (DMF) is obtained from Sigma Aldrich Co. H^1NMR (Polyacrylonitrile copolymer): CH_2 at 2.9ppm, CH at 3.2ppm, and dDMSO at 2.5ppm. The intrinsic viscosity and viscosity average molecular weight (M_v) of the received PAN is determined by viscometry[37] in DMF at 25°C to be 1.6dl/g and M_v 114,000g/mol, respectively. The number average molecular weight (M_n) and polydispersity index is determined by gel permeation chromatography in DMF against styrene standards to be 200,000g/mol (determined M_n is approximately twice the true

M_n) and 1.18, respectively. The polymer and solvent are dried before use; PAN powder was dried between 100°C and 120°C under vacuum for 2 hours and DMF is dried using a drying agent $MgSO_4$ and then distilled under vacuum. All solutions of PAN in DMF are prepared at room temperature under constant mixing. The solution viscosity is determined by using a cone and plate apparatus with an oscillatory method (with a frequency sweep of 0Hz to 100Hz) to determine the zero shear rate viscosity (Table 2.1).

Table 2.1: Viscosity at zero shear of electrospinning solutions of Polyacrylonitrile (PAN) in dimethylformamide as a function of concentration at room temperature

Concentration of PAN in DMF	8wt%	10wt%	15wt%
Viscosity	308cP	538cP	2594cP

2.5.2 Electrospinning Set-up

The electrospinning apparatus consists of a KD Scientific dual syringe infusion pump (Model 101), Gamma High Voltage Research high voltage power supply (Model RR20-3P/PRGI0V), and a grounded target. Solution is loaded into the syringe and an electrode is clipped onto the needle. The needle, electrode and grounded target are all enclosed in order to reduce the effect of air currents on the trajectory of the electrospun jet. The flow rate of solution to the needle tip is maintained so that a pendent drop remains during electrospinning. All air bubbles are purged prior to electrospinning and the solution is electrospun between 8-16kV horizontally onto the target. The grounded target is between 13-16cm from the charged capillary tip and is stationary (Scheme 2.1).

2.5.3 Electrospinning Velocity and Induced Draw ratio

The potential draw ratio of the electrospun fibers is determined by comparing the initial velocity of the solution with the final velocity of the collected fiber. The initial velocity of the polymer solution entering the electric field is determined based on the flow rate and the area of the needle orifice. The final velocity of the resulting electrospun fibers is determined based on collected mass[38] (Equation 2.1).

$$M = \rho V = \rho A l \qquad (2.1)$$

Where M is mass, ρ is the density, V is the volume, A is the cross-sectional area, and l is the length of the fiber. Splaying and the effects of solvent evaporation are ignored. The diameter of the jet is assumed to be the diameter of the dried fibers. Solutions of approximately 10wt% PAN in DMF are electrospun at 16kV over a distance of 11.5cm onto a weighed, stationary, grounded target for five minutes. The mass of the collected fibers on the target deviates from the theoretical collected mass, based on the flow rate and solution concentration, by 3% due to fiber loss resulting from air flow and fiber collection elsewhere. The collected sample is weighed and dried, the average fiber diameter was determined by field emission scanning electron microscopy (FESEM), and the density (1.18g/ml) is taken from the literature[39].

2.5.4 Laser Diffraction

The diameter of the electrospun jet of a 10wt% solution PAN in DMF is determined by light diffraction using Hughes Industrial Products Division 5mW helium-neon laser (λ = 632.8nm)[40] (Equation 2.2).

$$d_f = \frac{2\lambda s}{\delta_f} \qquad (2.2)$$

Where d_f is the fiber diameter, λ is the wavelength, s is the camera length, and δ_f is the width of the first maximum of the diffraction pattern. The electrospinning apparatus is repositioned vertically so that the grounded target was 9.5cm to 10.5cm below the charged capillary tip. The laser intercepted the jet at approximately 0.5cm below the capillary tip and the diffraction pattern is recorded for jets electrospun at voltages of 10kV, 13kV, and 16kV.

2.5.5 Microscopy

Electrospun fibers are observed by field emission scanning electron microscopy (FESEM) and polarized optical microscopy. Samples are mounted onto SEM plates, sputter coated with gold, and examined using a JOEL JSM 6320FXV electron microscope to determine fiber diameters. Measured fiber diameters include a 5% random error. All fibers are dried at approximately 170°C in vacuum for ~2 hours prior to observation.

2.5 Results and Discussion

During the electrospinning process, the droplet of solution at the capillary tip gradually elongates from a hemispherical shape to a conical shape or Taylor cone[13h] as the electric field is increased. A further increase in the electric field results in the ejection of a jet from the apex of the cone. The concentration, viscosity, conductivity of the solution as well as the applied voltage and distance between the charged electrode and the grounded target may be adjusted in order to obtain a stable jet. The diameter of

polyacrylonitrile (PAN) fibers collected onto a stationary, grounded target decrease as the applied voltage is increased, and increases as the concentration of the solution increases (Table 2.2). By increasing the electric field, while maintaining the distance between the charged capillary and the grounded target, the force pulling and stretching the polymer jet is increased; therefore a decrease in fiber diameter is expected. As the solution concentration is increased, the fiber diameter increases since the volume percent of solid in the solution and viscosity increase.

During the electrospinning process the spinning jet must undergo an extremely large draw ratio to generate fibers with diameters in the hundreds of nanometer

Table 2.2: Average diameter of electrospun Polyacrylonitrile (PAN) fibers as collected on a stationary, grounded target with increasing applied voltage and solution concentration, determined by scanning electron microscopy (SEM)[41]

	9.9wt% PAN in DMF	14.8wt% PAN in DMF
8kV	1.53 $\pm$0.1μm	1.67 $\pm$0.2μm
10kV	1.07 $\pm$0.4μm	1.15 $\pm$0.05μm
13kV	0.50 $\pm$0.03μm	0.59 $\pm$0.07μm
16kV	0.38 $\pm$0.03μm	

diameter range, therefore, it would be expected that the resulting collected fibers would contain some molecular orientation. Electrospun PAN fiber collected onto a stationary target are neither birefringent under cross-polars nor show a diffraction pattern by wide-angle x-ray diffraction (WAXD). Rather, the electrospinning process produces a delicate, amorphous, entangled web of PAN nanofibers (Figure 2.2) due to a lack of control of the forces that drive orientation and crystallization.

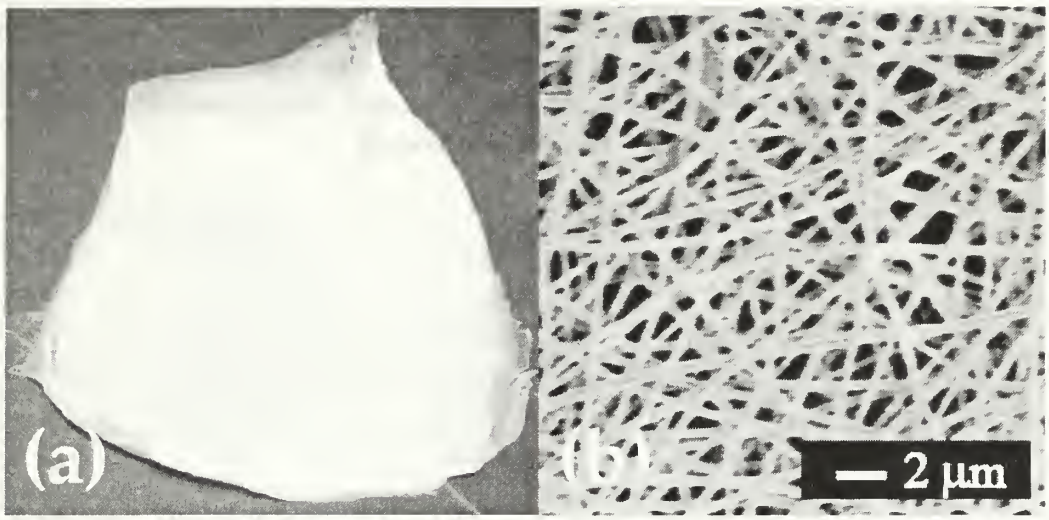

Figure 2.2: (a) Photograph and (b) a scanning electron microscopy (SEM) image of Polyacrylonitrile (PAN) fibers electrospun from 15wt% PAN solution in dimethylformamide (DMF) at 16kV onto a stationary target[17]

Since dimethylformamide (DMF) is a high boiling solvent, it is not expected that DMF has completely evaporated during the electrospinning process. A surface, or skin, forms on the jet due to the diffusion of moisture from humidity in the environment into the fiber and solvent remains in the core of the fiber; after drying (solvent is removed), the measured fiber diameter decreases (Table 2.3). The fibers are unconstrained after collection onto the target and tend to relax. The polymer chains are able to rearrange and any molecular orientation that may have been induced by the electrospinning process is lost. Due to this reason, it is common to produce fibers containing beads by the electrospinning process when the concentration of polymer in solution is low (as the fibers are allowed to relax into more energetically favorable spherical structures as the solvent is slowly removed).

Table 2.3: Average diameter of electrospun Polyacrylonitrile (PAN) fibers as collected onto a stationary, grounded target with increasing applied voltage and solution concentration before and after drying, determined by scanning electron microscopy

	9.97wt% PAN in DMF		14.8wt% PAN in DMF	
	As collected diameter	Diameter after drying	As collected diameter	Diameter after drying
8kV	1.54 ± 0.1μm	1.39 ± 0.2μm	1.68 ± 0.17μm	1.12 ± 0.5μm
10kV	1.08 ± 0.4μm	0.9 ± 0.04μm	1.52 ± 0.05μm	0.64 ± 0.08μm
13kV	0.5 ± 0.03μm	0.6 ± 0.03μm	0.59 ± 0.07μm	0.65 ± 0.04μm
16kV	0.39 ± 0.03μm	0.4 ± 0.03μm		

The draw ratio experienced by the electrospinning jet was determined by comparing the initial velocity of the polymer solution to the final velocity of the collected fiber. The initial velocity of the polymer solution through the spinneret at a constant flow rate of 0.016ml/min is determined to be 3.64E-4m/s. The final velocity of the collected fiber from a 9.9-9.8wt% PAN in DMF solution electrospun at 16kV is determined to be between 140-160m/s, from the mass collected in a period of time. The electrospun jet is treated as a monofilament in the velocity calculations; electrospinning generates one long, flowing, continuous, thinning jet. It is determined that the polymer jet experiences a 1:300,000 potential draw ratio across the 11.5cm gap from the charged capillary to the grounded target. Errors in the assumptions made during the final fiber velocity, due to fiber splaying or an increase in wet fiber diameter, would result in a decrease in the final spinning velocity; the true draw ratio may differ depending upon the validity of these assumptions. Not considering effects from solvent evaporation, the fiber diameter should theoretically decrease to 0.026% (0.253μm) of its original diameter. The diameter of fibers electrospun from a 10wt% PAN in DMF solution at

16kV and collected onto a stationary target is within in the range of 0.38-0.43μm, 0.039-0.045% of the original diameter.

The jet diameter was measured as a function of applied voltage at a constant distance of 0.5cm from the apex of the cone by laser diffraction (target position remained constant). The diameter of the jet appeared to increase as the voltage was increased (Table 2.4) and diameter of the jet was observed to decrease with increasing distance.

Table 2.4: Change in diameter of the electrospinning jet within the first 0.5cm traveled (from the syringe tip) as a function of applied voltage as determined by laser diffraction[17] (for a 10.1wt% PAN in DMF solution)

Voltage	10kV	13kV	16kV
Diameter	5.98 ±1.1μm	7.82 ±0.6μm	9.85 ±0.4μm

The draw ratio experienced by a jet of polymer solution electrospun at 16kV over a gap distance of 10.5cm is determined based on these results. Upon exiting the syringe, the jet (10.1wt% PAN in DMF solution) experiences a draw ratio of approximately1:9620 after just traveling a distance of 0.5cm from the syringe tip (based on the change in jet diameter), and within the next 10cm traveled, the jet experiences a further draw ratio of 1:600. During the electrospinning process, the fiber experiences a total draw ratio of approximately 1:582,000 as determined by comparing the diameter of the spinning jet entering the electric field and of the dried collected fiber; this is of the same magnitude as that determined earlier based on jet velocity (Section 2.5, pg. 76).

To prepare carbon fibers, the precursor fibers need to undergo a series of heat treatments; the PAN precursor fibers are initially oxidized under tension and then carbonized in an inert atmosphere. The electrospun webs are difficult to handle (the

webs are very delicate, randomly aligned, and amorphous) and it is difficult to keep the fibers in tension during stabilization. Carbon fibers with poor mechanical properties are expected from these precursor fibers. Generally the higher the degree of molecular orientation in the original PAN fiber results in carbon fibers with better mechanical properties particularly the tensile modulus[42]. Therefore, efforts to improve molecular orientation, alignment, and to enlarge the scale of the electrospinning process are necessary in order to prepare and evaluate carbon nanofibers prepared from electrospun precursor fibers.

2.6 Conclusions

Synthetic fibers of polymer have been produced for decades by conventional processes, such as melt spinning, dry spinning, or wet spinning. These techniques rely upon pressure-driven extrusion of a viscous polymer fluid and produce fibers that typically range from 10 to 500μm in diameter[43]. Electrostatic fiber spinning, or 'electrospinning,' is a novel process for forming fibers with diameters in the submicron range through the action of electrostatic forces; it provides a novel way to prepare continuous, carbon precursor fiber fabrics and yarns. Electrospinning permits for the production of non-directional, isotropic, nonwoven fabrics, unidirectional-oriented-nonwoven fabrics and yarns, as well as shaped preforms using isotropic, continuous precursor fiber. The high aspect ratio, large available surface area, surface morphology, and potential interlocking mechanism of load transfer make electrospun fibers of great interest as fillers in composite matrices.

2.7 References

(1) Ondarchuhu, T.; Joachim, C. *Europhys. Lett.* **1998**, *42*, 215.

(2) (a) Feng, L.; Li, S.; Li, H.; Zhai, J.; Song, Y.; Jiang, L. *Angew. Chem. Int. Ed.* **2002**, *41*, 1221. (b) Martin, C.R. *Chem. Mater.* **1996**, *8*, 1739.

(3) Ma, P.X.; Zhang, R. *J. Biomed. Mat. Res.* **1999**, *46*, 60.

(4) (a) Liu, G.J.; Ding, J.F.; Qia, L.J.; Guo, A.; Dymov, B.P.; Gleeson, J.T. *Chem.-A European J.* **1999**, *5*, 2740. (b) Whitesides, G.M.; Grzybowski, B. *Science.* **2002**, *277*, 1971.

(5) (a) Bognitzki, M.; Hou, H.; Ishaque, M.; Frese, T.; Hellwig, M.; Schwarte, C.; Schaper, A.; Wendorff, J.H.; Greiner, A. *Adv. Mater.* **2000**. (b) Czaplewski, D.A.; Verbridge, S.S.; Kameoka, J.; Craighead, H.G. *Nano Lett.* **2004**, *4*, 437. (c) Cazaplewski, D.; Kameoka, J.; Craighead, H.G. *J. Vac. Sci. Technol.* **2003**, *B21*, 2994.

(6) (a) Li, D.; Ouyang, G.; McCann, J.T.; Younan, X. *Nano Lett.* **2005**, *5*, 913. (b)

(7) Wang, X.; Kim, Y.G.; Drew, C.; Ku, B.C.; Kumar, J.; Samuelson, L.A. *Nano Lett.* **2004**, *4*, 331. (b) Chu, B.; Hsiao, B.S.; Fang, D.; Okamoto, A. U.S. Patent Appl. No. 10/674,464, **2003**. (c) Lennhoff, J.D. U.S. Patent Appl. No. 10/967,627, **2004**.

(8) (a) Gibson, P.W.; Schreuder-Gibson, H.L., Rivin, D. *AIChE Journal* **1999**, *45*, 190. (b) Schreuder-Gibson, H.; Gibson, P.; Senecal, K.; Sennett, M.; Walker, J.; Yeomans, W.; Ziegler, D.; Tsai, P.P. *J. Adv. Mater.* **2002**, *34*, 44.

(9) (a) Zong, X.; Kim, K.; Fang, D.; Ran, S.; Hsiao, B.S.; Chu, B. *Polymer* **2002**, 4403. (b) Khil, M.S.; Cha, D.I.; Kim, H.Y.; Kim, I.S.; Bhattarai, N. *J. Biomed. Res. B Appl. Biomater.* **2003**, *67*, 675.

(10) (a) Jiang, H.; Fang, D.; Hsiao, B.S.; Chu, B.; Chen, W. *Biomacromolecules* **2004**, *5*, 326. (b) Zheng, J.; Xu, X.; Chen, X.; Liang, Q.; Bian, X.; Yang, L.; Jing, X. *J. Controlled Release* **2003**, *92*, 227.

(11) (a) Boland, E.D.; Wnek, G.E.; Simpson, D.G.; Pawlowski, K. J.; Bowlin, G.L. *J. Macromol. Sci. –Pure Appl. Chem.* **2001**, *A38*, 1231. (b) Kim, K.; Yu, M.; Zong, X.; Chiu, J.; Fang, D.; Seo, Y.S.; Hsiao, B.S.; Chu, B.; Hadjiarqyrou, M. *Biomaterials* **2003**, *24*, 4977. (c) Ma, P.X.; Zhang, R. *J. Biomed. Mater. Res.*

1999, *46*, 60. (d) Xu, C.Y.; Inai, R.; Kotaki, M.; Ramakrishna, S. *Biomaterials* **2004**, *25*, 877.

(12) Madhugiri, S.; Dalton, A.; Gutierrez, J.; Ferraris, J.P.; Balkus, K.J. *J. Am. Chem. Soc.* **2003**, *125*, 14531.

(13) (a) Raleigh, Lord X. *London, Edinburgh, Dublin Philos. Mag.* **1882**, *44*, 184. (b) Zeleny, J. *Phys. Rev.* **1914**, *3*, 69. (c) Zeleny, J. *Proc. Cambridge Philos. Soc.* **1915**, *18*, 17. (d) Zeleny, J. *Phys. Rev.* **1917,** *10*, 1. (e) Macky, W.A. *Proc. R. Soc. A* **1931**, *133*, 565. (f) Nolan, J.J. *Proc. R. Irish. Acad.* **1926**, *37A*, 28. (g) Vonnegut, B.; Neubauer, R.L. *J. Colloid Sci.* **1952**, *7*, 616. (h) Taylor, G.I. *Proc. R. Soc. Lond. A* **1969**, *313*, 453.

(14) Cooley, J.F. U.S. Patent 692,631,**1902**.

(15) (a) Formhals, A. U.S. Patent 1,975,504, **1934**. (b) Formhals, A. U.S. Patent 2,160,962, **1939**. (c)Formhals, A. U.S. Patent 2,187,306, **1940**. (d) Formhals, A. U.S. Patent 2,323,025, **1943**. (e) Formhals, A. U.S. Patent 2,349,950, **1944**.

(16) Simmons, H.L. U.S. Patent 3,280,229, **1966**.

(17) Baumgarten, P.K. *J. of Colloid and Interface Sci.* **1971**, *36*, 71.

(18) Haung, Z.M.; Zhang, Y.Z.; Kotaki, M.; Ramakrishna, S. *Composites Science and Technology.* **2003**, *63*, 2223.

(19) Fridrikh, S.V.; Yu, J.H.; Brenner, M.P.; Rutledge, G.C. *Phys. Rev. Lett.* **2003**, *90*, 144502-1.

(20) (a) Warner, S.B.; Buer, A.; Ugbolue, S.C.; Rutledge, G.C.; Shin, M.Y. National Textile Center Annual Report No. 83-90, **1998**. (b) Shin, Y.M.; Hohman, M.M.; Brenner, M.P.; Rutledge, G.C. *Appl. Phys. Lett.* **2001**, *78*, 1149.

(21) (a) Reneker, D.H.; Yarin, A.L.; Fong, H.; Koombhongse, S. *J. Appl. Phys.* **2000**, *87*, 4531. (b) Yarin, A.L.; Koombhongse, S.; Reneker, D.H. *J. Appl. Phys.* **2001,** *89*, 3018. (c) Spivak, A.F.; Dzenis, Y.A. *Appl. Phys. Lett.* **1998**, *73*, 3067

(22) McKee, M.G.; Wilkes, G.L.; Colby, R.H.; Long, T.E. *Macromolecules.* **2004**, *37*, 1760.

(23) Deitzel, J.M.; Kleinmeyer, J.; Harris, D.; Beck Tan, N.C. *Polymer.* **2001**, *42*, 261.

(24) Demier, M.M.; Yilgor, I.; Yilgor, E.; Erman, B. *Polymer.* **2002**, *43*, 3303.

(25) Mit-uppatham, C.; Supaphol, P.; Nithitanaku, M. Society of Plastics Engineers Annual Technical Conference (ANTEC). **2003**, 1685.

(26) (a) Reneker, D.H.; Fong, H. *J. Polym. Sci.: Part B Polym. Phys.* **1999**, *37*, 3488. (b) Liu, H.Q.; Hsieh, Y.L. *J. Polym. Sci.: Part B Polym. Phys.* **2002**, *40*, 2119.

(27) Doshi, J.; Reneker, D.H. *J. Electrostatics.* **1995**, *35*, 60.

(28) Megelski, S.; Stephens, J.S.; Chase, D.B.; Rabolt, J.F. *Macromolecules.* **2002**, *35*, 8456.

(29) Casper, C.L.; Stephens, J.S.; Tassi, N.G.; Chase, D.B.; Rabolt, J.F. *Macromolecules.* **2004**, *37*, 573.

(30) Shkadov, V.Y.; Shutov, A.A. *Fluid Dyn. Res.* **2001**, *28*, 23.

(31) Huang, L.; MiMillan, R.D.; Apkarian, R.P.; Pourdeyhimi, B.; Conticello, B.P.; Chaikof, E.L. *Macromolecules.* **2000**, *33*, 2989.

(32) Deitzel, J.M.; Kleinmeyer, J.; Harris, D.; Beck Tan, N.C. *Polymer.* **2001**, *42*, 261.

(33) Reneker, D.H.; Yarin, A.L.; Fong, H.; Koombhongse, S.J. *Appl. Phys.* **1999**, *87*, 4531.

(34) Koombhongse, S.; Liu, W.; Reneker, D.H. *J. Polymer Sci.: Part B: Polymer Phys.* **2001**, *39*, 2598.

(35) Kang, Y.S.; Kim, H.K.; Ryu, Y.J.; Lee, D.R.; Park, S.J. *Polymer (Korea).* **2002**, *26*, 360.

(36) (a) Chun, I.; Reneker, D.H.; Fong, H.; Fang, X.; Deitzel, J.; Beck Tan, N.; Kearns, K. *Adv. Mater.* **1999**, *1*, 36. (b) Kim, C.; Yang, K.S. *Appl. Phys. Lett.* **2003**, *83*, 1216. (c) Yang, K.S.; Edie, D.D.; Lim, D.Y.; Kim, Y.M.; Choi, Y.O. *Carbon.* **2003**, *41*, 2039. (d) Wang, Y.; Santiago-Aviles, J.; Furlan, R.; Ramos, I. *IEEE Transactions on Nanotechnology.* **2003**, *2*, 39.

(37) Brandrup, J.; Immergut, E.H. and E.A. Grulke. Polymer Handbook. 4th Ed. New York, John Wiley & Sons Inc. **1999**, VII/11.

(38) Chun, I. Dissertation. University of Akron, **1995**.

(39) Brandrup, J. and E.H. Immergut. Polymer Handbook. 3rd Ed. New York, John Wiley & Sons Inc. **1989**, V/57.

(40) (a) Perry, A.J.; Ineichen, B. and B. Eliasson. *J. Mater. Sci.* **1974**, *9*, 1376. (b) Doshi, J. and D.H. Reneker. *J. Electrostatics* **1995**, *35*, 151.

(41) Fennessey, S.F.; Farris, R.J. *Polymer*. **2004**, *45*, 4217.

(42) (a) Bahl, O.; Mathur, R.; Kundra, K. *Fibre Sci. Tech.* **1981**, *15*, 147. (b) Chari, S.; Bahl, O.; Mathur, R. *Fibre Sci. Tech.* **1981**, *15*, 153.

(43) Ziabicki, A. Fundamentals of fibre formation: the science of fiber spinning and drawing. Wiley & Sons, Inc., New York, **1976**.

CHAPTER 3

MOLECULAR ORIENTATION AND ALIGNMENT

3.1 Introduction

Deposition of electrospun fibers onto a stationary target is essentially random due to the chaotic motion of the elctrospinning jet as it travels to the target. The small pore size obtained by the random morphology of the nonwoven electrospun mat is particularly advantageous for membrane and filter applications. This deposition process limits the use of electrospun fibers in a variety of reinforcement and 1-dimensional nanostructure applications. The random deposition is problematic; the collection of electrospun fibers in the form of a yarn, or tow, which could be post processed to improve mechanical performance or controlled fiber deposition onto a substrate in specific places, or patterns, is not possible by the present electrospinning process, as described, without further manipulation of the apparatus.

Researchers are exploring novel methods to focus and align continuous polymer and ceramic nanofibers (NFs); efforts have been made to improve the control of the electrospinning jet and its deposition by both mechanical and electrostatic means. Various alterations to the electrospinning apparatus have been proposed and examined to prepare aligned and oriented fibers by mechanical means, including the use of: grounded high-speed rotating drums, grounded metal frames and dual parallel plates. Attempts to manipulate the shape of the electrostatic field have been made to assist in the alignment of electrospun NFs. The literature is predominantly focused on applying these technologies to the preparation of 1-dimensional nanostructures (i.e. Nanowires)

rather than on the preparation of reinforcers. There is a lacking for application of these inventions to prepare aligned electrospun yarns and/or determine the mechanical properties of such yarns.

3.2 History

When a grounded, high- speed, rotating drum (target) is used, electrospun fibers are collected in textile form with the fibers generally oriented parallel to the direction of rotation[1]. Robust, one-centimeter wide strips of aligned electrospun nanofibers (NFs) have been prepared through the use of a collector consisting of cooper wires spaced evenly in the form of a circular drum[2]. Recent efforts to devise alternative approaches to further align electrospun NFs have focused on the use of electrostatic field assisted assembly techniques to prepare 1-dimensional nanostructures. The main objectives of these investigations focus on reproducibility in locating the NFs in specific positions and orientations. Theron et al. combined electrostatic field assisted assembly techniques with the electrospinning process to position and align individual NFs onto a grounded, rotating, tapered bobbin. Continuous lengths of polyethylene oxide NFs are wound onto the tapered edge of the bobbin providing a new approach to assemble NFs in parallel arrays while controlling the average separation distance between the fibers[3a]. Later this work was extended by Zussman et al. to prepare parallel periodic arrays and to provide a general strategy for the assembly of polymer NFs for the fabrication of structures needed in the creation of functional nanoelectronic devices. The rotating collector disc is equipped with a table that collects the NFs and which can be rotated about the z-axis. In order to prepare layers of NF arrays, each aligned at a set angle to

the layer below, the collector disk is stopped temporarily and the table is rotated the desired number of degrees[3b]. Kameoka et al. described a method to orient polymeric NFs by electrospinning a solution (horizontally) onto a rotating, planar silicon surface and integrate NFs with micro fabricated structures to allow for the possibility for on chip materials processing and functional nanostructure formation. In this process, a micro fabricated triangular tip, integrated with micro fluidics, is used as the electrospinning source; the tip acts as a wick and helps to establish a Taylor cone. Trenches are etched radially into the surface silicon wafer and electrospun nanofibers are deposited so to traverse the trenches at specific locations[4]. Recently, Sundaray et al. have aligned fibers (parallel and in cross patterns) on an insulated cylinder rotating at high speed (approximately 1200-1500rpm) through the use of a directing, thin, stainless steel pin with a sharp tip as a counter electrode. The electrospinning apparatus is vertically positioned with the steel pin counter electrode lying directly below the syringe tip (the syringe is holding the polymer reservoir). The rotating, insulated target is positioned horizontally near the counter electrode tip. The single, sharp pin counter electrode focuses the electrospinning jet/fiber by focusing the electric field configuration[5].

The mechanism demonstrated by Dersch et al. to prepare aligned and molecularly oriented NFs of polyamide using a metal frame collector has, also, been extended in the recent literature towards the development of 1-dimensional nanostructures. Dersch et al. proposed that the observed molecular orientation is due to the polymer jet jumping back and forth from one side of the rectangular frame to the other (due to electrostatic charging effects)[6]. Li et al. proposed a versatile method for

generating nanofibers in uniaxially aligned arrays using a dual parallel plate collector (gap separation method). Polymeric solution is electrospun onto two perpendicularly oriented conductive substrates that are separated by a gap[7a]. Later Li et al. extended this work to prepare aligned NFs with diameters less than 150nm by developing a new design for their counter electrode. They directly patterned the electrode on the surface of a highly insulating substrate; typically two gold electrodes are directly fabricated onto the surface of an insulator by thermal evaporation through a physical mask. It was found that electrospun NFs align across the gap between the two gold electrodes as long as the substrate is sufficiently insulating. Multilayered structures of aligned NFs with crossbar junctions are readily obtained by transferring (in a layer by layer fashion) uniaxially aligned nanofibers suspended across a void gap onto the same substrate by controlling the test pattern for the electrodes[7b]. Dalton et al. evolved the gap method of alignment to prepare a multifilament yarn of electrospun fibers. Their apparatus includes two grounded collection rings, or circular disks, equidistant from the spinneret; an array of fibers collects between the collection rings. The fibers are oriented between the two rings, continuous, and 3-dimensionally suspended in air. A twist can be applied to the fiber array by rotating one of the rings relative to the other after the completion of electrospinning[8]. Unfortunately, Dalton et al. did not complete any molecular orientation or mechanical characterization of the yarns.

Additionally, researchers have investigated the use of electrostatic fields, other than the one responsible for jet initiation, to dampen the bending instability inherent in the electrospinning process and control the fiber deposition particularly for application in the preparation of yarns. Deitzel et al. constructed a novel vertically oriented

electrospinning apparatus including three biased rings in between the two charged electrodes; positive polarity is applied to the syringe tip and rings while a negative polarity is applied to the target. Control of the shape and strength of the macroscopic electric field between the electrodes allows for the focusing of the fiber for deposition[9]. Reference in the literature to the application of this approach to yarns was not found as of the publication of this manuscript.

3.3 Proposal

Polyacrylonitrile nanofibers (NFs) prepared by electrospinning, as described previously (Chapter 2), are collected in amorphous and entangled webs, or mats, on stationary targets. These webs are extremely delicate and difficult to handle. Additionally, these materials are not oriented in any particular direction, which causes great complexities in regards to mechanical characterization and further processing required to prepare carbon NFs for reinforcement applications from these precursor fibers. Therefore, it is proposed that lengths of entangled precursor material (yarn) be prepared and a twist applied. The twisted yarn will be easily handled, can be mechanically characterized, and further processed to prepare yarns of carbon NF yarns.

In the present work, the change in velocity and fiber diameter measurements of electrospun Polyacrylonitrile (Chapter 2) are manipulated to scale-up fiber collection with the use of a high-speed, rotating target. Tows of unidirectional and molecularly oriented Polyacrylonitrile nanofibers are prepared. The effect of voltage and take-up speed on the alignment and molecular orientation of the generated fiber is examined.

The aligned tows are twisted into yarns and the mechanical properties of the yarns are determined as a function of twist angle.

3.4 Experimental

3.4.1 Materials

Polyacrylonitrile copolymer (PAN) is received from an industrial source and dimethylformamide (DMF) is obtained from Sigma Aldrich Co. The intrinsic viscosity in DMF at 25°C, M_v, M_n, and PDI are determined to be 1.6dl/g, 114,000g/mol, 200,000g/mol (determined M_n is approximately twice the true M_n) and 1.18, respectively, as described previously. The polymer and solvent are dried prior to use and solutions of 15wt% PAN in DMF with a viscosity of 2590cP at zero shear are prepared as described previously (Section 2.5.1).

3.4.2 Electrospinning Set-up

The electrospinning apparatus consists of a KD Scientific dual syringe infusion pump (Model 101), Gamma High Voltage Research high voltage power supply (Model RR20-3P/PRGI0V), and a grounded rotating target (Scheme 3.1). The grounded wheel is rotated from 0rpm to 2280rpm (12.3m/s) at a distance of approximately 13cm from the charged capillary tip. The enclosed apparatus is operated at 16kV as described previously (Section 2.5.2).

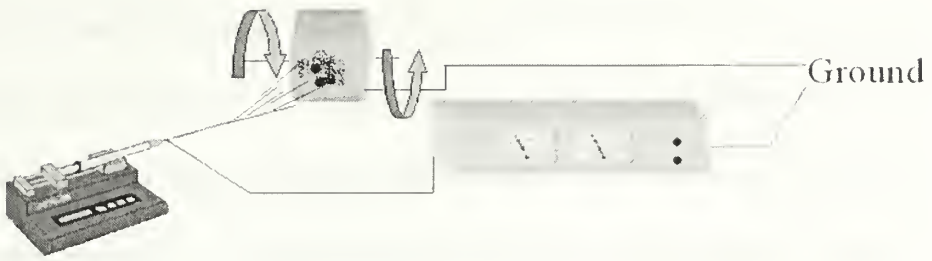

Scheme 3.1: Typical solution electrospinning apparatus with a rotating, grounded target

3.4.3 Microscopy

Electrospun fibers are observed by field emission scanning electron microscopy (FESEM), as described previously (Section 2.5.5), and polarized optical microscopy. Electrospun fibers are examined using an Olympus BX51, polarizing optical microscope, to detect birefringence. With the addition of a 1st order red plate, the sign of elongation is determined by comparing the direction of the fast and slow vibration component of the fiber[10]. All fibers are dried prior to observation, as described previously (Section 2.5.5).

3.4.4 IR Dichroism

Dried, electrospun fiber bundles are examined using a Perkin Elmer Spectrum 2000 infrared spectrometer (FTIR) with a polarized wire-grid to measure the dichroism of the nitrile-stretching (-C≡N) group vibration, 2240cm^{-1},[11] as a function of the target's surface velocity (fiber collection take-up speed). Spectra are acquired with the draw direction of the electrospun fibers positioned both parallel and perpendicular to the electric vector direction of the polarizer. Care is taken to examine the same region of fibers in both instances. Spectra are recorded over the range of 700-4000cm^{-1} with

typically 64 scans. The dichroic ratio, D, and the chain orientation factor (Herman's orienation function), f, are calculated (Equation 3.1, 3.2, and 3.3) using a transition moment angle of 73° [11b, 11f]. The transition moment angle is the angle between the direction of the nitrile group's dipole moment change and the chain axis.

$$D = A_{\Pi} / A_{\perp} \tag{3.1}$$

$$D_o = 2\cot^2 \alpha \tag{3.2}$$

$$f = \frac{\left(3\left\langle \cos^2 \Phi \right\rangle - 1\right)}{2} = \frac{(D-1)(D_o+2)}{(D_o-1)(D+2)} \tag{3.3}$$

Where $A_{//}$ is the absorbance of the nitrile-stretching vibration as the electric vector direction of the polarizer is oriented parallel to the fiber draw direction and $A_{\perp}$ is the absorbance as the electric vector is oriented perpendicular to the fiber draw direction, D_o is the dichroic ratio of an ideally oriented polymer, α is the transition moment angle, and Φ is the angle of the molecular segment relative to the fiber axis.

3.4.5 X-ray Diffraction

Dried, electrospun fibers are examined by wide angle X-Ray diffraction (WAXD) as a function of the target surface velocity (fiber collection take-up speed). A pin-hole collimated, monochromated CuKα radiation is used and a diffraction pattern of electrospun fiber bundles is collected with a GADDS detection system (Brucker) in air. Calcite is used as a reference to aid analysis (diffraction patterns contained an error of 0.2°). Diffraction patterns are collected after 10hours of exposure per sample and a

background is subtracted. The Herman's orientation function, f, is determined using the primary equatorial arcs from the (10 $\bar{1}$0) reflection at d~5.3Å (Equation 3.4).

$$f = \frac{\left[3\left\langle \cos^2 \beta \right\rangle - 1\right]}{2} = \frac{\int I|\sin\beta|\left[3\cos^2\beta - 1\right]/2\partial\beta}{\int I|\sin\beta|\partial\beta} \qquad (3.4)$$

Where β is the azimuthal angle between the axis of the molecular segment and of the fiber and I is the scattering intensity of the (10 $\bar{1}$0) reflection at that angle.

3.4.6 Twisted Yarns

Approximately 32cm x 2cm unidirectional tows of electrospun nanofibers are linked together and twisted using a Roberta electric spinner by Ertoel. The twisted yarns are rinsed in deionized water for 24 hours and dried under vacuum at 100°C. The twist per centimeter (tpcm), denier (g/9000m), and the angle of twist of the yarn are determined.

3.4.7 Mechanical Testing

The mechanical behavior of dried, twisted yarns of electrospun Polyacrylonitrile (PAN) nanofibers is examined using an Instron 5564 with a crosshead speed of 2mm/min (10%/min strain rate) in tension at room temperature. Samples are mounted with a 20mm gauge length onto paper tabs. The paper tab serves to define the gage length of the yarn, to assure proper alignment of the fiber, and to greatly simplify the handling of the yarns. A grid is designed and layed out onto a manila file folder (30cm x 56cm, opened). Vertical dashed lines are drawn every 15mm across the width of the

folder, so to define the width of the tab and to indicate where cuts will be made to separate the tab strips. Solid lines are drawn vertically down the center of each tab (7.5mm from each solid line); the solid lines are used to align the yarn through the center of the tab. Horizontal lines are laid out to define the gauge length of the tab and provide 10mm spacings at each end of the gauge length. The vertical tab strips are cut along the dashed lines and slots are removed from the gauge region using a hole punch and knife. A small piece of double-sided adhesive tape is placed at the center of each adjoining grip area and a single yarn is laid over the solid centerline of the tab strip. The yarn is affixed to the tab with a small droplet of crazy-glue; a rectangular tab (approximately 5mm x 10mm) is glued over the fiber at each edge of the gauge slot. The glue is allowed to cure overnight prior to testing[12]. The cross-sectional area is calculated based on the denier and the density of PAN (1.17g/ml) from the literature[13]. The initial modulus, ultimate strength, and elongation at ultimate strength are measured.

3.5 Results and Discussion

Discrete lengths of partially aligned and oriented Polyacrylonitrile (PAN) nanofibers with diameters in the range of 0.27μm to 0.29μm are prepared by electrospinning a ~15wt% PAN in DMF solution at 16kV onto a grounded, rotating collection wheel with a surface velocity of 3.5m/s to 12.3m/s (Figure 3.1). The collected fibers are observed to align relative to the direction of the rotating wheel, or draw direction, by optical microscopy (Figure 3.2) and to be birefringent under cross-polars. The alignment of the collected fibers is induced by the rotation of the target and improves as the surface velocity of the target is increased. The trajectory of the continuous electrospinning jet

is affected by the rotation of the target. The rotating target acts as an anchor for the continuous, electrospinning jet and affects its trajectory. As the fiber collects onto the target surface, it is electrostatically attached to the grounded surface and is used to stretch the fiber from its naturally spiraling path to align with the rotation direction of the target. Thus, the shape of the conical envelope of the electrospinning jet is altered through the use of a rotating target. As the surface velocity of the target increases the path of the electrospinning jet is further altered, the effective draw is increased, and the alignment of the collected fiber improves; the

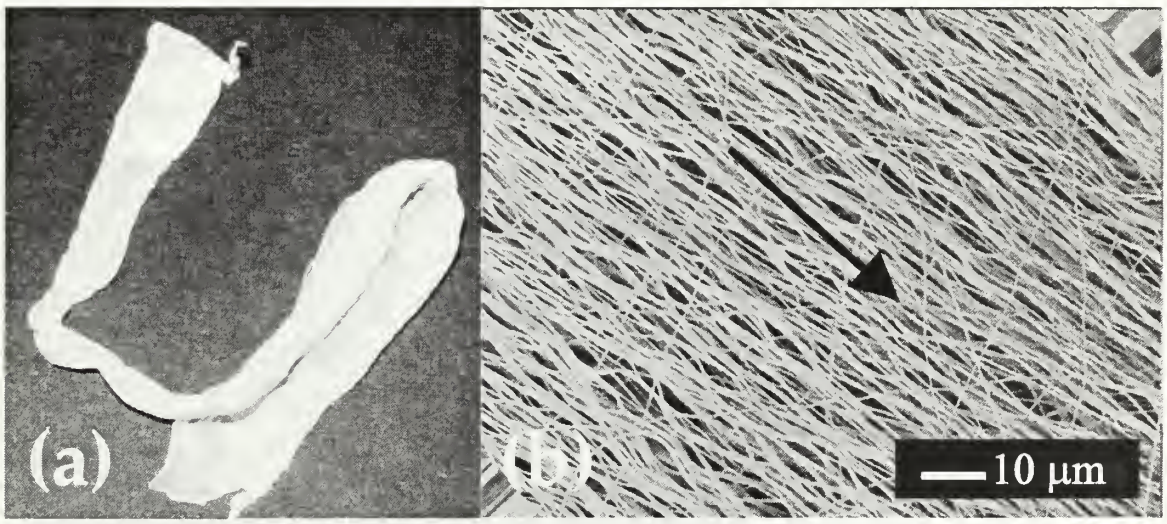

Figure 3.1: (a) Photograph and (b) a field emission scanning electron microscopy (FESEM) image of Polyacrylonitrile (PAN) fibers from a 15wt% solution with dimethylformamide electrospun at 16kV and collected onto a grounded take up wheel rotating with a surface velocity of 9.8m/s

deviation between the fiber and rotation direction due to the influence of the looping jet trajectory lessens (Figure 3.2).

Molecular orientation is induced with rotation of the target and the fibers are birefringent, exhibiting positive elongation. When observed under cross-polars with a 1st order gypsum red plate, the slow component, higher index of refraction, is observed

to vibrate approximately parallel to the draw direction of the fiber (Figure 3.3). The overall average diameter of fibers prepared from a ~15wt% solution electrospun at 16kV range onto a rotating target are smaller then those prepared under similar conditions onto a stationary target (Table 3.1). Polyacrylonitrile fibers collected onto the rotating target are constrained; the fiber diameter of fiber collected onto a rotating target is smaller than that collected onto a station a stationary target since the opportunity of the fiber to relax is minimized.

The molecular orientation of the nanofibers is examined by infared dichroism (FTIR) and wide angle x-ray diffraction (WAXD). The dichroism of the nitrile-stretching vibration is measured for ~15wt% solutions electrospun at 16kV over a

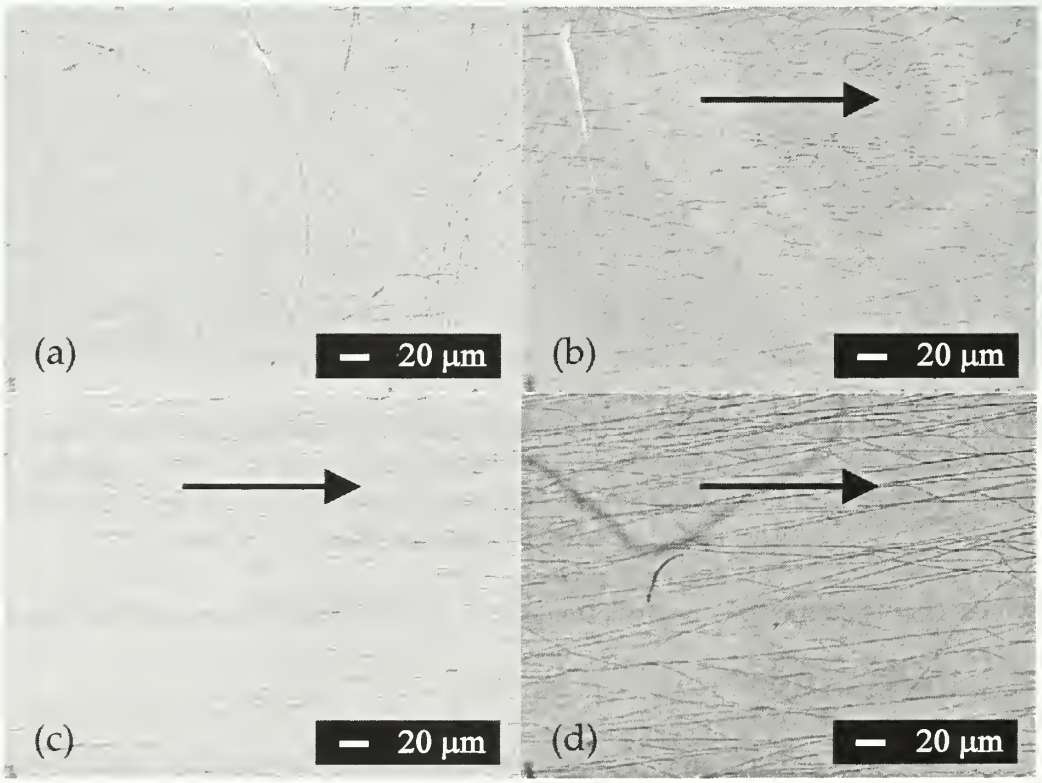

Figure 3.2: Optical micrograph of Polyacrylonitrile (PAN) fibers collected onto a take-up wheel rotating with a surface velocity of (a) 0m/s, (b) 3.5m/s, (c) 6.1m/s, and (d) 12.3m/s

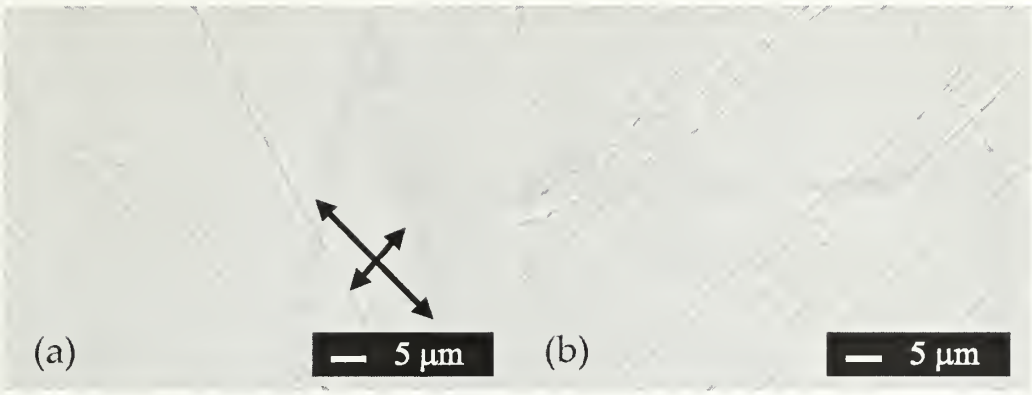

Figure 3.3: Polyacrylonitrile fibers collected onto a take-up wheel rotating with a surface velocity of 9.8m/s observed under cross-polars with a 1st-order Red plate: (a) subtraction position, (b) addition position

distance of ~15cm onto a collection wheel rotating between 0m/s and 12.3m/s by FTIR. The nitrile group is oriented approximately perpendicular to the draw direction of the fiber; the absorbance

Table 3.1: Electrospun Polyacrylonitrile fiber diameter as a function of target surface velocity as measured by field emission scanning electron microscopy (FESEM) after sputter coating with gold

0m/s	*3.7m/s*	*6.1m/s*	*12.3m/s*
0.280 ± 0.05μm	0.270 ± 0.03μm	0.270 ± 0.04μm	0.290 ± 0.05μm

for the nitrile-stretching vibration with the electric vector polarized perpendicular (to the fiber axis) is expected to be greater than that for parallel polarization, as molecular orientation within the fiber improves. The nitrile-stretching vibration of electrospun polyacrylonitrile fiber bundles shows a strong perpendicular dichroism (Figure 3.4) [11c] and the dichroic ratio decreases from approximately unity at 0m/s take-up speed to 0.75 at 9.8m/s (Figure 3.5). The electrospun fibers are unoriented, or isotropic, when collected onto a stationary target and gradually orient as the surface velocity of the take-up wheel is increased to 9.84m/s (Figure 3.8 and Table 3.2). At a take-up speed above 9.8m/s, the dichroic ratio was found to increase to 0.91 and 0.88 at 11.0m/s and 12.3m/s

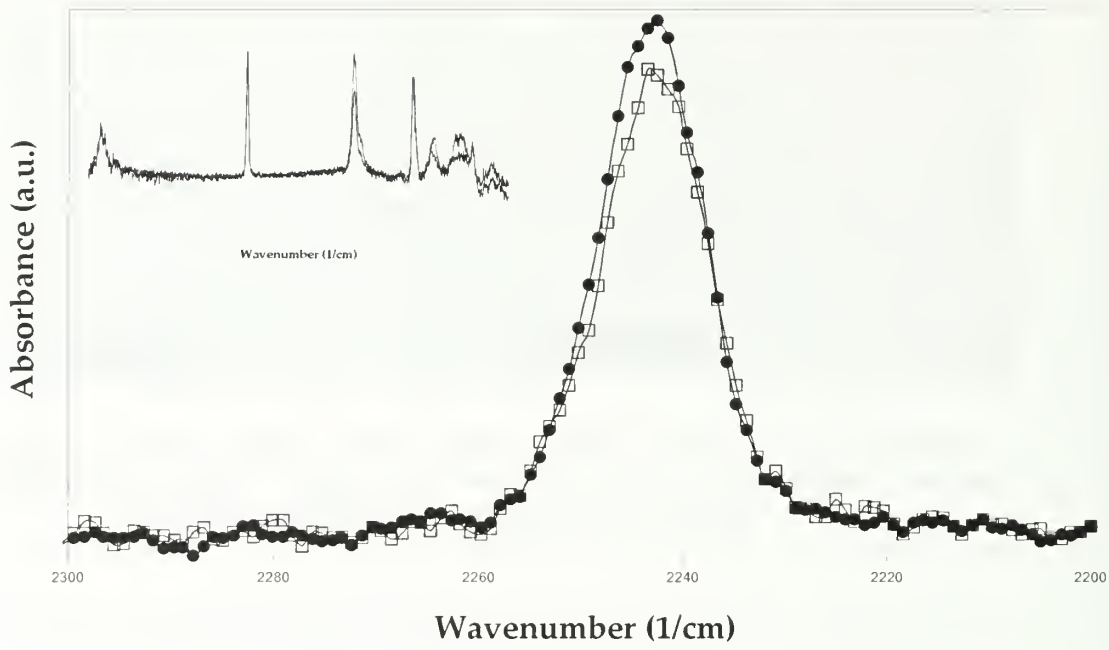

Figure 3.4: Upper Left: Polarized infrared (FTIR) spectrum of Polyacrylonitrile (PAN) electrospun at 16kV onto a target rotating with a surface velocity of 9.8m/s. Center: Nitrile stretching vibration with the electric field vector (□) parallel and (●) perpendicular to the draw direction, respectively

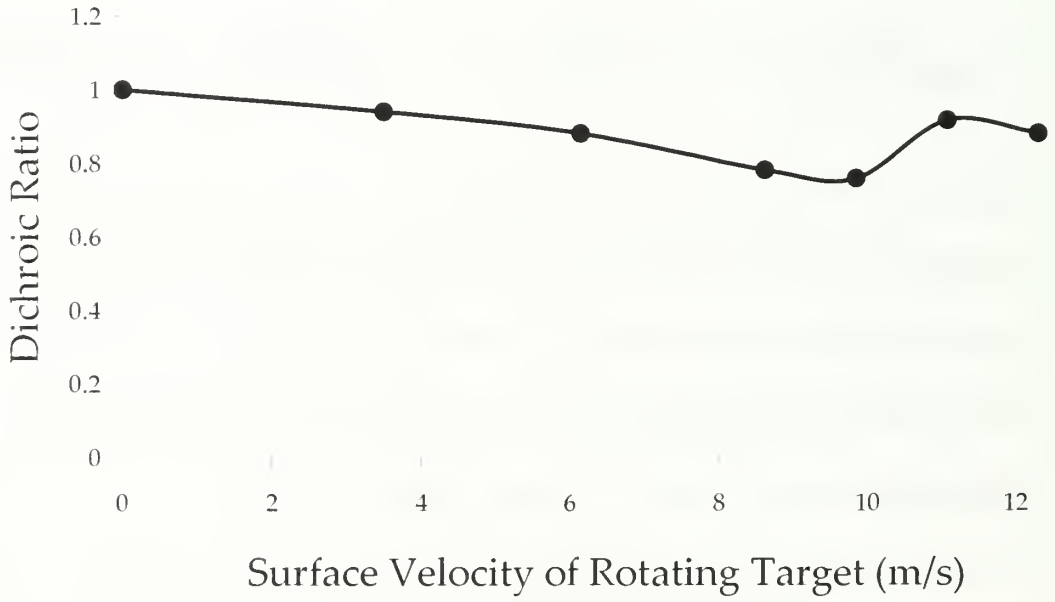

Figure 3.5: Dichroic ratio of the nitrile stretching vibration as a function of target surface velocity

take-up speeds, respectively. The chain orientation factor followed a similar trend to the dichroic ratio, with a maximum orientation of 0.23 for the nitrile-stetching vibration at fibers electrospun from approximately 15wt% solutions at 10kV and 13kV under the same conditions.

Wide angle X-ray diffraction (WAXD) patterns are collected from bundles of fibers electrospun at 16kV from a 15wt% PAN in DMF solutions at 16kV collected onto a target rotating with a surface velocity between 0m/s and 12.3m/s. The diffraction pattern show two equatorial peaks; a weak peak at $2\theta = 29.5°$ corresponding to a spacing of $d \approx 3.03Å$ from the (1120) reflection and a strong peak at $2\theta = 16°$ corresponding to a spacing of $d \approx 5.3Å$ from the $(10\ \bar{1}0)$ reflection. Equatorial peaks at $2\theta = 29.5°$ and $2\theta = 16°$ are common to the fiber diffraction pattern of PAN with hexagonal packing[14]. The diffraction pattern as well as a plot of intensity versus azimuthal angle of the $d \approx 5.3Å$ peak shows arcs indicating that the fibers are oriented (Figure 3.6 and 3.7). The arc width of the strongest equatorial reflection provides an

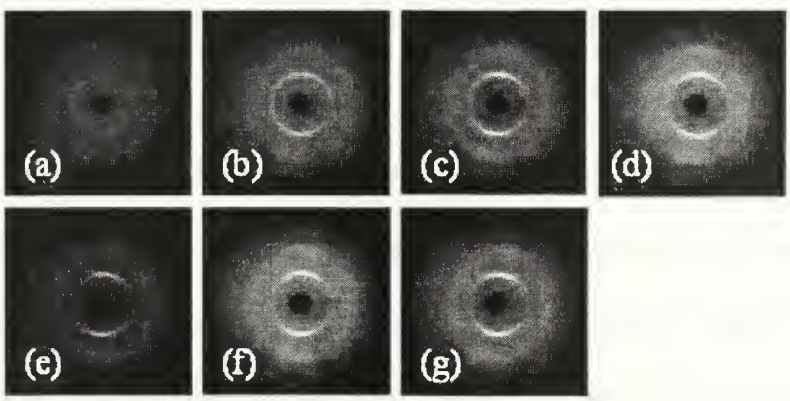

Figure 3.6: Wide angle X-ray diffraction (WAXD) of bundles of Polyacrylonitrile (PAN) fibers electrospun at 16kV onto a rotating target with a surface velocity of (a) 0m/s, (b) 3.5m/s, (c) 6.1m/s, (d) 8.6m/s, (e) 9.8m/s, (f) 11.1m/s, and (g) 12.3m/s

indication of the degree of molecular orientation within the fibers. The Herman's orientation function increases gradually with take-up speed from 0 at 0m/s to 0.23 ±0.01 at 8.61m/s and plateau to 0.21 ±0.07 at between 9.81m/s and 12.3m/s. The trend in the orientation measurement from the dichroism and the WAXD are in agreement (Figure 3.8 and Table 3.2). Overall the orientation measurements determined by dichroism are

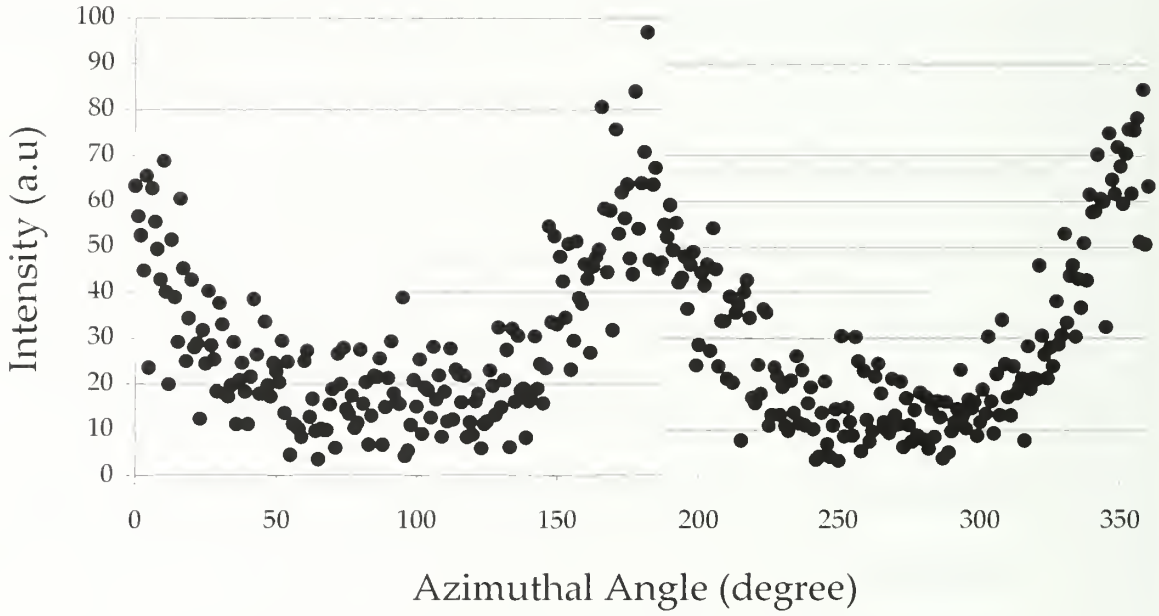

Figure 3.7: Plot of intensity versus azimuthal angle of the strong equatorial peak at $2\theta = 16°$ from the $(10\ \bar{1}0)$ reflection, corresponding to a spacing of $d \approx 5.3$Å

lower than those determined by WAXD; dichroism measures the orientation in the amorphous and the crystalline region while WAXD only measures the crystalline region. The molecular orientation is observed when fibers are electrospun onto a high-speed, rotating target; it appears to increase with increasing target surface velocity to a speed of approximately 8.61m/s. As the surface velocity of the target is increased further the molecular orientation of the fibers appears to decrease and plateau (within the error), although, the fibers do not appear to be experiencing core-shell effects with target surface velocities greater than 9.8m/s.

As the fiber has a lessened ability to relax (with use of the rotating target), orientation induced through the electrospinning process is maintained within the fiber. As the surface velocity increases, the measured molecular orientation within the fiber

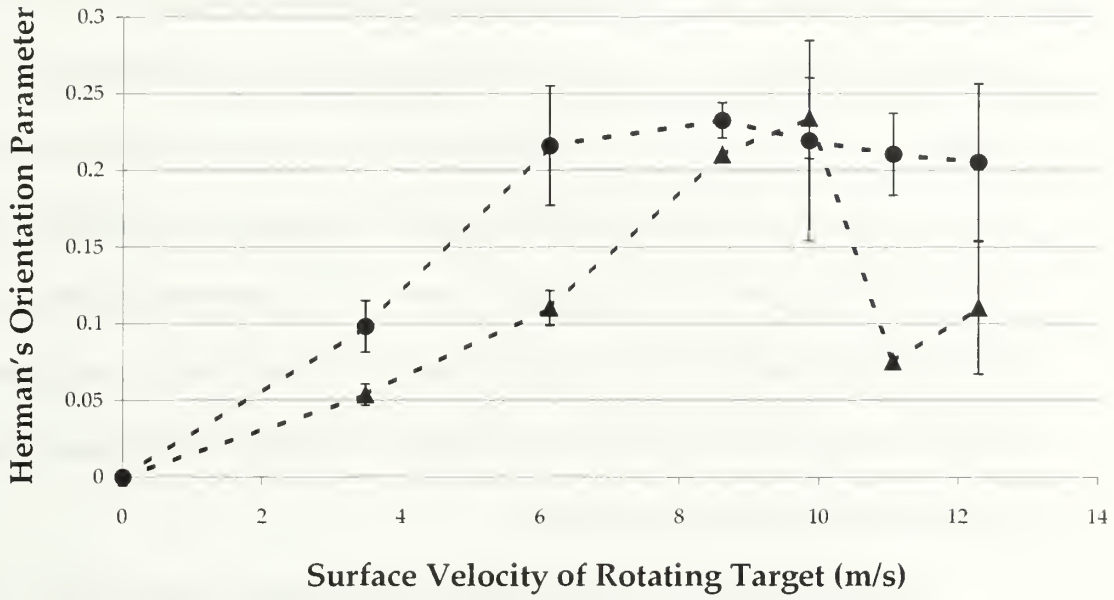

Figure 3.8: Herman's Orientation Parameter versus surface velocity of the rotating target determined by (— •—) wide angle X-ray diffraction (WAXD) of the 5.3Å equatorial peak and (▪ ▲ ▪) dichroism using a transition angle of 73°

Table 3.2: Orientation Parameter as a function of rotating target surface velocity as measured by wide anlge X-ray diffraction (WAXD) and dichroism

	Dichroism (*f*)	**WAXD (*f*)**
0*m/s*	-0.0005 ± 0.01	0
3.5*m/s*	0.05 ± 0.01	0.1 ± 0.02
6.1*m/s*	0.11 ± 0.01	0.22 ± 0.04
8.6*m/s*	0.21	0.23 ± 0.01
9.9*m/s*	0.23 ± 0.03	0.22 ± 0.07
11.1*m/s*	0.08	0.21 ± 0.03
12.3*m/s*	0.11 ± 0.04	0.21 ± 0.05

appears to increase to a maximum of approximately 23% and then plateau with further increase in rotation speed. Two effects contribute to the measured orientation: the improvement of molecular orientation within the individual fiber and the improved

alignment of the fibers within the electrospun bundles with increasing rotation speed. Since Polyacrylonitrile fibers collected onto stationary targets contain no appreciable molecular orientation, as observable by polarized optical microscopy and wide angle X-ray diffraction, it is believed that the rotating target acts as a source of constraint on the relaxation of the fibers. The rotating target acts to alter the electrospinning jet trajectory, but does not draw the spinning jet, or fiber, as shown by the lack of fiber diameter fluctuation with variable rotation speed. The measured orientation is due to the electrospinning process; it is actually a measure of the improved alignment of the fibers within the bundle. Above a surface velocity of 9.8m/s, the fiber alignment becomes constant and does not improve further. The maximum orientation measured for the electrospun fiber is low overall.

Unidirectional tows of PAN nanofibers prepared from ~15wt% PAN in DMF solution electrospun at 16kV onto a target rotating with a surface velocity of 9.8m/s are linked (using English knots) and twisted into yarns. The induction of a twist into the yarn allows for the evaluation of the mechanical properties of the yarn without concern for defects within the individual fibers. Yarns of twisted electrospun PAN nanofibers are prepared with an angle of twist ranging from 1.1° to 16.8° and a denier between 326 and 618 with the average yarn denier being 446. The stress-strain behavior of the yarns is examined and the modulus, ultimate strength, and elongation at ultimate strength are measured as a function of twist angle (Figure 3.9 and Table 3.3).

The initial modulus and ultimate strength increase gradually with twist angle from 3.8 $\pm$ 1.1GPa and 91.1 $\pm$ 5.5MPa with a twist angle of 1.1° to 5.8 $\pm$ 0.4GPa and 163 $\pm$ 12MPa with a twist angle between 9.3° and 11.0°, respectively. The modulus

and ultimate strength of the yarns decreases with angles of twist greater than 11.0°. The elongation at ultimate strength followed a similar trend; it initially increased

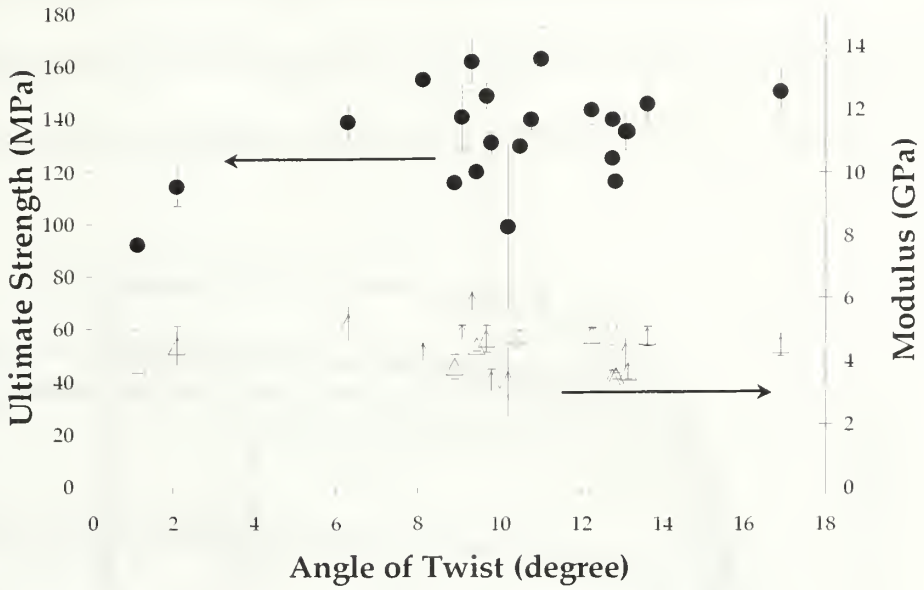

Figure 3.9: The ultimate strength (●, MPa) and modulus (△, GPa) versus angle of twist (°) for Polyacrylonitrile (PAN) fibers electrospun at 16kV onto a target rotating with a surface velocity of 9.8m/s

Table 3.3: The ultimate strength, modulus, and strain as a function of angle of twist for electrospun Polyacrylonitrile (PAN) yarn with an average denier of 446

Angle of Twist (°)	Ultimate Strength (MPa)	Modulus (Gpa)	Ultimate Strength (g/denier)	Modulus (g/denier)	Strain (%)
1.1	91.9 ± 5.5	3.8 ± 1.1	0.88 ± 0.05	32 ± 2.1	34 ± 6
6.3	139± 6.8	5.2 ± 0.6	1.32 ± 0.07	47 ± 7.5	35 ± 0.3
9.3	162 ± 8.4	5.9 ± 0.3	1.55 ± 0.08	55 ± 4.7	43 ± 8
11.0	163 ± 12	5.8 ± 0.4	1.57 ± 0.1	54 ± 1	27 ± 7
13.1	135 ± 7.1	4.3 ± 05	1.30 ± 0.07	40 ± 3.5	38 ± 8

with angle of twist and then decreased. The broken yarns are observed by field emission scanning electron microscopy (FESEM); the surface of the broken filaments

appear to have been damaged or roughened due to the frictional and normal forces in action as the twisted yarns are exposed to tension.

The stress-strain behavior of the yarns (Figure 3.10) appears to be similar to that of commercially produced PAN fibers. Commercial PAN fiber has an ultimate strength of approximately 512MPa (after post-treatment), according to the literature[15].

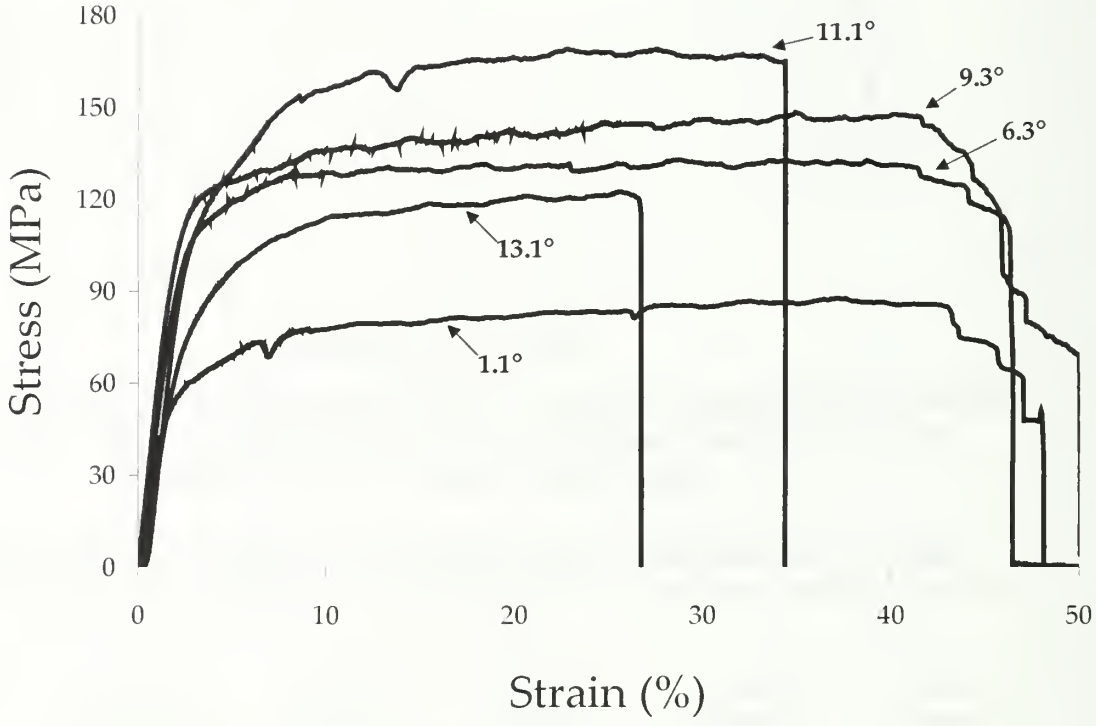

Figure 3.10: The stress-strain behavior of Polyacrylonitrile (PAN) fibers electrospun at 16kV onto a target rotating with a surface velocity of 9.8m/s as a function of twist angle (°)

Commercial PAN precursor fibers are drawn prior to stabilization which decreases the fiber diameter and reduces the probability of encountering a critical flaw in a given test length. The ultimate strength of commercial PAN precursor fibers is approximately three times larger than the yarns of electrospun nanofibers; the twisted yarns were not drawn. PAN precursor fiber with a diameter of 155μm, as measured by laser

diffraction, and an average denier of 80 was prepared by dry-jet solution spinning in our laboratory from a 28wt% solution of PAN and DMF into a coagulation bath of 40:60 wt. H_20:DMF The mechanical properties of the laboratory precursor fiber are measured under the same conditions as described previously for the twisted electrospun yarn (Section 3.4.7). The fiber is not drawn prior to measurement in order to prepare a suitable comparison with the twisted electrospun yarns. The initial modulus and ultimate strength of the dry-jet solution spun fiber iss 2.6 $\pm$0.1GPa and 56 $\pm$13MPa, respectively. The initial modulus and ultimate strength of the twisted electrospun PAN yarn with a twist angle of 1.1° and 11° are both approximately 1.5 times, and 2.2 and 2.9 times greater than that of the dry-jet solution spun PAN fiber prior to post-drawing, respectively. Neither the dry-jet solution spun fiber nor the yarn of electronspun fibers are post drawn[16].

3.6 Conclusions

It is generally thought that the better the degree of molecular orientation in the original Polyacrylonitrile fiber, the better the mechanical properties, in particular the modulus, of the resultant carbon fiber[17]. The presence of molecular orientation within the fibers suggests that carbon nanofibers prepared from these electrospun Polyacrylonitrile nanofibers should outperform those prepared previously by other researchers (which collected their precursor fibers onto a stationary target and failed to report any orientation). The ability to orient the precursor fibers during the fabrication of the fabrics allows for the production of carbon nanofibers with mechanical properties comparable to those of carbon fibers prepared by conventional methods.

The ease in fabrication of unidirectional fabric of sub-micron fibers without the use of complicated equipment and sizing is presented. Improved fiber alignment provides the opportunity to mechanically characterize and further process (ie. to oxidize under tension) the carbon precursor nanofibers with greater ease. The mechanical properties of electrospun yarns are improved with the addition of twist.

3.7 References

(1) (a) Doshi, J.; Reneker, D.H. *J. Electrostatics* **1995**, *35*, 151. (b) Lee, S.H.; Yoon, J.W.; Suh, M.H. *Macromol. Res.* **2002**, *10*, 282. (c) Ding, B.; Kim, H.; Lee, S.; Lee, D.; Choi, K. *Fibers and Polymers* **2002**, *3*, 73. (d) Kang, Y.; Kim, H.; Ryu, Y.; Lee, D.; Park, S. *Polymer (Korea)***2002,** *26*, 360. (e) Matthews, J.; Wnek, G.; Simpson, D.; Bowlin, G. *Biomacromolecules* **2002**, *3*, 232.

(2) Katta, P.; Alessandro, M.; Ramsier, R.D.; Chase, G.G. *Nano. Lett.* **2004**, *11*, 2215.

(3) (a) Theron, A.; Zussman, E.; Yarin, A.L. *Nanotechnology* **2001**, *12*, 384. (b) Zussman, E.; Theron, A.; Yarin, A.L. *Appl. Phys. Lett.* **2003**, *82*, 973.

(4) (a) Kameoka, J.; Orth, R.; Yang, Y.; Czaplewski, D.; Mathers, R.; Coates, G.W.; Craighead, H.G. *Nanotechnology* **2003**, *14*, 1124. (b) Kameoka, J.; Craighead, H.G. *Appl. Phys. Lett.* **2003**, *83*, 371.

(5) Sundaray, B.; Subramanian, V.; Natarajan, T. S.; Xiang, R.Z.; Chang, C.C.; Fann, W.S. *Appl. Phys. Lett.* **2004**, *84*, 1222.

(6) Dersch, R.; Liu, T.; Schaper, A.K.; Greiner, A.; Wendorff, J.H. *J. Polym. Sci.* **2003**, *41*, 545.

(7) (a) Li, D.; Wang, Y.; Xia, Y. *Nano. Lett.* **2003**, *3*, 1167. (b) Li, D.; Wang, Y.; Xia, Y. *Adv. Mater.* **2004**, *16*, 361.

(8) Dalton, P.D.; Klee, D.; Moller, M. *Polymer* **2005**, *45*, 611.

(9) Deitzel, J.M.; Kleinmeyer, J.D.; Hirvonene, J.K.; Beck Tan, N.C. *Polymer* **2001**, *42*, 8163.

(10) Chamot, E.; Mayson, C. Handbook of Chemical Microscopy Volume 1. New York, John Wiley & Sons 1938, Ch.10.

(11) (a) Bashir, Z.; Church, S.; Waldron, D. Polymer 1994, 35, 967. (b) Bashir, Z.; Tipping A.; Church, S. Polymer International1994, 33, 9. (c) Bashir, Z.; Atureliya, S.; Church, S. J. Mater. Sci. 1993, 28, 2731. (d) Dalton, S.; Heatley, F.; Budd, P. Polymer 1999, 40, 5531. (e) Zbinden, R. Infared Spectroscopy of High Polymers. New York, Academic Press 1964, Ch V. (f) Jasse B.; Koenig, J. J. Macromol. Sci.- Rev. Macromol. Chem. 1979, C17, 61.

(12) Allen, S.R. 'Mechanical and Morphological Correlations in Poly(p-phenylene benzobisthiazole Fibers.' Thesis, Unviersity of Massachusetts Amherst (**1983**), Appendix 1.1.

(13) Brandrup, J. and E.H. Immergut. Polymer Handbook. 3rd Ed. New York, John Wiley & Sons Inc. 1989, V/57.

(14) (a) Bashir, Z. Acta Polymer 1996, 47, 125. (b) Davidson, J.; Jung, H.; Hudson, S.; Percec, S. Polymer 2000, 41, 3357.

(15) Moncrieff, R.W. Man-Made Fibres, 6th Ed. New York, John Wiley & Sons **1975**.

(16) Fennessey, S.F.; Farris R.J. *Polymer* **2004**, *45*, 4217.

(17) (a) Bahl, O.; Mathur, R.; Kundra, K. *Fibre Sci. Tech.* **1981**, *15*, 147. (b) Chari, S.; Bahl, O.; Mathur, R. *Fibre Sci. Tech.* **1981**, *15*, 153 Bashir, Z.; Church, S.; Waldron, D. *Polymer* **1994**, *35*, 967.

CHAPTER 4

POST-TREATMENT & MECHANICAL PARAMETERS

4.1 Introduction

One of the most important features of carbon fibers is the high value of the Young's modulus, which in combination with their low density makes this material very attractive for composites[1]. The mechanical properties of carbon fiber prepared from Polyacrylonitrile (PAN) precursor fiber depend upon the orientation imparted by the precursor fiber. Generally, the better the orientation of the precursor fiber, the more preferred the orientation and the better the mechanical properties, in particular the modulus, of the resultant carbon fiber[2].

Most fiber processes include a drawing operation, which reduces the denier (g/9000m) of the filaments and increases the molecular orientation, to yield desirable fiber tensile properties. To produce high modulus carbon fiber from any given precursor, it is essential to have a highly preferred orientation of the ribbons in the direction parallel to the fiber axis. The value of the Young's modulus depends upon the two following factors: the degree of orientation and degree of perfection of the crystallites. Therefore it is believed the better the orientation of the crystallites, the higher is the value of the ultimate Young's modulus.

Molecular orientation, within the PAN precursor, may be brought about by stretching the fiber at various stages of development, including: during the spinning of the precursor[3a], the low-temperature stabilization, and/or carbonization[3c]. The modulus, tensile strength, and orientation of the PAN fiber increase with stretch ratio during

spinning. Some comonomers are introduced to cause an increase in crystalline orientation of the fiber. If the fiber is not restrained during the early stages of pyrolysis (stabilization), then length shrinkage and loss of preferred orientation occurs. During carbonization, there is a marked improvement in orientation with increasing heat treatment temperature[3c].

4.2 History

There has been a tremendous growth of research activities dedicated to exploring the technology of electrospinning and its use in the fabrication of nonwoven fibrous membranes. A majority of the studies are dedicated to the generation of new nanostructured materials and their applications, but few researchers have investigated the effect of post treatment to control the mechanical properties of electrospun material. Zong et al. investigated the use of post-treatment to tailor the mechanical and biodegradation properties of entangled, electrospun, poly(glycolide-co-lactide), nonwoven membranes. They studied the control of structure, morphology, and mechanical and biodegradation properties of the membranes by post-stretching and annealing treatments. They found that the degree of crystallinity within the fibers could be increased with annealing at elevated temperatures, although, annealing did not improve the overall molecular orientation. Rather, it was found that the crystal orientation improved significantly when the membrane was mechanically drawn and then annealed. As the elongation ratio is increased, the degree of orientation and the tensile strength of the membrane increased. Additionally, the fibers were observed to

align with the direction of the applied draw and the diameter of the pores, or gaps, between the fibers decreased as the percent draw was increased[4].

4.3 Proposal

Electrospinning with a rotating collection system provides a technique to prepare oriented and aligned carbon precursor nanofiber yarns with fiber diameters in the sub-micron range (Chapter 3). Improvement of the orientation within the precursor fiber will result in an improvement in the mechanical properties of the precursor as well as the resultant carbon nanofiber. In the present work, the effect of post stretching of unidirectional electrospun PAN fiber yarns at elevated temperature on the mechanical properties is investigated. Unidirectional tows of PAN nanofibers prepared by electrospinning onto a rotating target with a surface velocity of 9.8m/s are drawn above the glass transition temperature, T_g, and the mechanical properties are evaluated.

4.4 Experimental

4.4.1 Materials

Polyacrylonitrile copolymer (PAN) is received from an industrial source and dimethylformamide (DMF) is obtained from Sigma Aldrich Co. H^1NMR (Polyacrylonitrile copolymer): CH_2 at 2.2, CH at 3.2ppm, and dDMSO at 2.5ppm. The number average molecular weight (M_n) and polydispersity is determined by gel permeation chromatography in DMF against styrene standards to be 165,000g/mol (determined M_n is approximately twice the true M_n) and 2.03, respectively. The glass transition temperature (T_g) of the pure copolymer and the electrospun fiber (containing

solvent) is determined to be between 92 - 114°C and 75 - 104°C, respectively, by differential scanning calorimetry (DSC). The polymer and solvent are dried and ~15wt% solutions of PAN in DMF are prepared at room temperature under constant mixing as described previously (Section 2.5.1).

4.4.2 Electrospinning Set-up

An electrospinning apparatus including a high speed, rotating target, as described previously (Section 3.4.2), is used to collect yarns that are approximately 2.5cm x 36cm long. Solutions (flow rate of 0.0016ml/min) are electrospun at a voltage of 16kV over a gap distance of ~13cm onto a grounded target rotating with a surface velocity of 9.8m/s. All experiments are conducted in an enclosure.

4.4.3 Batch Stretching

Yarns are mounted, as described previously (Section 3.4.7), with a 100mm gauge length, submerged in boiling water, and drawn in tension using an Instron 5654 with a constant crosshead speed of 10mm/min (strain rate of 10%/min). A steel cylinder and heating coil (maintained at 100°C) is slid down to surround the mounted yarn and grips (Scheme 4.1).

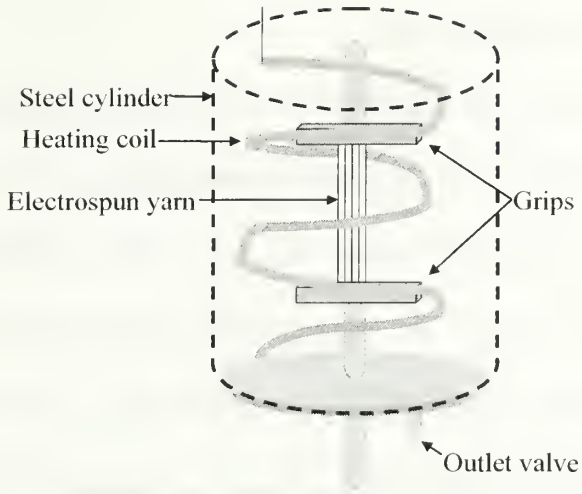

Scheme 4.1: Batch stretching apparatus

Boiling water is poured into the vessel to cover the system and the yarn is drawn. The yarn is held in tension for approximately 3min after drawing is complete, then the heated water is drained from the vessel through a valve underneath the gripping apparatus and the vessel is disassembled. The yarn is removed from the grips and immediately quenched in liquid nitrogen.

4.4.5 Mechanical Properties

Samples are re-mounted with a 20mm gauge length and the mechanical behavior of dry, drawn yarns of electrospun Polyacrylonitrile (PAN) nanofibers is examined using an Instron 5564 in tension, as described previously (Section 3.4.7). Cross-sectional area is calculated from yarn denier and density, as described previously (Section 3.4.7). The initial modulus, ultimate strength, and elongation at ultimate strength are measured.

4.4.6 Wide angle X-ray diffraction

X-ray diffraction (XD) is performed on dry, elongated, electrospun yarn with a Rigaku RU-H3R rotating anode x-ray diffractometer (Rigaku, Tokyo, Japan) equipped with a multiplayer focusing optic (Osmic Inc., type CMF23-46Cu8) and an evacuated Statton type scattering camera. The sample to detector distance is 460mm which corresponds to a q range of $0.0698\text{Å}^{-1} \le q \le 0.625\text{Å}^{-1}$ with $q = (4\pi/\lambda)\sin(\theta/2)$; θ is twice the Bragg angle and λ is the incident beam wavelength (1.54Å). Scattering patterns are acquired with 10cm x 15cm Fuji ST-VA image plates in conjunction with a Fuji BAS-2500 image plate scanner. The X-ray scattering intensity profile is obtained from radial averages of the scattering pattern intensities, using procedures developed for the Igor Pro software package (Wavmetrics, Inc. Lake Oswego, OR). Tricosane is used as a reference to aid in analysis.

4.5 Results and Discussion

Unidirectional tows of electrospun Polyacrylonitrile (PAN) nanofibers are drawn at/above their glass transition temperature, T_g, and the mechanical properties of the elongated yarns are determined. The yarns are drawn to a maximum of 100% strain (a draw ratio 2x): the unidirectional tows could not be drawn more than 100% strain (at temperatures of 85- 90°C) and provide reproducible results (Figure 4.1). The initial modulus and ultimate strength of the yarns increase with draw ratio from 3.0 $\pm$ 0.3 GPa and 114 $\pm$ 11 MPa at zero percent strain to 4.8 $\pm$ 0.5 GPa and 253 $\pm$ 47 MPa at 100% strain, respectively (Figure 4.2 and Table 4.1). The elongation at break decreases from 25 $\pm$ 6% at zero percent strain to 9.4 $\pm$ 2% at 50% strain, and then remains

approximately constant with increased draw to 100% strain. The ultimate strength of unidirectional yarns drawn to 100% strain is approximately half that of commercial

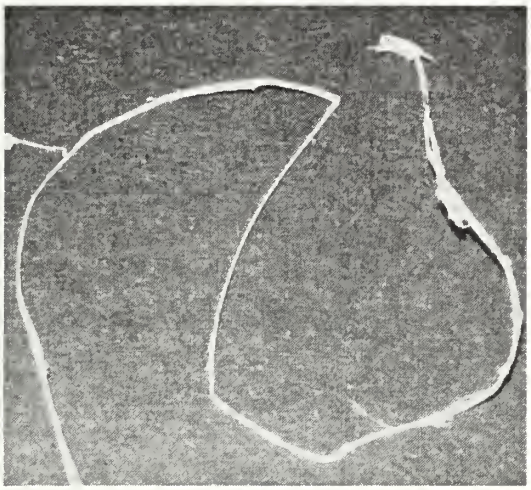

Figure 4.1: Photograph of electrospun Polyacrylonitrile (PAN) yarn stretched to a draw ration of 1:2 in boiling water

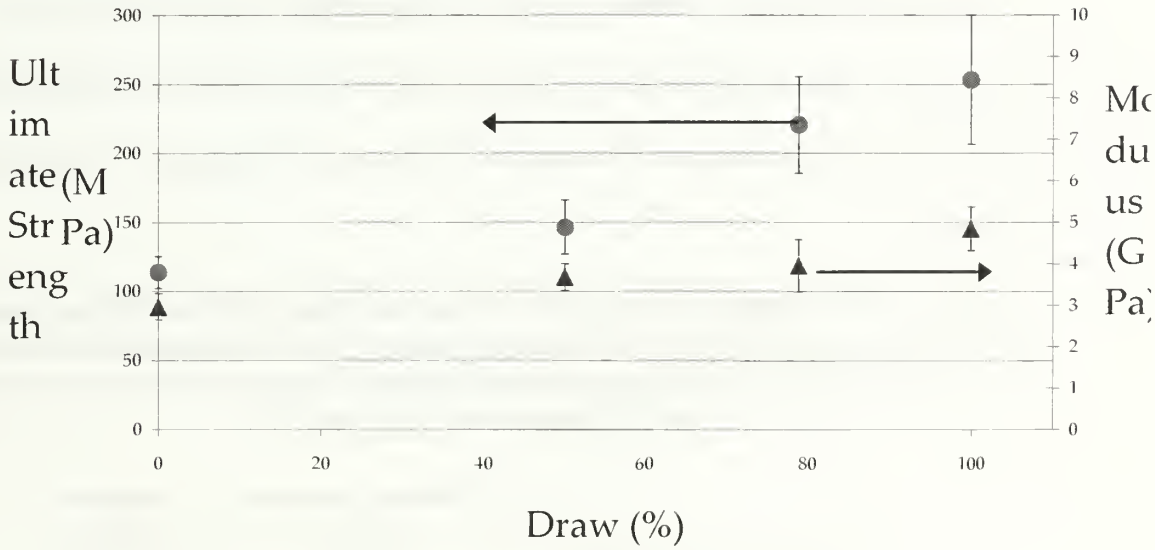

Figure 4.1: The ultimate strength (MPa) versus modulus (GPa) as a function of percent draw (%) of Polyacrylonitrile (PAN) yarn electrospun at 16kV onto a target rotating with a surface velocity of 9.8m/s and drawn in boiling water at a strain rate of 10%/min

Table 4.1: The ultimate strength and modulus as a function of strain (%) and denier for electrospun Polyacrylonitrile (PAN) yarn

Strain (%)	Ultimate Strength (MPa)	Modulus (GPa)	Denier (g/9000m)	Ultimate Strength (g/denier)	Modulus (g/denier)	Strain (%)
0	113 ± 12	3 ± 0.3	464	1.1 ± 0.1	27 ± 2	26 ± 7
50 ± 0.1	147 ± 19	3.7 ± 0.3	310	1.4 ± 0.2	37 ± 2	10 ± 2
78 ± 1.7	221 ± 35	4 ± 0.6	260	2.1 ± 0.1	39 ± 4	12 ± 1
100	253 ± 47	4.8 ± 0.5	230	2.8 ± 0.6	47 ± 9	11 ± 1

PAN precursor fiber (ultimate strength of post treated commercial precursor fiber is 512MPa[5]), which are drawn to a maximum of 600% elongation (Table 4.2).

For comparison, a PAN precursor fiber with a diameter of 113μm, as measured by laser diffraction, iss prepared by dry-jet solution spinning in our laboratory; a 27.6wt% PAN and DMF solution is spun into a coagulation bath of 40:60 wt. H_20: DMF. The mechanical properties of the fiber are measured under the same conditions as the drawn electrospun yarn, although, the fiber was not drawn prior to measurement. The initial

Table 4.2: The ultimate strength (MPa) and modulus (GPa) of Polyacrylonitrile (PAN) fiber prepared by dry-jet solution spinning into a coagulation bath of 40:60 DMF: H_2O without post treatment drawing and of post treated commercial PAN fiber (value from the literature[3])

	Ultimate Strength (MPa)	Modulus (GPa)
Laboratory Precursor	44 ± 13	2.3 ± 0.6
Commercial Precursor *(after post-treatment)*	512	

modulus and ultimate strength of the dry-jet solution spun fiber is 2.3 ±0.6GPa and 44 ±13MPa, respectively (which is less than that of the virgin electrospun yarn) (Table 4.2).

Since the degree of orientation determines the mechanical properties of precursor Polyacrylonitrile (PAN) fiber, it is inferred from the improvement of mechanical properties that the molecular orientation within the precursor fiber is, also, improved with draw ratio. The wide angle X-ray diffraction (WAXD) pattern is collected from electrospun PAN yarn drawn to a draw ratio of 1:2 (Figure 4.3). It exhibits sharp arcing of two equatorial peaks;

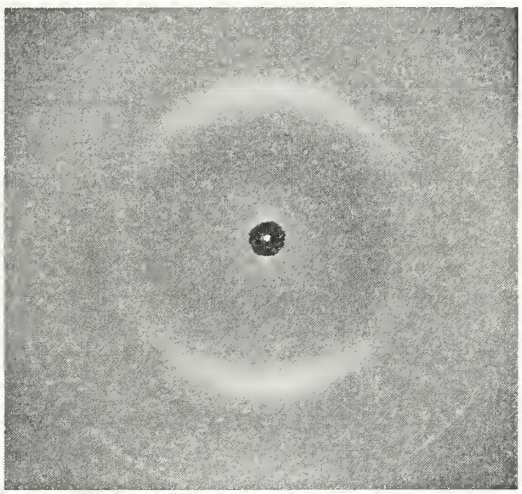

Figure 4.3: Wide angle X-ray diffraction (WAXD) pattern of electrospun Polyacrylonitrile (PAN) yarn drawn to 100% strain

a weak peak at $2\theta = 29.5°$ corresponding to a spacing of $d \approx 3.03Å$ from the (1120) reflection and a strong peak at $2\theta = 16°$ corresponding to a spacing of $d \approx 5.3Å$ from the $(10\ \bar{1}0)$ reflection. The WAXD pattern is affected by both the molecular orientation of the crystals within the electrospun fibers as well as the alignment of the individual fibers to the direction of draw. Although, the sharp arcing suggests that both the molecular orientation and the alignment within the yarn has improved with drawing[6].

4.6 Conclusions

Electrospun fibers collected onto a stationary target are isotropic, with little or no molecular orientation, and entangled. The molecular orientation and alignment of electrospun fibers is controlled and altered through the use of a rotating collection device. Post treatment of electrospun fibers increases their axial orientation and mechanical strength. Aligned, electrospun fibers with a high degree of orientation are expected to surpass conventional fibers in the reinforcement of composites due to the increased surface area available for adhesion, their high aspect ratio (l/d), and expected property improvement with smaller diameter fibers.

4.7 References

(1) Ruland, W. "The Relationship Between Preferred Orientation and Young's Modulus of Carbon Fibers." J. Preston, Ed. High Temperature resistant Fibers from Organic Polymers. John Wiley & Sons, Inc. New York (**1969**), pp. 293.

(2) (a)Bahl, O.; Mathur, R.; Kundra, K. *Fibre Sci. Tech.* **1981**, *15*, 147. (b)Chari, S.; Bahl, O.; Mathur, R. *Fibre Sci. Tech.* **1981**, ***15***, 153 Bashir, Z.; Church, S.; Waldron, D. *Polymer* **1994**, *35*, 967.

(3) (a) Tsai, J.S. *J. Mater. Sci. Lett.* **1992,** *11*, 140. (b) Tsai, J.S. *J. Mater. Sci. Lett.* **1994**, *13*, 1162. (c) Tsai, J.S.; Lin, C.H. *J. Matter. Sci. Lett.* **1990**, *9*, 921.

(4) Zong, X.; Ran, S.; Fang, D.; Hsiao, B.S.; Chu, B. *Polymer* **2003**, *44*, 4959.

(5) Moncrieff, R.W. Man-Made Fibres, 6th Ed. John Wiley & Sons, New York (1975).

(6) Fennessey, S.F.; Pedicini, A.; Farris, R.J. 'Mechanical Behavior of Nonwoven Electrospun Fabrics and Yarns.' Reneker, D.H.; Fong, H.F. American Chemical Society Symposium Series 918: Polymeric Nanofibers. American Chemical Society, Wahsington. (**2006**), Ch. 21.

CHAPTER 5

STABILIZATION & CARBONIZATION

5.1 Introduction

The high quality carbon fiber present in today's market place is based on Polyacrylonitrile copolymer (PAN) (more than 95%). Particularly in aerospace applications, the use of fibers with a strain to failure ratio of at least 1.5% is a primary requirement of design engineers. High strength (stiff) fibers, with modulus values of approximately 220-290GPa, can achieve such values of strain to failure; they experience brittle fracture behavior similar to all carbon fiber.

The Young's modulus of the carbon fiber is directly related to the extent of preferred orientation of the basal planes. Orientation may be achieved through pre-orientation of the macromolecules within the polymer fiber (with post-treatment stretching. Additionally, the orientation may be increased (improved) by heat treatment of the carbon fiber at the high temperature, although, at high temperature crystal growth occurs and crystalline defects in the carbonaceous structure heal, resulting in low fiber shear strength (thus, low compressive and flexural strength).

One way to increase the tensile strength of carbon fiber is through the reduction of the fiber diameter, resulting in an increase in the strength of the monofilament. The enhancement of fiber tensile strength achieved by the industry during the late 1980's is explained mainly by the reduction of the average monofilament diameter from 8μm to 6μm[1].

5.2 History

Carbon fibers have been investigated extensively and have found use in a wide variety of applications including: structural materials and composites. Regardless of the whether they are produced from organic precursor fibers, or deposited from the gas phase, the diameter of carbon fiber is in the several microns size scale range[2]. With the renewed interest in the electrospinning technique, researchers have attempted to prepare ultrafine carbon fiber (with diameters in range of a few microns to 100s of nanometers) from thermally treated electrospun carbon precursor fiber. Thus far, investigations have been limited to studying the resultant fiber's diameter and surface. The effectiveness of the pyrolysis treatment (in regards to graphitic structure) has not been examined until just recently, although mechanical characterization has not been completed.

In 1999, Chun et al.[3] pyrolyzed electrospun Polyacrylonitrile (PAN) and meosphase pitch fibers into carbon fibers with diameters in the range of 100nm to a few microns. A solution of pure PAN polymer dissolved in dimethylformamide (DMF) was collected onto a grounded carbon fabric, stabilized at 270°C for 15min in air without tension, and carbonized at 800°C for 1h in an inert atmosphere. Not surprisingly, the linear dimensions of the nanofiber sheet shrunk by ~10% and detach from the carbon fabric during the heat treatment. It is presumed, by the present author, that the precursor fibers are not fully stabilized prior to carbonization resulting in shrinkage of the fibers upon further heat treatment. Most likely, the resultant fibers possess low crystallinity and orientation, and therefore, no structural characterization is reported.

Chun et al. used a similar protocol to stabilize and carbonize electrospun, mesophase pitch nanofibers; the resultant fiber was examined wide angle X-ray

diffraction (WAXD), in addition to electron microscopy. An interplanar *d* spacing, calculated from the 002 reflection using Bragg's equation (Equation 5.2), of the graphite layers of 0.349nm is determined for the carbon nanofibers; graphite fiber has an interplanar spacing of 0.355nm according to the literature[4,5]. The crystal size was determined to be 1.68nm, while the literature value is reported to be between 3.5nm to 4.5nm for larger diameter fibers carbonized to 1300°C[2]. Crystal size parameter increases as a function of carbonization temperature and a carbonization temperature of 800°C is too low to produce the necessary high crystalline order of carbon fiber.

Wang et al. [6] structurally characterized carbon nanofibers prepared from electrospun PAN precursor fibers by Raman scattering; carbon polymorphs are a well-known Raman active group of materials. Carbon fibers with diameters in order of 100nm were prepared from solution in DMF and pyrolyzed in vacuum between 600°C and 1200°C. Raman characterization revealed order-induced (D), 1360cm-1, and Raman-allowed (G), 1580cm-1, peaks, characteristic of the disordered carbon and graphite in the nanofibers. The integrated Raman intensity of the D (I_D) and G (I_G) peak is proportional to the number of scattering disordered and ordered sp^2 bonding carbon atoms; the ratio (R) of I_D to I_G describes the disorder within the sample. From the value of R, the in-plane graphitic crystallite size (L_a) and the mole fraction of graphite (x_g) is estimated to be between 1.5nm to 1.5nm (based on work done by Knight et al.[7b]) and 0.25 and 0.37, respectively; both L_a and x_g increase with pyrolyzing temperature[7].

Kim et al. [8] completed work similar to that of Wang et al. on PAN-based carbon nanofibers pyrolyzed between 700°C to 1000°C. In addition, Kim et al. examined the

structure of the resultant nanofibers; they determined apparent crystalline size in the along the crystallographic a- and c-direction ($L_{a(002)}$ and $L_{c(10)}$, respectively) of the fiber by wide angle X-ray diffraction (WAXD). $L_{a(002)}$ and $L_{c(10)}$ are calculated from the (002) and (10) reflections at $2\theta = 24°$and 44°C, respectively. As the maximum pyrolysis temperature was increased to 1000°C, $L_{a(002)}$ and $L_{c(10)}$ were found to increase to a maximum of 2.15nm and 3.36nm, respectively. The interplanar spacing, $d_{(002)}$, decreased to 0.360nm at maximum pyrolysis temperature of 1000°C.

Conductivity of both the carbon microfiber and nanofiber derived from PAN is sensitive to the pyrolyzing temperature and time. Both Wang et al. [9a] and Kim et al.[9b] extended the previous works to show that the electrical conductivity of the carbonized web increases with carbonization temperature and exposure time (in accordance with increasing crystal size and improved ordering).

Based on the work by Chun et al., Park et al. [10] prepared isotropic webs of carbon nanofibers from pitch precursor fibers electrospun from solution with tetrahydrofuran and subjected the webs to a carbonization temperature of 1200°C in argon. Examination of the fiber surface led to the finding that that the cross-section of the resultant fibers were ribbon-like; the cylindrical fibers had most probably collapsed upon heating, as residual solvent is removed, resulting in a flattening of the cross section (oval cross section). Flat ribbon-like morhology are commonly observed of electrospun fibers in the literature. The width of the pitch based carbon fibers was between 2μm and 3μm. Similar to the previous work done on PAN-based nanofibers, Park et al. found that the electrical conductivity of pitch-based carbon nanofibers improves with increasing carbonization temperature.

Despite these investigations, there are no reports in the literature regarding the preparation or use of carbon nanofibers for use as a reinforcer. Nor are there any reports of mechanical properties of carbon nanofibers prepared from electrospun precursor fibers; this is not surprising considering that all of the previously mentioned literature made no efforts to control/maintain the molecular orientation of the precursor during the thermal processing as expressed by the reported small crystal size.

5.3 Proposal

In the present work, unidirectional tows of Polyacrylonitrile (PAN) nanofibers post-stretched above the glass transition temperature, Tg, of the polymer (Chapter 4) are stabilized and carbonized at elevated temperatures. Parameters, including: heating rate, oxygen consumption, temperature, and exposure time, are evaluated in order to determine the ideal oxidation conditions for the precursor nanofiber yarn. The effect of the final carbonization temperature on the translational order within the graphite sheets and the crystal size is investigated. The mechanical properties of the resultant carbon nanofiber yarn are described and evaluated as a function of processing temperature and time.

5.4 Experimental

5.4.1 Materials

Polyacrylonitrile copolymer (PAN) received from an industrial source and dimethylformamide (DMF) from Sigma Aldrich Co. are used to prepare solutions for electrospinning, as described previously (Section 4.4.1). Yarns are prepared by

electrospinning and drawn (draw ratio of 1:2) above the glass transition temperature, Tg, prior to high temperature pyrolysis, as described previously (Section 4.4.2 and 4.4.3, respectively).

5.4.2 Thermal Properties

The effect of heating rate on the thermal decomposition of electospun Polyacrylonitrile (PAN) yarn in air is determined using a TA Instruments 2050 thermogravimetric analyzer (TGA). Samples of approximately 5mg are heated at various heating rates (between 0.1°C/min and 10°C/min) to 800°C; the decomposition profile and percent weight loss is examined for each heating rate.

The effect of environment on the oxygen consumption during decomposition is determined by Pyrolysis-combustion flow calorimetry (PCFC). A 1.0mg to 5.0mg sample of virgin electrospun fiber is inserted into a pyrolyzer (preheated to 150°C) and then heated to 900°C at 1°C/s under nitrogen. Tthe decomposition volatiles are swept into a combustion chamber by a continuous flow of N_2 and O_2 and completely combusted at 900°C. The input and output flow of O_2 is measured continuously by an oxygen analyzer; the heat release capacity and the char yield is measured. The final value of the heat-release rate is the average of five measurements.

The amount of oxygen consumed at the maximum point of combustion and the total amount of oxygen consumed during the decomposition is calculated as a function of combustion atmosphere. The maximum instantaneous consumption of oxygen, $\Delta \dot{m}_{O_2}$, is determined from the total heat release integrated area, *HR*, by Equation 5.3.

The total amount of oxygen consumed during combustion, $\Delta \dot{m}_{o_2}^{\max}$, is calculated from the measured heat release capacity, η_c, by Equation 5.4.

$$\Delta \dot{m}_{O_2} = (HR * m_o)/E \tag{5.3}$$

$$\Delta \dot{m}_{O_2}^{\max} = (\eta_c \beta m_o)/E \tag{5.4}$$

Where $\Delta \dot{m}_{O_2}$ is in units of g_{O_2}/s, HR is in kJ/g, m_{O_2} is the initial mass of the sample (g), E is 13.1 + 0.6x103 J/g_{O_2}/, $\Delta \dot{m}_{o_2}^{\max}$ is in g_{O_2}, η_c is in J/g*K s, and β is the heating rate (K/s).

5.4.3 Batch Stabilization

Drawn (post treated to a draw ratio of 1:2), electrospun, (Polyacrylonitrile) PAN yarn is held at constant length and stabilized (oxidized) in batch in a Thermolyne 4800 furnace. A length of yarn is held on a graphite rod (1in x 1/4in dia.) with v-grooves at each end (Scheme 5.1); the yarn is wound around the rod the tied off. The oven is purged with preheated air and heated to a specific temperature. The rod and sample are placed into the oven and the sample is heated according to a preset program. Oxidation is completed in batch to avoid unnecessary complexities involving heating rates.

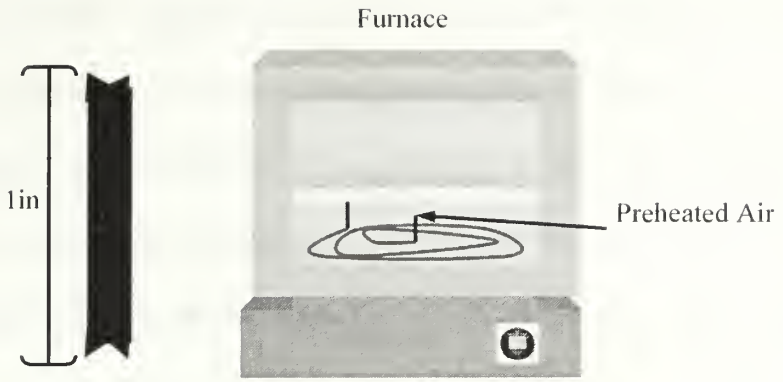

Scheme 5.1: Diagram of a graphite rod used to hold the electrospun yarn sample and furnace set up used during the batch stabilization

5.4.3.1 IR Spectroscopy

Stabilized yarn is examined by transmission infrared spectroscopy using a Perkin Elmer Spectrum 2000 infrared spectrometer (FTIR); the extent of reaction is monitored and ideal processing temperatures are determined. Spectra are recorded over the range of 700-4000cm^{-1} with typically 64 scans. The course of the stabilization process is evaluated; the ratio of absorbances of the nitrile-stretching group vibration (-C≡N), 2240cm^{-1}, and the aliphatic methyl group vibration (CH_2, CH), 2940cm^{-1}, are compared to those vibrations related to the ladder structure of stabilized PAN, including bands stemming from the aromatic ring, as a function of temperature and time. The absorbance at 810cm^{-1} due to C=CH group, at 2200cm^{-1} due to a nitrile group bound to an olefinic chain (=C-C≡N), and absorbances in the region of 1600cm^{-1} related to the C=N-, -C=C-, and NH groups are monitored.

5.4.4 Batch Carbonization

Yarn stabilized in air, as described in Section 5.4.4), is carbonized under N_2. The stabilized yarn is exposed to a high temperature pyrolysis treatment in a Lindberg

59545 tube furnace. The oxidized yarn (still wound on a graphite rod) is inserted into a steel vessel and the vessel is purged with oxygen free nitrogen gas (<5ppm O_2) for 10minutes. The vessel is a 3ft long tube of 618 steel with a 3/8in internal diameter; one end of the tube is fitted with a 2-way valve and the other with a cap seal (Scheme 5.2). Copper gaskets are used with the seal and connector fittings. Spacers (1/4in steel rod) are used to

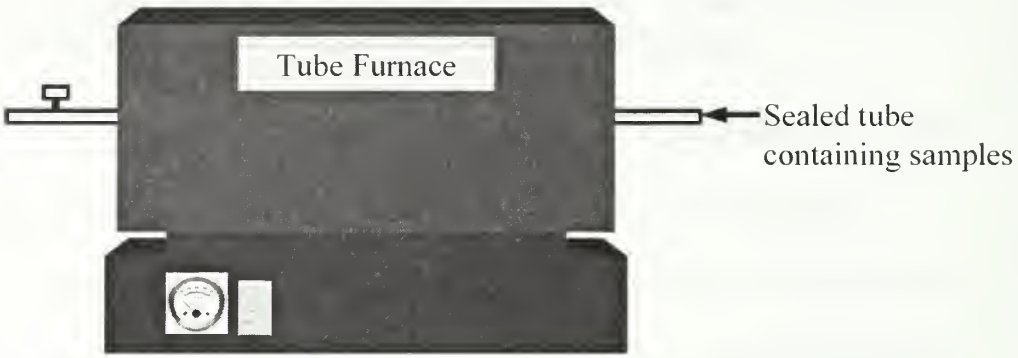

Scheme 5.2: Batch carbonization set-up

position the samples into the center of the furnace. After purging is complete, the tube is sealed at both ends. The sample(s) are heated in the closed vessel under constant tension in an oxygen free atmosphere; any residual oxygen is reacts with the copper gaskets. The final pyrolysis temperature is held for 15min then the vessel is removed from the furnace and allowed to cool to room temperature before it is opened.

5.4.4.1 Raman Scattering

Carbonized yarn is examined by Raman scattering using a laser confocal Raman spectrometer (Jobin Yvon HORIBA LabRam HR 800 Raman microscope) with CCD detector in order to characterize the structure of the carbon fiber. The instrument is equipped with a conical focus capable of high spatial resolution of approximately 1μm^2.

A ¼ λ plate is inserted into the path of the beam in order to randomize the direction of polarization of the laser beam. Spectra centered around 1400cm^{-1} are collected with ten 10s scans with a hole setting of 1100μm, slit of 100μm, and grating of 600; spectral resolution is kept at 1cm^{-1}.

The disorder-induced (D) line with a peak near 1360cm^{-1} and the Raman-allowed (G) line near 1580cm^{-1} are observed. The ratio of the integrated intensity of the disorder-induced (D) and the Raman-allowed (G) line $R = I_D / I_G$ provides a sensitive characterization of the disorder in the sample (where I_D and I_G are proportional to the number of observed scattering disordered and ordered sp2 bonding carbons, respectively)[11].

5.4.5 Wide Angle X-ray diffraction

The aromatization index *AI*, the degree of oxidation, of the stabilized yarn is determined by X-ray diffraction (XD) using a Rigaku RU-H3R rotating anode x-ray diffractometer (Rigaku, Tokyo, Japan) equipped with a multiplayer focusing optic (Osmic Inc., type CMF23-46Cu8) and an evacuated Statton type scattering camera, as described previously (Section 4.4.6) (Equation 5.1).

$$AI = \left[I_a / \left(I_a + I_p \right) \right] \times 100\% \qquad (5.1)$$

Where I_a is the measured intensity of the aromatic structure (ladder structure) at 2θ = 26°, and I_p is the diffraction intensity of Polyacrylonitrile (PAN) crystal at ~2θ = 17°[12].

The lattice parameters of carbonized yarn are determined by XD using a PANanlytical X'pert Pro powder diffractomer as a function of final pyrolysis temperature. A copper mirror assembly with Ni 0.002 attenuator and a 1/2° slit is used

to collimate the CuKα source; K_β radiation is removed and only $K\alpha_1$ and $K\alpha_2$ radiation is used (λ = 1.54Å). Scattering is collected using a X-celerator detector with an internally calibrated goniometer. The yarn is laid on top of a zero backgrounded Silicon III wafer and scanned over a range of 5° to 75° at a speed of 0.04°/s. A background is subtracted.

The average interplanar spacing, d_{002}, and the crystallite dimension $L_{a(10)}$ and $L_{c(002)}$ are determined from the (10) and (002) reflections at 2θ = 44° and 24°, respectively, using the Bragg (Equation 5.2) and Scherer equations (Equation 5.3 and 5.4).

$$d = n\lambda/2\sin\theta \qquad (5.2)$$

$$L_a = 1.84\lambda/\beta\cos\theta \qquad (5.3)$$

$$L_c = 0.91\lambda/\beta\cos\theta \qquad (5.4)$$

Where L_a is the crystallite dimension in the a-direction as determined from the (10) reflection, and L_c is that in the c-direction as determined from the (002) reflection, λ is the wavelength, β is the half maximum line width in radians, and θ is the scattering angle.

5.4.6 Microscopy

Stabilized and carbonized fibers are observed by field emission scanning electron microscopy (FESEM), as described previously (Section 2.5.5).

5.4.7 Mechanical Parameter

The mechanical behavior of the stabilized and carbonized yarn is examined using an Instron 5564 and Instron 5800, as described previously (Section 3.4.7). The cross-sectional area of the laboratory prepared yarns is calculated from the denier and density, while the area of the commercial fiber is determined by laser diffraction, as described previously (Section 2.5.4). The density of the stabilized yarn is assumed to be 1.4g/ml, as determined by ASTM D3800-9 of tow stabilized PAN fiber from an industrial source. The density of the carbonized yarn is assumed to be 1.78g/ml from the literature. The initial modulus, ultimate strength, and elongation at ultimate strength is measured.

5.5 Results and Discussion

Of the three previously presented precursors: Rayon, Pitch, and Polyacrylonitrile (PAN), PAN has proven to be the most suitable for developing the carbon structure needed to produce high strength fibers. Currently, the PAN process is the standard commercial method used for manufacturing of the majority of industrial carbon fibers. The process begins with the production of the PAN precursor fiber; the fiber is subsequently subjected to a controlled transformation to carbon fiber through a series of heat treatment steps in different environments at progressively increasing temperatures.

The stabilization step converts the precursor from a linear polymer to a highly condensed, thermally stable structure, as detailed in Section 1.2.4.2. Stabilization involves a low temperature heat treatment between 180°C and 280°C in air of the

precursor fiber under normal atmospheric pressure. The chemical processes taking place during stabilization and the structure of the stabilized fiber are known up to now only in the main features; the fibers become insoluble at a relatively early stage of the stabilization process. Furthermore, the possibility to generalize the results of many analyzing methods is limited as there are a variety of precursor materials. Generally the following reactions take place during the stabilization process: ring formation, (cyclization) via nitrogen atoms, leading to a ladder structure; dehydrogenation and thereby formation of conjugated double bonds; and oxidation. Typically the fiber, considered well stabilized in terms of further processing, is subjected to only partial cyclization and dehydrogenation; its structure is a mixture of heteroaromatic and nonaromatic rings, and olefinic and aliphatic structural units[13]. To ensure optimum properties, the cyclization is usually conducted so as to promote a slow release of heat, minimizing both the loss of orientation and fragmentation of the polymer molecules. The technology is slightly modified and optimized by each producer depending upon the chemical composition of the copolymer, the applied stretch, and the diameter of the fiber[14].

Due to the critical importance of the cyclization step in the production of PAN-based carbon fiber and the obvious advantages offered by a controlled and a decreased reaction time, the kinetics and mechanism for the conversion of electrospun PAN fibers to cyclized ladder structure is investigated. The effect of heating rate and environment on the decomposition of electropun PAN nanofibers is evaluated. The effect of heating rate on the decomposition of electrospun precursor fiber is determined by thermal gravimeteric analysis (TGA). The decomposition of the nanofibers consists of two

steps occurring between 220°C and 260°C, and 370°C and 490°C, respectively, depending upon the heating rate (Figure 5.1). Weight loss observed between approximately 90°C and 105°C is due to the removal of residual water (from high temperature drawing in water). As the heating rate is increased from 0.1°C/min to 10°C/min, the decomposition profile becomes more abrupt and the decomposition temperature of each event rises due to slow heat transfer. The complete decomposition of the nanofiber bundles, as observed in Figure 5.1 (char yield varied between 2% and 5%), is expected, since the analysis is conducted in the presence of air throughout the entiare temperature range (room temperature to 800°C). It is known that the presence of more than several parts per million (ppm) of oxygen during the carbonization process (at temperatures greater than 600°C) has severe, negative effects on carbon materials and results in degradation. Therefore, it is not possible to determine a true char yield from this data.

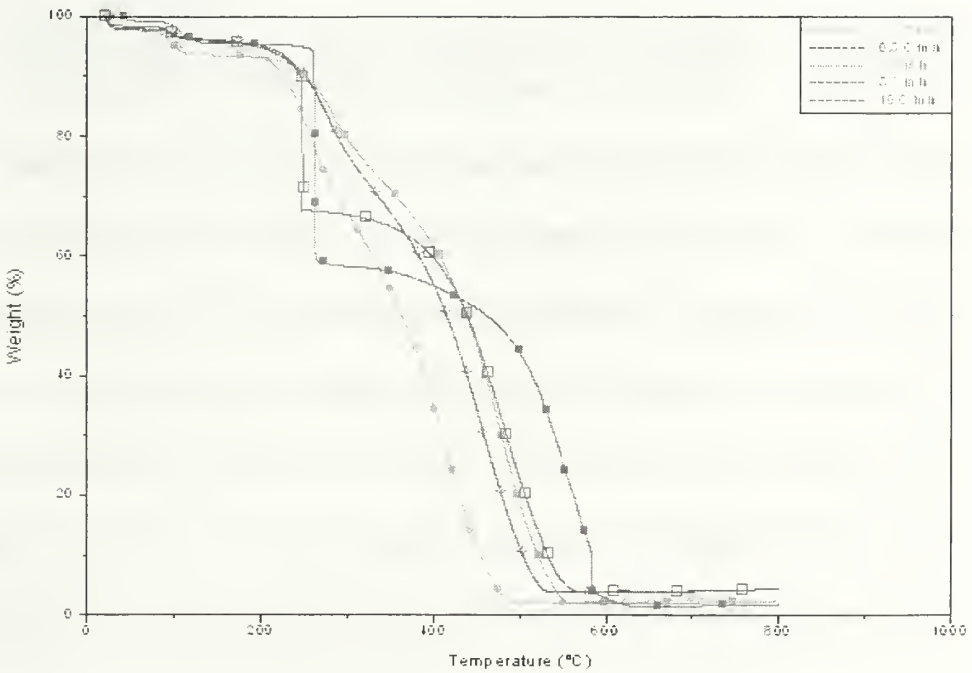

Figure 5.1: Decomposition of electrospun Polyacrylonitrile fibers as a function of heating rate; thermal gravimetric analysis (TGA) at a heating rate of (a) 0.1°C/*min* (•), (b) 0.5°C/*min* (■), (c) 1°C/*min* (◙), (d) 5°C/*min* (□), and (e) 10°C/*min* (+)

The effect of environment on the stabilization of precursor nanofiber is evaluated by pyrolysis combustion flow calorimetric (PCFC); the amount oxygen consumed by the nanofiber bundle during combustion is determined in an air (80:20 composition of N_2:O_2) and an oxygen rich (50:50 composition of N_2:O_2) environment (Table 5.1). The total oxygen consumed by the nanofibers during combustion in the two environments is

Table 5.1: Effect of environment on the consumption of oxygen during the decomposition of electrospun Polyacrylonitrile fibers determined by Pyrolysis Combustion Flow Calorimetry (PCFC)

Environment (N_2:O_2)	Char Yield (%)	Heat Release Capacity (J/g*K)	Total Heat Release (kJ/g)	Oxygen Consumed at Maximum Point of Combustion, normalized ($g_{O_2}/g_{polymer}$)	Total Oxygen Consumed, normalized ($g_{O_2}/g_{polymer}$)
80:20	42.8 ± 2	172 ± 38	12.3 ± 0.3	0.94 ± 0.02	13.1 ± 2.8
50:50	49.1 ± 1	160 ± 43	11.0 ± 0.47	0.84 ± 0.03	12.2 ± 3.3

comparable; an oxygen rich atmosphere is not necessary for the stabilization of the nanofibers. A char yield of approximately 40% is determined (without any previous oxidative treatment). In comparison, commercially stabilized Polyacrylontirile (PAN) fibers consume 16.7 times their weight of oxygen during combustion in air (80:20 N_2:O_2) (Table 5.2). It is inferred from the PCFC results that commercially oxidized fiber is not fully stabilized, as expected (Section 1.2.4.2). The char yield of the electrospun precursor nanofiber is expected to between 40% and 60% with stabilization.

Table 5.2: Oxygen consumed during the decomposition of commercially stabilized (oxidized) Polyacrylonitrile fibers determined by PCFC

Char Yield (%)	Heat Release Capacity (J/g*K)	Total Heat Release (kJ/g)	Oxygen Consumed at Maximum Point of Combustion, normalized	Total Oxygen Consumed, normalized
62.6 ± 0.5	51.0 ± 3.5	8.5 ± 0.5	0.65 ± 0.04	16.7 ± 1.2

In order to reduce the number of variables affecting the oxidation of the precursor nanofibers, a batch stabilization process in air (80:20 N_2:O_2) is designed. The effect of temperature and exposure time on the oxidation and subsequent cyclization reactions is evaluated; the optimum stabilization conditions are determined. Post treated, electrospun PAN yarn, held at constant length, is subjected to oxidation in batch. The extent of reaction is monitored by transmission infrared spectroscopy (Trans FTIR); the cyclization and dehydrogenation reactions are observed during stabilization (Figure 5.2). A major decrease in the nitrile stretching at 2240cm^{-1} and methylene band at 2940cm^{-1}, and a growth of three new bands at 1725cm^{-1}, 1660cm^{-1}, and 1595cm^{-1} in the carbonyl-stretch frequency region is observed after stabilization of the precursor nanofibers to 240°C (Table 5.3). Bands in the region of 1600cm^{-1} are related to the groups of C=N-, C=C, and NH, but evaluating them is difficult due to strong overlap. The absorption bands at 1725cm^{-1} and 1660cm^{-1} are due to the C=O stretch vibrations of the aliphatic ketone and the conjugated ketone, respectively. The band at 1725cm^{-1} comes from free ketones generated in the hydronaphthridine rings and the band at 1660cm^{-1} is due to conjugated ketones in the acridone ring. The band at 1595cm^{-1} is due to a combination of the C-N and C-C stretching, and NH in-plane bending of the ladder-frame structure of the stabilized PAN. As the temperature is increased further, an increase in dehydrogentation and cyclization reactions are observed. A band at

2200cm^{-1} due to nitrile groups bonded to an olefinic chain, indicates the existence of dehydrogenated, noncyclized structural units; this band and that at 2240cm^{-1} disappear

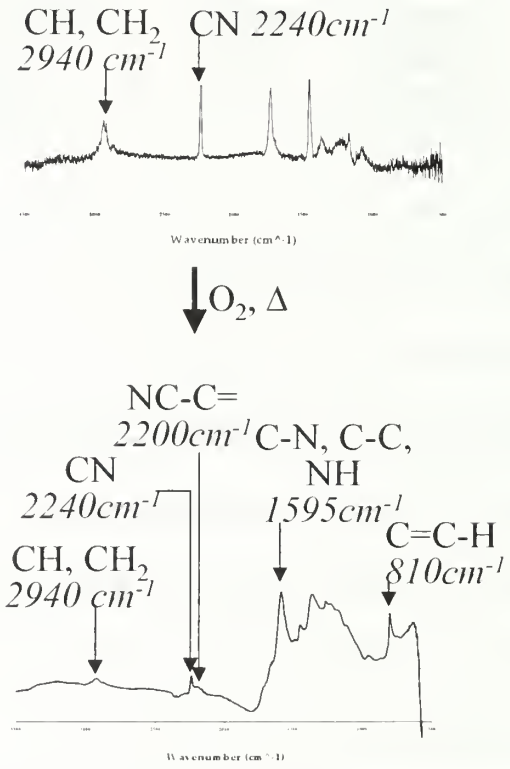

Figure 5.2: Transmission infrared spectrum of electrospun Polyacrylonitrile fiber and commercially prepared, partially stabilized (oxidized) Polyacrylonitrile fiber

at high degrees of stabilization (complete cyclization). A band at 810cm^{-1} stemming from the C=C-H group in the aromatic ring is also observed.

Absorption bands describing the linear polyacrylonitrile copolymer are compared to those referring the cyclized ladder structure of the stabilized material (Table 5.4). The nitrile-stretching (2240cm^{-1}) and methylene group (2940cm^{-1}) absorbance is compared to that of the bands referring to the cyclization and ladder structure (1595cm^{-1}, 2200cm^{-1}, and 810cm^{-1}) of the post-treated yarn. The results are

Table 5.3. Infrared absorbance of electrospun Polyacrylonitrile fiber with post-treatment stretching and oxidized under various conditions, reaction progress monitored by transmission infrared spectroscopy (Trans IR)

	Post treatment										Ladder Structure	
						$C\equiv N$	*CH, CH_2*	*NC-C=*	*C=O aliphatic ketone*	*C=O conjugated ketone*	*C-N, C-C, NH*	*C=C-H*
Temp °C	**180**	**220**	**240**	**260**	**300**	**cm^{-1}**	**2940**	**2200**	**1725**	**1660**	**1595**	**810**
	Polyacrylonitrile Fiber					Abs	0.47	0.23				
Time *(min)*	15	30					0.20	0.074		0.16		0.15	
	15	15	30				0.094	0.036	0.012	0.25	0.15	0.38	0.014
	15	15	15	30			0.078	0.030	0.028	0.14	0.33	0.73	0.031
	15	15	15	15	30		0.038		0.049	0.25	0.60	1.09	0.036
	15	15	15	15	15		0.024	0.001	0.021	0.11	0.29	0.59	0.026
	15	15	15	30	15		0.018		0.023	0.11	0.30	0.64	0.0186
	15	15	30	30			0.039	0.013	0.018	0.092	0.21	0.45	0.021
		15	15	15			0.089	0.027	0.023	0.12	0.29	0.63	0.03
		15	30	30			0.068	0.014	0.039	0.18	0.47	0.94	0.042
		15	30	15			0.049	0.012	0.028	0.12	0.34	0.73	0.03

compared to those of commercial stabilized fiber of the same precursor compolymer composition (Table 5.5) and a batch stabilization process is determined. The optimal batch stabilization in air procedure is formulated to include three segments of 15min each at: 220°C, 240°C, and 260°C. All stabilized nanofiber yarns described from herein are stabilized under these conditions.

Table 5.4: Electrospun Polyacrylonitrile (PAN) nanofiber after various low temperature, oxidative post treatments monitored by transmission infrared spectroscopy (Trans IR). Accepted batch stabilization conditions are highlighted.

	Post treatment						***Ratio:***				
Temp (°C)	**180**	**220**	**240**	**260**	**300**	**cm^{-1}**	***2240: 1595***	***1595:2240***	***2940: 2200***	***2200: 2940***	***2940: 810***
Time (*min*)	15	30				**Abs.**	1.30				
	15	15	30				0.25	0.16	2.95	0.34	2.43
	15	15	15	30			0.11	0.39	1.08	0.93	0.98
	15	15	15	15	30		0.035	0.94	0.02	51	0.027
	15	15	15	15	15		0.04	1.09	0.068	15	0.056
	15	15	15	30	15		0.028	1.04	0.095	11	0.12
	15	15	30	30			0.088	0.54	0.70	1.43	0.6
		15	15	15			0.14	0.34	1.16	0.86	0.89
		15	30	30			0.072	0.62	0.36	2.79	0.33
		15	30	15			0.067	0.62	0.41	2.45	0.38

Table 5.5: Commercial stabilized (oxidized) Polyacrylonitrile fiber characterized by transmission infrared spectroscopy (Trans IR)

	C≡N	*CH, CH_2*	*NC-C=*	*C-N, C-C, NH*	*C=C-H*	***Ratio:***				
cm^{-1}	**2200**	**2940**	**2200**	**1595**	**810**	***2240: 1595***	***1595:2240***	***2940: 2200***	***2200: 2940***	***2940: 810***
Abs.	0.035	0.015	0.012	0.23	0.08	0.15	2.44	1.21	0.83	0.18

As Polyacrylonitrie (PAN) fiber is subjected to stabilization, the polymer becomes colored and the intensity of the color depends upon the intensity and duration

of the treatment. The chromophore in PAN is a conjugated imine-nitrone system and it is formed by the polymerization of the nitrile groups, rather than by dehydrogenation[16]. As heating is prolonged (in a oxygen containing atmosphere), dehydrogenation of the backbone occurs and PAN is converted into a nonflammable form. PAN nanofiber,stabilized according to the batch procedure described above, appear dark brown (Figure 5.3). Additionally, the nanofiber morphology is maintained by the batch stabilization.

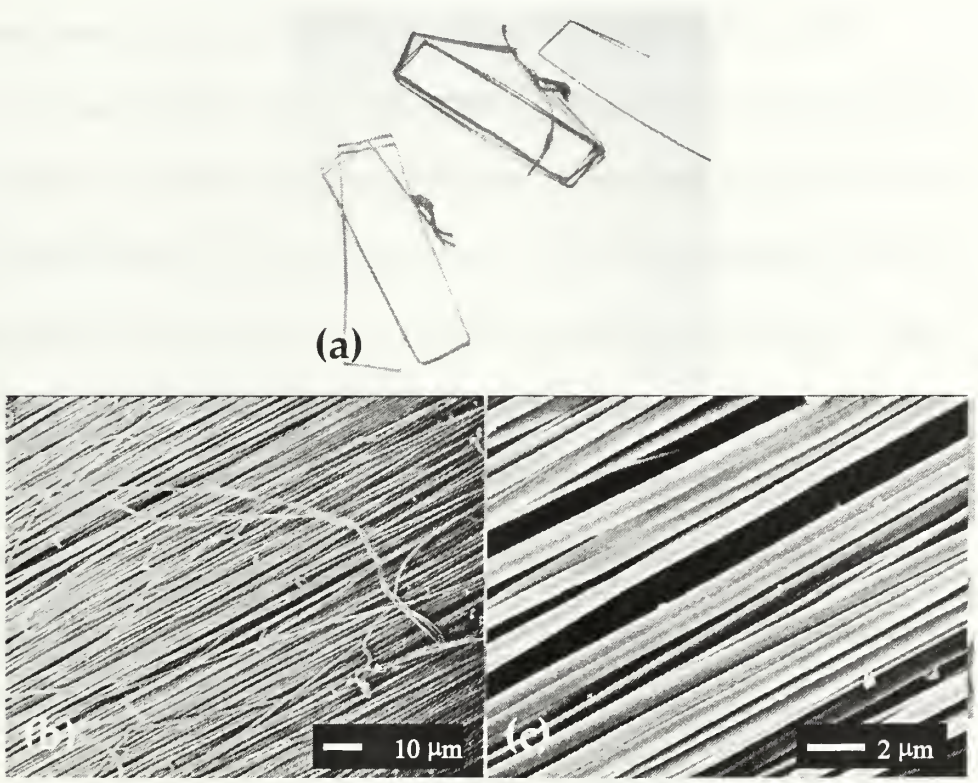

Figure 5.3: (a) Photograph and (b-c) field emission scanning electron microscopy (FESEM) image of batch stabilized, electrospun Polyacrylonitrile (PAN) nanofiber yarn

The chemical composition of the stabilized PAN fiber can have a dramatic influence on the mechanical properties of the final carbon fiber. The oxygen content

required for optimum final fiber properties varies for different PAN copolymers; in general, the oxygen content of the precursor fiber increases from 8% to 11%. During the stabilization process, the simultaneous evolution of CO_2, a product of decarboxylation reactions, and HCN, evolved in the reaction of uncyclized nitrile groups, causes the carbon content of the PAN fiber to decrease from approximately 68% to 65%. The hydrogen content, also, decreases with the evolution of HCN and H_2O (by product of dehydrogenation reactions). During the stabilization process the fiber experiences a net weight loss of between 5% and 8%[14].

Due to experimental difficulties involved with preparing large quantities of stabilized nanofiber yarn, density measurement of the stabilized yarn is not possible and it cannot be used to qualitatively describe the extent of oxidation. Rather, the fiber is evaluated qualitatively by flame test and quantitatively by X-ray diffraction (XD). A flame test consists of subjecting a stabilized material to the core of a flame (oxygen free area); if the material glows red, it is assumed that the material is adequately stabilized and will survive if exposed to high temperature pyrolysis (carbonization). If the material burns and disintegrates, it is assumed that the material is not adequately stabilized and will not survive further pyrolysis treatments. The batch stabilized yarn is observed to initially shrink (slightly) and then glow red when subjected to a flame; this suggests that the yarn is partially stabilized.

The aromatization index *AI*, or degree of oxidation, is determined by XD (Equation 5.1); *AI* of the nanofiber yarn is determined to be 54% (Figure 5.4 and Table 5.6). It is well known that the *AI* value of an oxidized fiber is a very important characteristic for monitoring the degree of oxidation of the precursor fiber; the *AI* value

is one of many factors that affect the properties of carbon fiber. It has been shown that an *AI* value greater than 50% results in low mechanical properties of the oxidized and the resultant carbon fiber[17]. The *AI* of the commercial stabilized fiber is not defined and it could not be determined due to the lack of an available commercial PAN fiber for the comparison.

As previously mentioned, the preferred orientation needed for the final high performance carbon fiber is generated by stretching the precursor fiber prior to stabilization. The chemical reactions that take place during the low temperature oxidation can disrupt the orientation of the molecular chains and result in fiber shrinkage. Additionally, the disruption can significantly influence the modulus of the final carbon fiber. The mechanical properties of the stabilized yarn are evaluated and compared to those of commercial stabilized fiber (Table 5.7). The ultimate strength of the batch stabilized yarn is approximately half that of the commercial stabilized fiber while the modulus of the two materials is comparable within the error. The batch stabilized, electrospun yarn is weaker than the commercial fiber, overall.

Once PAN fibers are stabilized, they are subjected to pyrolysis (carbonization), as described previously (Section 1.2.4.3). This high temperature treatment eliminates most of the non-carbon elements from the fiber, converting the fiber into a carbon fiber. Carbonization is conducted in a inert atmosphere, usually ultra pure nitrogen, at temperatures ranging from 1000°C to 1500°C; thermally stable pyridinic structure forms and subsequently collapses into a turbostratic, stacked ring structure. During the initial low temperature range of 300°C and 600°C, the foundation of the carbon building block is laid. Most of the chemical reactions involve intermolecular cross-

linking, reorganization, and coalescence of cyclized sections. These reactions lead to the evolution of water, ammonia, hydrogen cyanide, carbon dioxide, carbon monoxide, methane, and a small amount of low molecular weigh nitriles. In the range of 600°C to

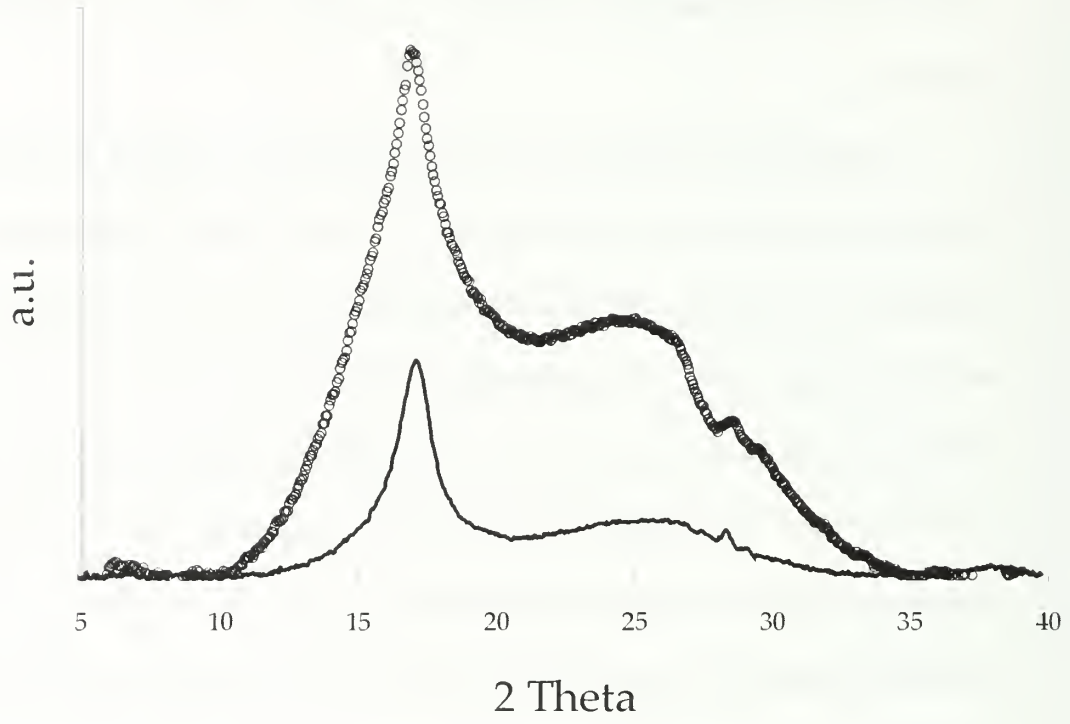

Figure 5.4: Intensity versus 2θ of the post-treated (percent draw of 100%) electrospun Polyacrylonitrile (PAN) yarn before (—) and after stabilization (○)

Table 5.6: Aromatization index of laboratory post-treated, stabilized, electrospun Polyacrylonitrile (PAN) yarn

I_a	I_p	*AI* (%)
26.7	22.8	54

Table 5.7: Mechanical properties of stabilized, electrospun, Polyacrylonitrile (PAN) yarn of denier 635 and commercial stabilized single fiber of denier 1.8. A density of 1.4g/ml is assumed in the stabilized, electrospun yarn calculation

	Ultimate Strength (MPa)	Modulus (Gpa)	Ultimate Strength (*g/denier*)	Modulus (*g/denier*)	Strain at Break (%)
Batch, stabilized, electrospun yarn	160 ± 29	7.1 ± 1.1	1.3 ± 0.2	57 ± 9	4.4 ± 1
Commercial stabilized single fiber	310 ± 45	7.4 ± 0.7	2.2 ± 0.3	54 ± 6.5	14 ± 2

1000°C, intermolecular cross-linking takes place causing hydrogen, hydrogen cyanide and water to be evolved. The carbon content of the fiber increases to about 92%, the nitrogen content decreases to 7%, and the hydrogen contnet decreases to 0.3% during this stage. Both temperature and heating rate are important during all stages of the carbonization process.

Carbon, nanofiber yarn is prepared from the partially stabilized, electrospun yarn through a batch carbonization process. The yarn is heated to various temperatures (heated to 500°C at a rate of approximately 16°C/min, 800°C at 13°C/min, or 1000°C at 11°C/min) in an inert, oxygen free atmosphere and held for 15min before cooling to room temperature. The resultant material is black and it is structurally characterized by Raman spectroscopy and wide angle X-ray diffraction (WAXD). Raman scattering provides a spectroscopic technique for the identification of the symmetries of the structure and bonding of carbon. Raman spectra of solids are very sensitive to changes that break the translational symmetry of carbon bonds; lattice defects, as occur in carbon fibers, cause a breakdown of the translational symmetry. Disorder gives rise to a disorder-induced (D) line with a peak near 1360cm^{-1} and a broadening of the Raman-allowed (G) line near 1580cm^{-1}. The ratio of the integrated intensity of the disorder-

induced (D) and the Raman-allowed (G) line $R = I_D/I_G$ provides a sensitive characterization of the disorder in the sample (where I_D and I_G are proportional to the number of observed scattering disordered and ordered sp^2 bonding carbons, respectively)[11]. The ratio of the integrated intensities of batch carbonized, electrospun yarn is compared to that of batch carbonized, commercial stabilized fiber and commercial carbon fiber prepared from the same precursor copolymer (Figure 5.5, and Table 5.8 and 5.9). By varying the heat treatment temperature (T_{HT}), the ratio R of the carbonized material varies; the intensity of R decreases and the line width of the Raman-allowed peak decreases with increasing T_{HT}. The R of the commercial carbon fiber is equivalent to that of the electrospun yarn carbonized to a final temperature of 1000°C.

The WAXD pattern of the carbonized electrospun yarn is examined as a function of T_{HT} to qualitatively verify the general structural features of carbon fiber. The WAXD pattern of carbon fiber exhibits two peaks near $2\theta = 24°$ and 44° corresponding to the refection of the (002) and (10) layer of the graphite structure[18]. The XD patterns collected from the carbonized nanofiber yarns exhibit broad peaks, which narrow the T_{HT} is increased (Figure 5.6). The lattice parameters of the carbonized nanofiber yarn are determined and compared to those of the commercial stabilized yarn that has been carbonized under similar conditions in batch as a function of T_{HT} (Table 5.10) and to those of commercial carbon fiber (Table 5.11). The average interlayer spacing d_{002} and the crystallite dimension $L_{c(002)}$ and $L_{a(10)}$ are determined using the Bragg (Equation 5.2) and Scherer equations (Equation 5.3 and 5.4). The crystallite size in the a- direction, L_a, cannot be accurately determined for the carbonized nanofiber yarns due to weak

scattering intensity. The interplanar spacing, $d_{(002)}$, of carbonized, nanofiber yarn and the commercial carbon fiber is comparable (graphite fiber has an interplanar spacing of 0.355nm according to the literature[7]).

Although the carbonized nanofiber yarn exhibits the basic structural requirements to be termed 'carbon,' it is extremely delicate and brittle. It is not possible to evaluate the mechanical properties of the carbonized nanofiber yarn. The weakness

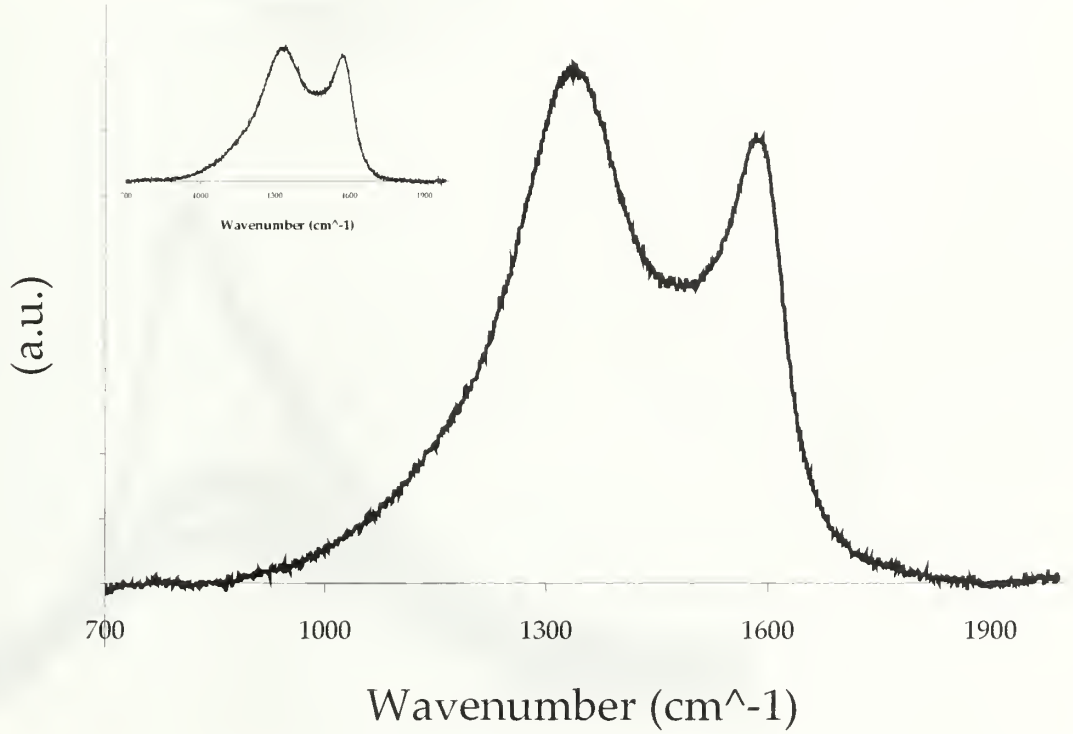

Figure 5.5: Raman spectrum of commercial carbon fiber (upper left) and electrospun fiber batch carbonized to a temperature of 1000°C. The spectrum highlighs the disorder-induced (D) peak at ~1360cm^{-1} and the Raman-allowed (G) peak at ~1580cm^{-1}

Table 5.8: The ratio of integrated intensities *R* of carbonized, electrospun yarn are compared to those of commercial stabilized fiber that has been carbonized under similar conditions as a function of carbonization temperature

Carbonization Temp.	I_D/I_G of Post-treated, electrospun yarn	I_D/I_G Commercial, stabilized fiber
800°C	1.27 ± 0.03	1.27 ± 0.021
1000°C	1.14 ± 0.04	1.06 ± 0.01

Table 5.9: The ratio of integrated intensities *R* of commercial carbon fiber

I_D/I_G of Commercial, carbon fiber
1.13 ± 0.03

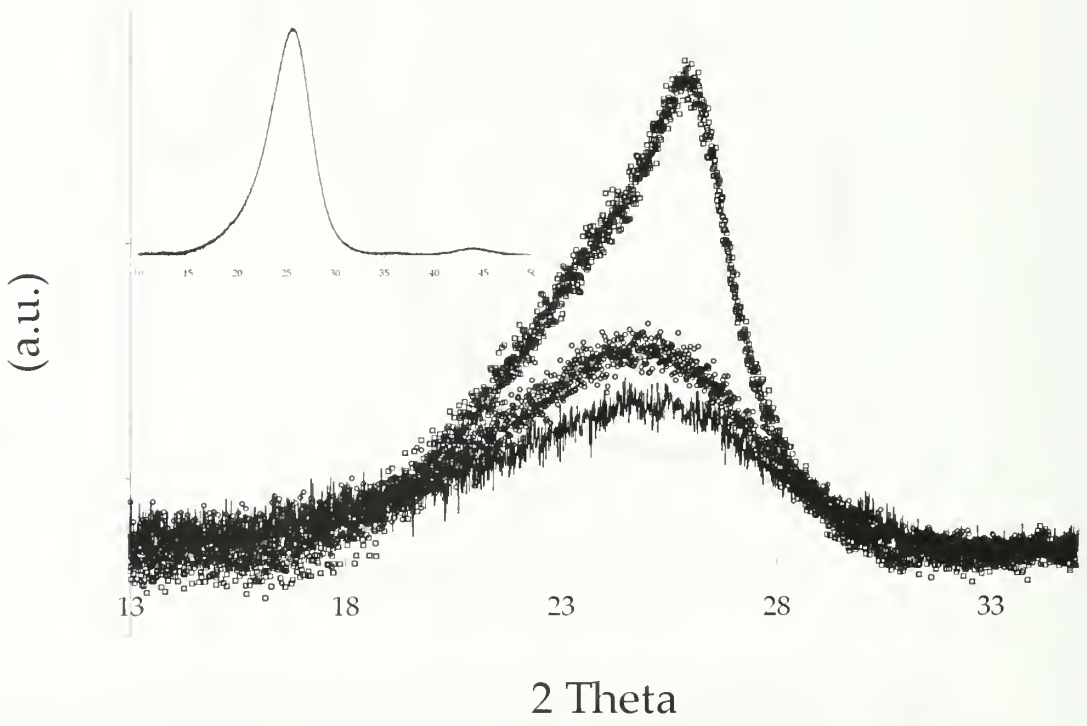

Figure 5.6: Wide angle X-ray diffraction pattern of commercial carbon fiber (upper left) and patterns of electrospun yarn carbonized to (center): (a) 500°C (—), (b) 800°C (○), (c) 1000°C (□)

Table 5.10: Lattice parameters as determined by wide angle X-ray diffraction (WAXD) of carbonized, electrospun yarn compared to commercial stabilized fiber that has been carbonized under similar conditions as a function of carbonization temperature

	Carbonization Temp.	$d_{(002)}$ (nm)	L_c (Å)	No. of graphite sheets (L_c/d)	L_a (Å)
Nanofiber yarn	500°C	0.348	11.3	3.2	
	800°C	0.354	11.4	3.2	
	1000°C	0.342	21.6	6.3	
Commercial stabilized fiber	500°C	0.337	12.9	3.8	
	800°C	0.354	11.4	3.2	
	1000°C	0.345	14.1	4.1	40.5

Table 5.11: Wide angle X-ray diffraction (WAXD) data of commercial carbon fiber

$d_{(002)}$ (nm)	L_c (Å)	No. of graphite sheets (L_c/d)	L_a (Å)
0.347	16.5	4.8	48.3

of the resultant nanofiber yarn is most probably due to the minimal size and lack of orientation of the crystallites produced during the incomplete stabilization and low temperature carbonization process. Even with longer oxidation times and a higher carbonization temperature, the mechanical properties of the resultant fiber are limited by the use of batch processing. During stabilization, for example, the yarn is held at fixed length in a batch process rather then under constant tension (as in continuous processing) permitting the loss of preferred orientation within the fibers.

With the aid of Dr. D. Edie and Dr. A. Naskar in the Chemcial Engineering department of Clemson University, South Caroloina, the effect of the carbonization temperature on the structural and mechanical properties of carbon nanofibers prepared from electrospun precursor was undertaken. The stabilized yarn is carbonized to 2000°C under helium (He) in an Astro Carbonization Furnace (Model 1000A) (maximum furnace temperature of 2400°C) (Figure 5.7a). The Clemson University chamber is oriented horizontally, so that samples may be stacked (Figure 5.7b). Samples are loaded into the chamber in Grafoil dishes; the chamber is purged and

evacuated with He to an over pressure of 5psi twice. The chamber is set to have a constant He overpressure of 5psi during the heat treatment; the pressure is regulated by equilibrated gas inlet and outlet flows. The furnace is manually heated to 425°C and then subjected to the following heating profile: ramp to 1700°C in 1h, ramp to 2000°C in 30min, and hold at 2000°C for 30min. An infrared pyroprobe is used to monitor the temperature. At completion of the heating program, a water jacket

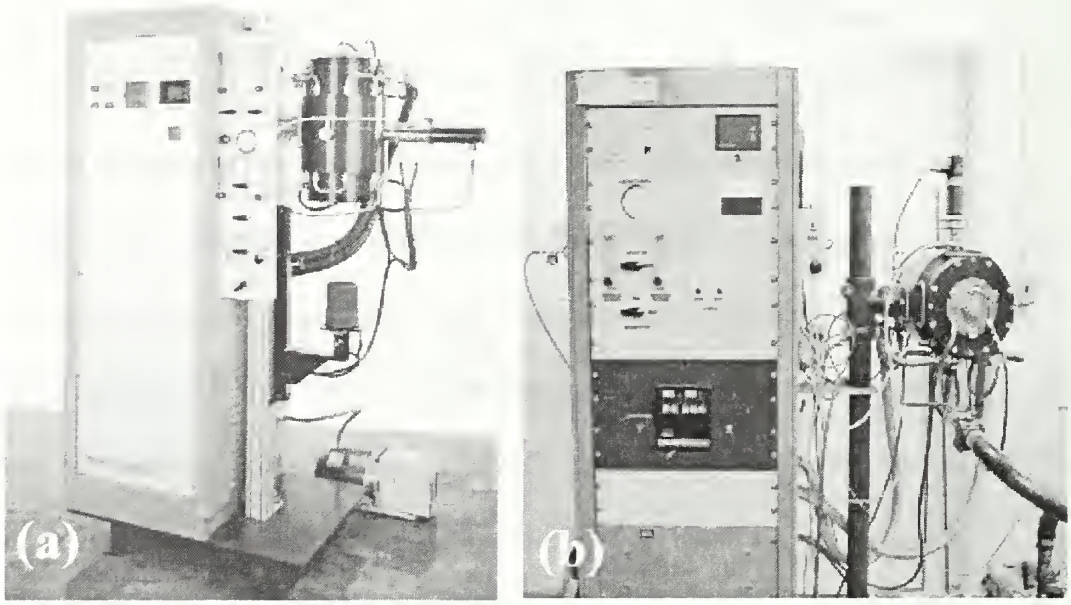

Figure 5.7: Astro Carbonization Furnace (Model 1000A) with its heating chamber oriented (a) vertically and (b) horizontally

is used to cool the chamber. The resultant yarn is black; the unconstrained yarn experienced shrinkage during the high temperature pyrolysis. Although the carbonized yarn is kinked and entangled, it maintained its' fiber structure after the pyrolysis, although, damage is evident (Figure 5.8). The nanofibers appear ribbon-like after examination by field emission scanning microscopy (FESEM).

5.5.1 Residual Stress

During cooling from processing temperatures, radial and hoop residual stresses develop within a carbon fiber due to the transverse preferred orientation in the fiber. These residual stresses are the result of differences in the coefficient of thermal

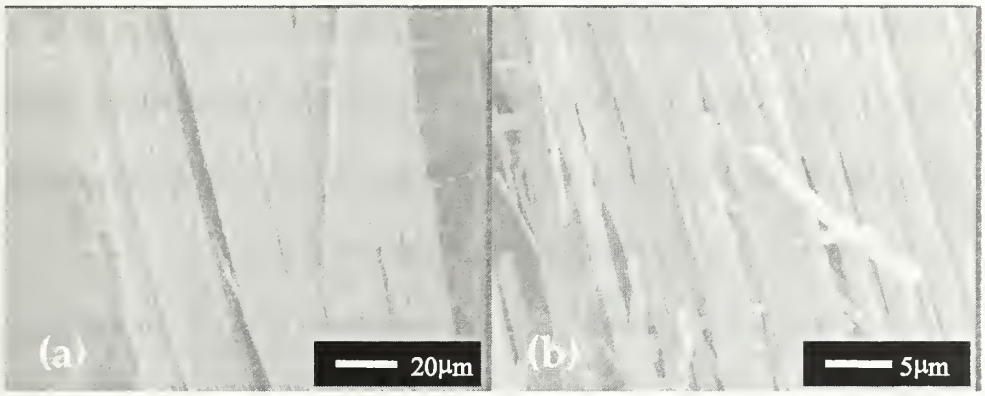

Figure 5.8: (a-b) Field emission scanning electron microscopy image of electrospun yarn carbonized to 2000°C in helium

expansion between the radial and hoop transverse direction of the fiber and can cause cracks to develop parallel to the fiber axis that degrade the fiber strength. Chen et al.[19] examined the axial residual stresses in commercial high modulus carbon fiber. Chen removed successive surface layers of carbon fibers by gaseous oxidation, wet oxidation, and ion milling and measured the contraction of the fiber segment in comparison to a reference fiber. As the compressive surface layers were removed during the sputtering, the fiber shrank; the fiber was observed to arc as it contracted. A measurement of the separation distance between the initial reference position and the arced fiber gave an indirect measure of the residual stress of the specimen fiber. Commercially available carbon fiber in a free state is straight and residual stresses within the fiber are balanced. As the surface layer on just one side of the fiber is ion milled away, the stresses within

the straight fiber are no longer balanced; the moment that is created will cause the fiber to curl and seek a state where the moment is again zero. The origin of residual stresses is postulated to predominantly arise during cooling from the final processing temperature. Chen heated curled fibers, which had been produced by sputtering away one side only of a fiber, and the fibers were observed to partially straighten. If the curl is due to differential contraction produce on cooling form the graphitization temperature, the differential strain within the fibers, upon heating, should decrease, which would result in a straightening of the curled fibers.

Graphite fibers exhibit either an onion-skin or a radial arrangement of the graphite basal planes. Allen[20] estimated the stress state in a model graphite fiber of perfect radial and onion-skin morphology. Allen determined that in axial tension the onion-skin morphology is characterized by tensile hoop and radial stresses; the fiber center having a value of 0.64% of the applied axial stress. At the fiber surface the radial stress is zero while the hoop stress is compressive (relative magnitude of 2.8%). The radial morphology exhibits a tensile hoop stress at the fiber surface of 0.0052 σ_z, with zero radial stress; both hoop and radial stresses at the fiber center approach infinite compression.

While high surface compression minimizes the effect of surface flaws, axial tensile stress in the interior of the fiber decreases the strength of the fiber by causing fracture to initiate at flaws in the interior rather than at the surface. Transverse residual stresses generate micro-cracks parallel to the fiber axis, which results in a fibrous fracture surfaces. Modifications of the residual stress pattern might allow increased tensile and/or compressive strengths to be obtained in high modulus carbon fibers.

Additionally a modulus gradient exists within carbon fibers; the modulus of the surface layers is about twice the average fiber modulus where the interior modulus is only about one half the average. The modulus gradient suggests that higher modulus carbon fibers could be produced if the modulus at the interior of these fibers could be increased. Carbon fibers with a ribbon-like morphology, or oval cross section, would have a residual stress pattern differing greatly from that of cylindrical carbon fiber with a circular cross section. The morphology of carbon nanofibers, prepared from electrospun precursor, are expected to contain low residual stress induced during cooling due to their ribbon-like morphology. The strength and modulus of these nanofibers may surpass those of cylindrical nanofibers prepared by different methods.

5.5.2 Graphitic Structure

The resultant yarn is characterized by Raman spectroscopy and WAXD; the value of R suggests that the translational order within the graphite sheets is significantly interrupted (Table 5.12). The lattice parameters and crystal structure determined by WAXD is distinctive of carbon fibers (Figure 5.9 and Table 5.13). There is improvement of the packing of the graphite layers in the c-direction with increased carbonization temperature (2000°C), although the scattering intensity is too weak for determination of the crystallite size in the a-direction (L_a). Due to the entangled and delicate nature of these yarns, it is not possible to determine their mechanical properties.

Table 5.12: The ratio of integrated intensities of the partially stabilized, electrospun yarn carbonized to 2000°C determined by Raman spectroscopy

Carbonization Temp.	I_D/I_G of Partially stabilized, electrospun yarn
2000°C	1.58 ± 0.01

The effect of oxidative exposure time on the mechanical properties of electrospun precursor nanofibers carbonized to 2000°C is examined. Previously stabilized yarn is subjected to a further, extended, stabilization step; the partially stabilized yarn, held at constant length on a metal frame, is heated in a Fisher Scientific Isotemp Oven in air from room temperature to 250°C in 1h, held at 250°C for 2h, ramped to 280°C in 1h, and held at 280°C for 2h. The stabilized yarn is then pyrolysized at 2000°C in helium, as described previously. The yarn did not shrink during the pyrolysis; the resultant yarn is black and it contains its original fiber morphology (Figure 5.10).

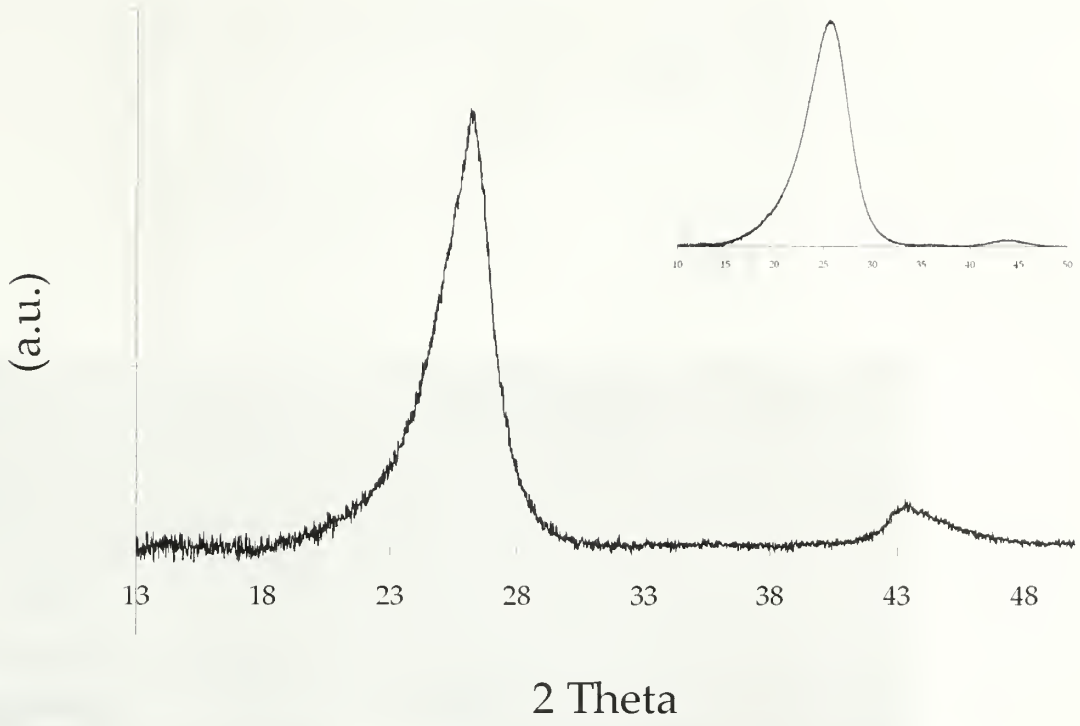

Figure 5.9: Intensity versus 2θ profile of a wide angle X-ray diffraction (WAXD) pattern of commercial carbon fiber (upper right) and of that of a nanofiber yarn carbonized to 2000°C (center) in helium

Table 5.13: Lattice parameters of a nanofiber yarn carbonized to 2000°C in helium as determined by the Bragg and Scherer equation from a wide angle X-ray diffraction (WAXD) pattern

$d_{(002)}$ (nm)	L_c (Å)	No. of graphite sheets (L_c/d)	L_a (Å)
0.341	35	10.2	7.2

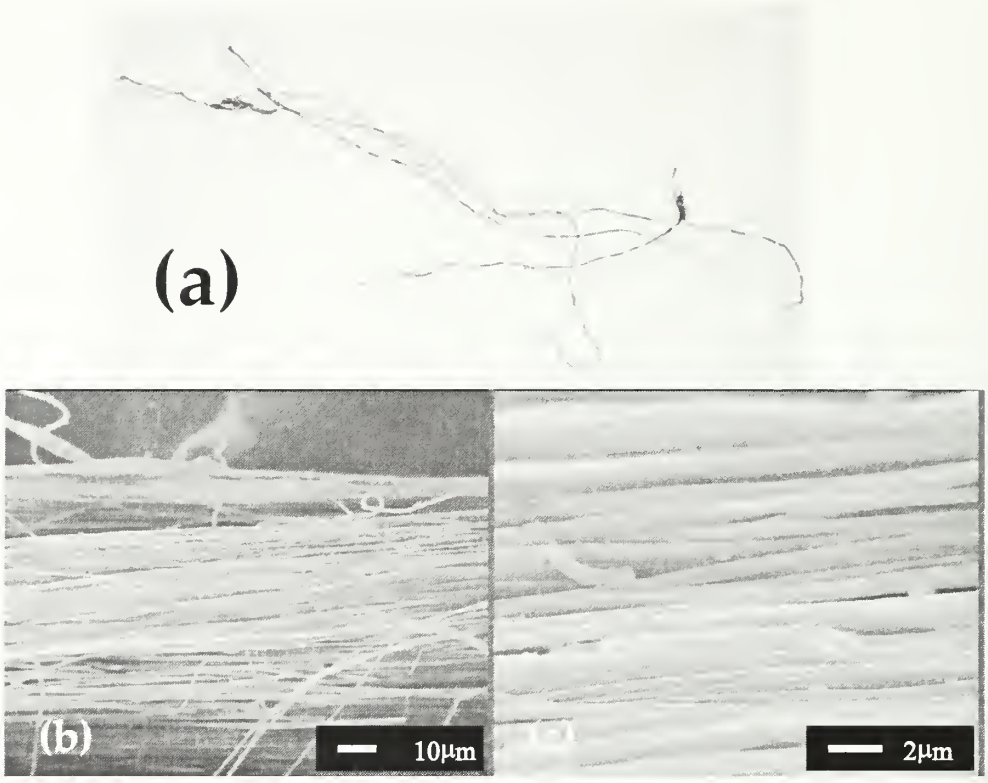

Figure 5.10: (a) Photograph and (b-c) Field emission scanning electron microscopy (FESEM) image of electrospun yarn batch stabilized to 280°C in air and carbonized to a final temperature of 2000°C in helium

The resultant yarn is characterized by Raman spectroscopy and WAXD; the ratio *R* of the resultant yarn shows improved translational order within the graphite sheets (with further stabilization) (Table 5.14). The lattice parameters improved with increased stabilization temperature and exposure time (Table 5.15); the crystal structure observed by WAXD pattern is distinctive of carbon fibers (Figure 5.11 and Table 5.15). It is concluded that the extended stabilization time and the increased carbonization temperature result in the improvement of the structure and properties of the resultant carbon nanofiber. The resultant yarns are markedly less brittle than those prepared using partially stabilized yarn, although the mechanical properties are still too weak for measurement by our equipment.

Table 5.14: The ratio of integrated intensities of the fully stabilized, electrospun yarn carbonized to 2000°C determined by Raman spectroscopy

Carbonization Temp.	I_D/I_G of Stabilized, electrospun yarn
2000°C	1.3 ± 0.03

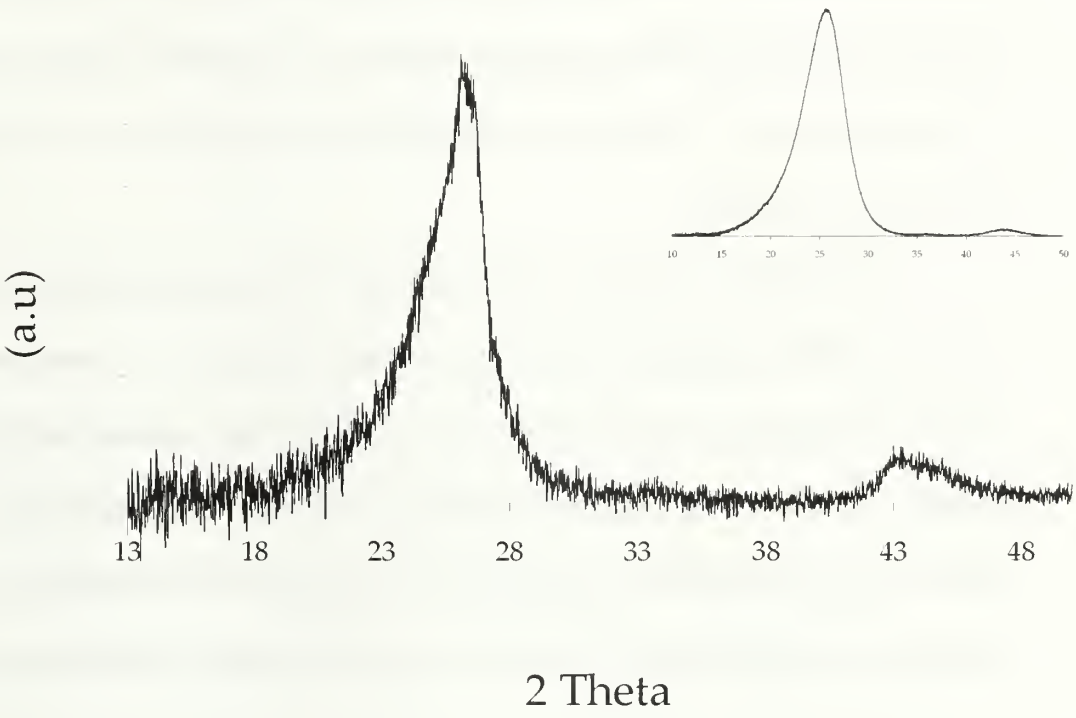

Figure 5.11: Wide angle X-ray diffraction of commercial carbon fiber (upper right) and that of fully stabilized, electrospun nanofiber yarn carbonized to 2000°C (center)

Table 5.15: Lattice parameters of the stabilized, electrospun yarn carbonized to 2000°C determined by wide angle X-ray diffraction (WAXD)

$d_{(002)}$ (nm)	L_c (Å)	No. of graphite sheets (L_c/d)	L_a (Å)
0.341	34	10	7.6

5.6 Conclusions

In the production of Polyacrylonitrile (PAN) based carbon fibers, the stabilization process, transforming the PAN material into a nonmeltable and inflammable fiber, is an important technological step that essentially influences the

properties of the resultant carbon fiber. The stability in the structure of the PAN is achieved through the conversion of an open chain structure into a closed chain or aromatic structure, and aromaticity is developed. Stabilization conditions are determined for electrospun PAN nanofiber yarns and the effect of the conditions on the structural characteristics and mechanical properties of the resultant carbon nanofiber yarn are determined. The effect of partial stabilization on the properties of the resultant carbon fiber is examined.

Carbonization temperature influences the structure and mechanical properties of carbon nanofibers prepared from electrospun precursor material. It is concluded that improved stabilization and high temperature ($\leq 2000°C$) carbonization results in carbon nanofibers with improved mechanical properties. It is, also, suggested that the deficiencies in the mechanical properties of the presented carbon nanofibers are a result of batch processing and loss of molecular orientation during the stabilization process.

5.7 References

(1) Fitzer, E.; Frohs, W. *Chem. Eng. Technol.* **1990**, *13*, 41.

(2) 'Carbon fibers electrical conductivity found to offer new uses.' *Composites News* **1998**, 3.

(3) Chun, I.; Reneker, D.H.; Fong, H.; Fang, X.; Deitzel, J.; Beck Tan, N.; Kearns, K. *J. Adv. Mater.* **1999**, *31*, 36.

(4) Fitzer, E.; Manocha, L.M. Carbon Reinforcements and Carbon/Carbon Composites. Springer-Verlag, New York (**1998**), Ch. 1.

(5) Mochida, I.; Yoon, S.H.; Takano, N.; Fortin, F.; Korai, Y.; Yokoawa, K. *Carbon* **1996**, *34*, 941.

(6) Wang, Y.; Serrano, S.; Santiago-Aviles, J.J. *Synthetic Metals* **2002**, *138*, 423.

(7) (a) Tuinstra, F.; Koenig, J.L. *J. Chem. Phys.* **1970**, *53*, 1126. (b) Knight, D.S.; White, W.B. *J. Mater. Res.* **1989**, *4*, 385.

(8) Kim, C.; Park, S.H.; Cho, J.I.; Lee, D.Y.; Park, T.J.; Lee, W.J.; Yang, K.S. *J. Raman. Spectrosc.* **2004**, *35*, 928.

(9) (a) Wang, Y.; Santiago-Aviles, J.J.; Furlan, R.; Ramos, I. *IEEE Transactions on Nanotchnology* **2003**, *2*, 39. (b) Kim, C.; Yang, K.S. *Appl. Phys. Lett.* **2003**, *83*, 1216.

(10) (a) Park, S.H.; Kim, C.; Choi, Y.O.; Yang, K.S. *Carbon* **2003**, *41*, 2653. (b) Park, S.H.; Kim, C.; Yang, K.S. *Synthetic Metals* **2004**, *143*, 175.

(11) Dresselhaus, M.S.; Dresselhaus, G.; Pimenta, M.A.; Eklund, P.C. "Raman Scattering in Carbon Materials." Pelletier, M.J. Ed. Analytical Applications of Raman Spectroscopy. Blackwell Science, Inc., Malden, MA (**1999**), Ch. 9.

(12) (a) Uchida, T.; Shinoyama, I.; Ito, Y.; Kukuda, K. Proc. 10th Biennial Conf. On Carbon, Bethlehem, PA (**1971**), p. 31. (b) Tsai, J.S. *J. Mater. Sci. Lett.* **1994**, *13*, 1162.

(13) Frigge, K.; Buchtemann, A.; Fink, H.P. *Acta Polymerics* **1991**, *42*, 322

(14) Fitzer, E.; Manocha, L.M. Carbon Reinforcements and Carbon/Carbon Composites. Springer-Verlag, New York (1998), Ch. 1.

(15) Shimada, I.; Takahagi, T.; Fukuhara, M.; Morita, K.; Ishitani, A. *J. Polym. Sci. Part: A* **1986**, *24*, 1989.

(16) Peebles, L.H. *J. Polym. Sci. Part: A-1* **1967**, *5*, 2637.

(17) Tsai, J.S. *SAMPE Quarterly* **1993**, *Apr.*, 21.

(18) Babu, V.S.; Seehra, M.S. *Carbon* **1996**, *34*, 1259.

(19) Chen, K.; LeMaistre, C.W.; Wang, J.H.; Diefendorf, R.J. *Polymer Preprints. Division of Polymer Chemistry, American Chemical Society* **1981**, *22*, 212.

(20) Allen, S.R. 'Mechanical and Morphological Correlation in Poly(p-phenylene benzobistrhiazole) Fibers.' Thesis, University of Massachusetts Amherst (**1983**), Chapter 3.

CHAPTER 6

CONTINUOUS PROCESSING

6.1 Introduction

A major limitation on the conversion of Polyacrylonitrile (PAN) precursor fiber into carbon arises from the slow oxidation step (stabilization); it is essential to stabilize the oriented structure of the fiber against fusion during the high temperature treatment (carbonization). The time required for stabilization is diffusion limited; the rate of oxidation is affected by the heating rate, temperature, environment, copolymer composition, and precursor fiber diameter. A small diameter precursor fiber (fine filament) is considered more suitable for the preparation of carbon fiber than a large diameter fiber, because it requires less time for oxidative stabilization[1].

Electrospun precursor nanofibers with diameters in the range of several 10s to 100s of nanometers should be ideal for the preparation of high strength carbon nanofibers. Advancement of the electrospinning method is necessary in order to prepare bundles of aligned electrospun yarn, which can undergo continuous processing. Continuous processing of precursor tows, or yarns, would alleviate the limitations imposed by batch processing methods on the mechanical properties of the resultant nanofiber yarn. Particularly, continuous oxidation would be beneficial to the final structure and properties of the carbon yarn. The continuous method of oxidation allows for the precursor yarn to be held under constant tension during the stabilization process. During continuous oxidation, a length of yarn is unwound from one roller, drawn through a preheated tube furnace in air, and collected onto another roller. Loss of

preferred orientation within the nanofiber yarn is minimized and, potentially, may be enhanced during oxidative processing.

6.2 History

The random orientation of electrospun fiber in the form of nonwoven webs, or mats, is acceptable for use in some applications, such as: filtration, wound dressings, and tissue scaffolding. However, to expand the use of electrospun fiber into commercial fiber for textile applications, researchers need to provide a mechanism to obtain a continuous single nanofiber, or uniaxial fiber bundle[2]. Researchers have attempted to obtain aligned electrospun fibers by various approaches, including: spinning onto a rotating drum[2a] or onto the sharp edge of a thin rotating wheel[2b], introducing an auxiliary electrode or electrical field[2c, 2d], rapidly oscillating a grounded frame within the jet[2e], and using a metal frame as a collector[3f] (as described in Section 3.2). Various degrees of fiber alignment are obtained by these approaches, although only relatively short tows of aligned fiber is obtained.

Presently there is a need to advance the electrospinning technique and develop a method to prepare continuous electrospun fiber, or yarn. The present author has shown that unidirectional tows of electrospun nanofibers can be linked and twisted, allowing for the determination of the yarns' mechanical properties[4] (as described in Section 3.4.6 and 3.5). Ko et al.[5] manufactured continuous composite yarns of Poly(lactic acid) and Polyacrylonitrile (PAN) with single wall carbon nanotubes, but did not provide a detailed description of the process or the characteristics of the resultant yarn. Smit et al.[6] presented a technique to obtain continuous uniaxial fiber yarns by electrospinning

into a liquid reservoir collector. Polymer solution is electrospun into a shallow water bath containing a grounded collector electrode. Fibers form on the surface of the water; the fibers are drawn across the surface of the water and are hand fed onto a roller located outside of the bath. The yarn is then drawn with the use of a motor and collected on the roller; the lab-scale process can be used to prepare 180m of yarn per hour. Smit characterized the collected fiber and yarn morphologically, but not mechanically. Kim et al.[7] described a method to prepare continuous lengths of Poly(ε-caprolactone) from solution using a multi-head spinneret (Scheme 6.1). Many filaments are simultaneously produced and they are drawn toward a

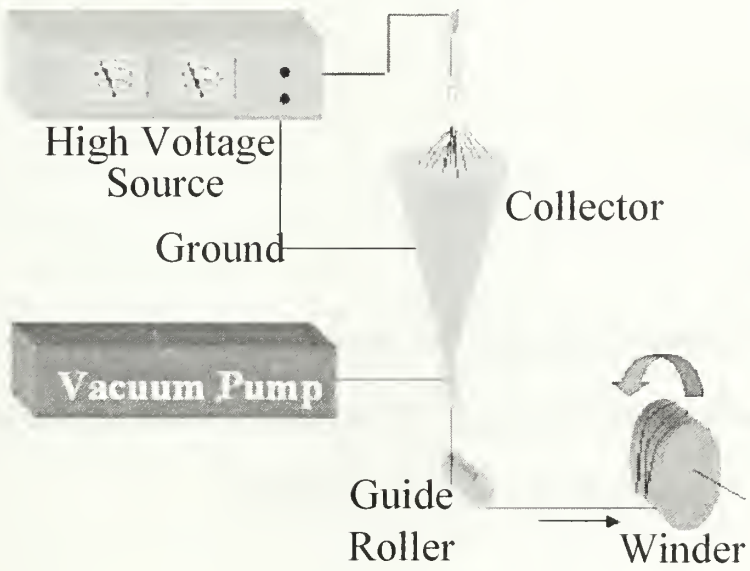

Scheme 6.1: Diagram the altered of the electrospinning apparatus that consists of a multi head spinneret, a grounded conical collector with rotary vacuum pump, guide roller and winder

conical collector (following the induced electric field). The filaments are combined into a multifilament yarn and directed through the conical collector towards a guide roller with the application of vacuum. A slight twist is induced in the yarn and the yarn is collected onto a rotating winder[7]; the spinning speed is 35m/min. The surface and core

morphology of the collected Poly(ε-caprolactone) yarns are examined. Kim et al., also, showed that the mechanical properties of these yarns are improved with high temperature drawing.

6.3 Proposal

In the present work unidirectional, continuous yarns of Polyacrylonitrile (PAN) nanofibers are post-stretched above the glass transition temperature, Tg, of the polymer and stabilized continuously. The yarns are carbonized in batch at elevated temperatures and the effect of continuous processing on the properties of the resultant yarn is determined.

6.4 Experimental

6.4.1 Materials

Polyacrylonitrile copolymer (PAN) received from an industrial source and dimethylformamide (DMF) from Sigma Aldrich Co. are used to prepare solutions for electrospinning, as described previously (Section 4.4.1).

6.4.2 Electrospinning Set-up

Through a collaborative effort with Dr. H.Y. Kim of Chonbuk National University, South Korea, a continuous electrospun yarn of Polyacrylonitrile nanofibers is prepared. The basic electrospinning apparatus is altered to include a multi head spinneret, a grounded conical collector with rotary vacuum pump, guide roller and winder, as described earlier (Section 6.2 and Scheme 6.1).

6.4.3 Post-treatment

The electrospun yarn is stretched, or drawn, in batch in order to determine the limitations of the yarn due to yarn structure. The results of batch stretching are evaluated and manipulated in order to design and construct a continuous stretching set-up.

6.4.3.1 Batch Stretching

Multiple (approximately 8 to 10 yarns) yarns are mounted simultaneously with a gauge length of 100mm, similar to those described previously (Section 3.4.7), and drawn in batch with a strain rate of 10%/min, as described previously (Section 4.4.3).

6.4.3.2 Continuous Stretching

Tows of the electrospun yarn are drawn continuously in boiling water to various draw ratios. The continuous stretching set-up includes: a tank filled with preheated deionized water and a heater, an unwinding and winding spindle, and a resistance wheel (Scheme 6.2). A length yarn is wound onto the unwinding spindle and submerged into the tank. The unwinding spindle is connected to a rotating shaft and a resistance wheel, located outside of the tank, is attached to the other end of the shaft. The winding spindle, partially submerged and connected to a 58rpm motor, draws the yarn from the unwinding wheel through the heated water. Resistance is applied to the yarn; air pressure, applied to the resistance wheel, is used to induce a back tension on the yarn as it is drawn. The tension is calibrated; the force required to impose a particular draw ratio on the yarn is determined by

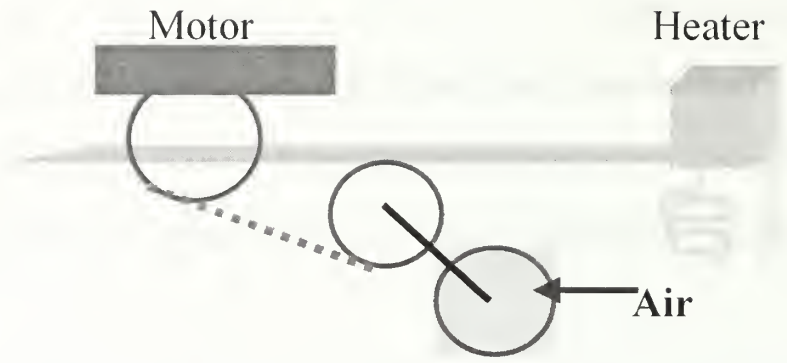

Scheme 6.2: Continuous yarn stretching apparatus consisting of a heater and tank, a winding and unwinding spindle, and a resistance wheel

stretching a single yarn in batch while monitoring the applied force versus elongation (Table 6.1). The draw ratio experienced by the yarn is determined by mass.

Table 6.1: Strain (%) as a function of gram force, g^f (g^f = N(1000g/kg)/(9.8m/s^2)), required to draw continuous, electrospun Polyacrylonitrile (PAN) yarn

Strain (%)	100	80	50
Force (g^f)	19	15	9

6.4.4 Stabilization

Polyacrylonitrile (PAN) yarn with a draw ratio of 1.5x, prepared as described previously (Section 6.4.3.2), is stabilized (oxidized) continuously in a Lindburg 55035 tube furnace (Scheme 6.3). The drawn yarn is wound onto an unwinding spindle, drawn through the preheated tube furnace (purged with preheated air), and collected onto a winding spindle at the opposite end of the furnace; the residence time is 13min. The samples are heated in batch to avoid unnecessary complexities involving heating rates.

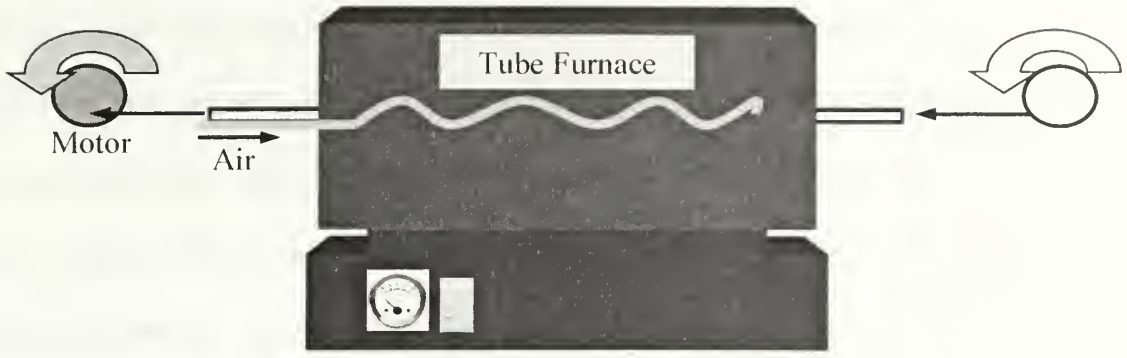

Scheme 6.3: Continuous stabilization apparatus consists of a tube furnace, and a unwinding and a winding wheel. A borosilicate tube with steel tubing (gas line) coiled around it is inserted into the furnace and guides the yarn through the furnace

6.4.4.1 IR spectroscopy

Attenuated total reflectance infrared spectroscopy (ATR IR) is used to monitor the extent of cyclization and oxidation during stabilization process so to determine the ideal stabilization temperatures, as described previously (Section 5.4.3.1). A Jobin Yvon Horiba LabRam-IR HR800 is used; the 632.8nm line of a HeNe gas laser is used for excitation. Spectral resolution is $4cm^{-1}$ near the Rayleigh line. A CCD detector is used and the exact band positions are calibrated to polyethylene standards.

6.4.5 Carbonization

Through a collaborative effort with Dr. D. Edie and Dr. A. Naskar in the Chemcial Engineering department of Clemson University, South Carolina, stabilized yarn is carbonized to 2000°C under helium (He) in an Astro Carbonization Furnace (Model 1000A) (maximum furnace temperature of 2400°C), as described previously (Section 5.5). The chamber is oriented horizontally, so samples may be stacked. The samples are wound around Grafoil tubes and loaded into the chamber; the chamber is

purged with He to an over pressure of 5psi and vacuum evacuated twice. The furnace chamber has a constant overpressure of 5psi of He during the heat treatment; the pressure is regulated by equilibrated gas inlet and outlet flows. The furnace is manually heated to 425°C and then subjected to the following heating profile: ramp to 1700°C in 1h, ramp to 2000°C in 30min, and held at 2000°C for 30min. An infrared pyroprobe is used to monitor the temperature. At completion of the heating program, a water jacket is used to cool the chamber.

6.4.5.1 Raman Scattering

Carbonized yarn is examined by Raman scattering using a laser confocal Raman spectrometer (Jobin Yvon HORIBA LabRam HR 800 Raman microscope) with CCD detector (spectral resolution is kept at $1cm^{-1}$) to characterize the structure of the carbon fiber, as described previously (Section 5.4.4.1).

6.4.5.2 Wide angle X-ray diffraction

The lattice parameters of carbonized yarn are determined from wide angle X-ray diffraction (WAXD) patterns collected with a PANanlytical X'pert Pro powder diffractomer, as described previously (Section 5.4.5). The interplanar spacting $d_{(002)}$ and the crystalline dimensions L_a and L_c are calculated using Equation 5.2, 5.3, and 5.4.

6.4.6 Microscopy

Stabilized and carbonized yarn is observed by field emission scanning electron microscopy (FESEM), as described previously (Section 2.5.5).

6.4.7 Mechanical Properties

The mechanical behavior of the stabilized yarn is examined using an Instron 5564 and Instron 5800, as described previously (Section 3.4.7). The cross-sectional area of the laboratory prepared yarns is calculated from the denier and density; the density of the stabilized yarn is assumed to be 1.4g/ml, as described previously (Section 5.4.7). The initial modulus, ultimate strength, and strain at break is measured.

The ultimate strength of the carbonized yarn is measured; mounted samples with a gauge length of 6mm tested in tension with a crosshead speed of 0.6mm/min (strain rate of 10%/min). The density of the carbonized yarn is assumed to be 1.78g/ml from the literature.

6.5 Results and Discussion

Continuous, electrospun Polyacrylonitrile (PAN) yarn with a diameter of 68 $\pm$ 5μm, as determined by laser diffraction (Section 2.5.4), and a denier of 14.8 (Section 2.5.4) is evaluated as a precursor material for the production of carbon nanofibers. The yarn consists of entangled fibers with an average diameter of 220 $\pm$ 0.05nm, as determined by field emission scanning electron microscopy (FESEM) (Figure 6.1). The ultimate strength of yarn, as received, is approximately half of that of the previously described lengths of aligned electrospun yarn (described in Section 4.5) without post-treatment (Table 6.2). The modulus of the two electrospun yarns is comparable.

Batch stretching of the yarn in boiling water is completed in order to improve the molecular orientation within the yarn and subsequently improve the its' mechanical properties. The yarn is drawn in batch to a maximum of 100% strain; at a draw ratio

greater than 2x, the results are not reproducible. The yarn tends to break at a maximum of 140% strain. The ultimate strength and modulus of the yarn is determined as a function of percent strain (Figure 6.2 and Table 6.3). The initial modulus and ultimate strength of the yarn increases with draw ratio from 2.9 ± 0.3 GPa and 62 ± 16 MPa at zero percent strain to 4.9 ± 0.6 GPa and 240 ± 48 MPa at 100% strain, respectively. The ultimate strength, modulus and strain at break at a draw ratio of 2x is comparable to those of previously prepared aligned electrospun yarn: 253 ± 47 MPa, 4.8 ± 0.5 GPa, and 11± 1%, respectively (as described previously in Section 4.5).

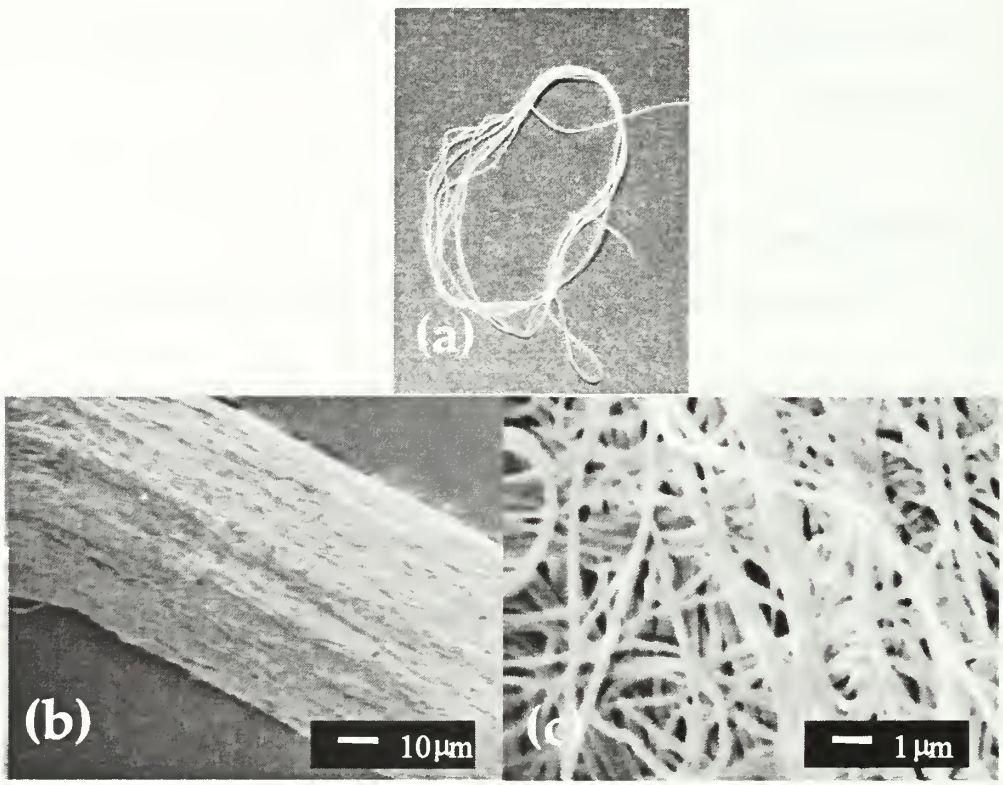

Figure 6.1: (a) Photograph and (b-c) Field emission scanning electron microscopy image (FESEM) of a continuous, electrospun yarn of Polyacrylonitrile (PAN)

Table 6.2: The ultimate strength, modulus, and strain at break of a continuous, electrospun Polyacrylonitrile (PAN) yarn with a denier of 14.8

Ultimate Strength (MPa)	Modulus (GPa)	Ultimate Strength (g/denier)	Modulus (g/denier)	Strain at Break (%)
62 ± 16	2.9 ± 0.4	0.6 ± 0.2	30 ± 3	18 ± 9

The use of a continuous filament, or yarn, allows for continuous processing methods. Continuous processing of materials results in improved reproducibility of conditions experienced and of the resultant structure and properties between samples relative to those produced by batch methods. The yarn is drawn continuously to a maximum of 50% strain; at a draw ratio greater than 0.5x, the results are not reproducible. The yarn tends to break when stretched continuously to a draw ratio greater than 1.5x. The surface morphology of the continuously post treated yarn shows that the overall alignment of the fibers relative to

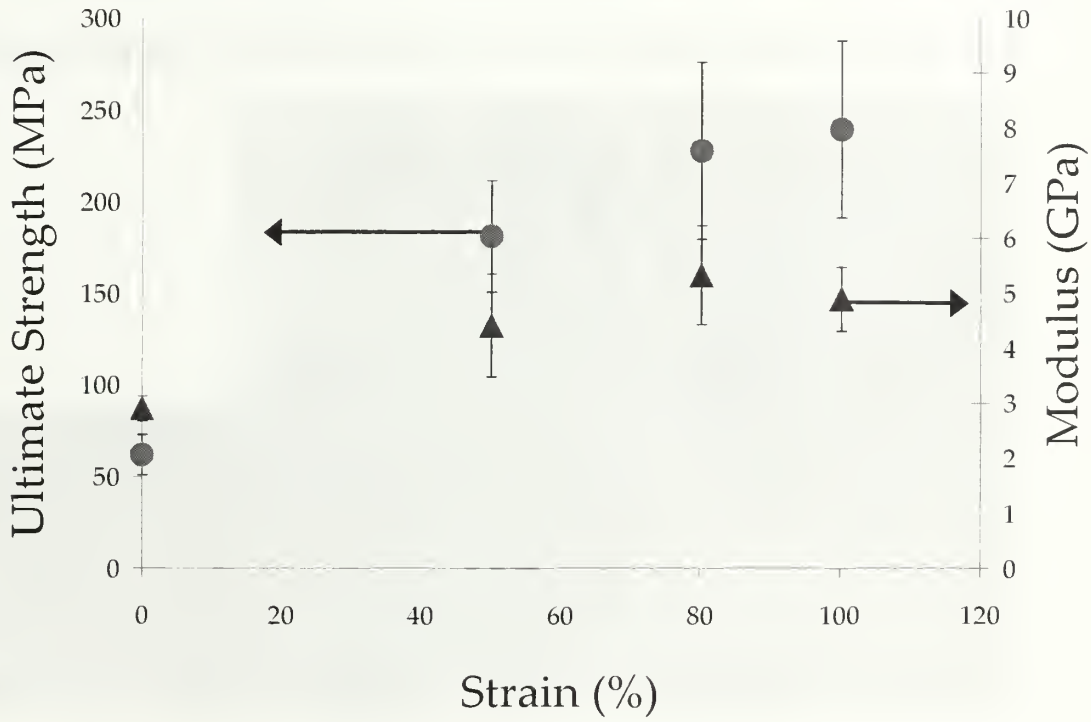

Figure 6.2: The ultimate strength (MPa) (●) versus modulus (GPa) (▲) as a function of percent draw (%) of continuous, electrospun Polyacrylonitrile (PAN) yarn drawn in boiling water at a strain rate of 10%/min

Table 6.3: The ultimate strength (MPa) versus modulus (GPa) as a function of percent draw (%) for continuous, electrospun Polyacrylonitrile (PAN) yarn

Draw (%)	Ultimate Strength (MPa)	Modulus (GPa)	Denier (g/9000m)	Ultimate Strength (g/denier)	Modulus (g/denier)	Strain (%)
0	62 ± 16	2.9 ± 0.3	14.9	0.6 ± 0.2	30 ± 3	18 ± 9
50 ± 0.02	180 ± 31	4.4 ± 0.9	9.9	1.7 ± 0.3	41 ± 7	10 ± 2
80 ± 0.02	228 ± 33	5.3 ± 0.9	8.2	2 ± 0.4	51 ± 9	9.5 ± 1
100 ± 0.07	240 ± 48	4.9 ± 0.6	7.4	2.2 ± 0.5	47 ± 5	9.1 ± 1

the yarn axis improves with increased stretching, although the alignment is not optimum (Figure 6.3). The ultimate strength and modulus of the of yarn increases with percent strain (Figure 6.4 and Table 6.4); the strength and modulus of a yarn stretched continuously to a draw ratio of 1.5x is 170 ± 18MPa and 5.9 ± 0.8GPa, respectively.

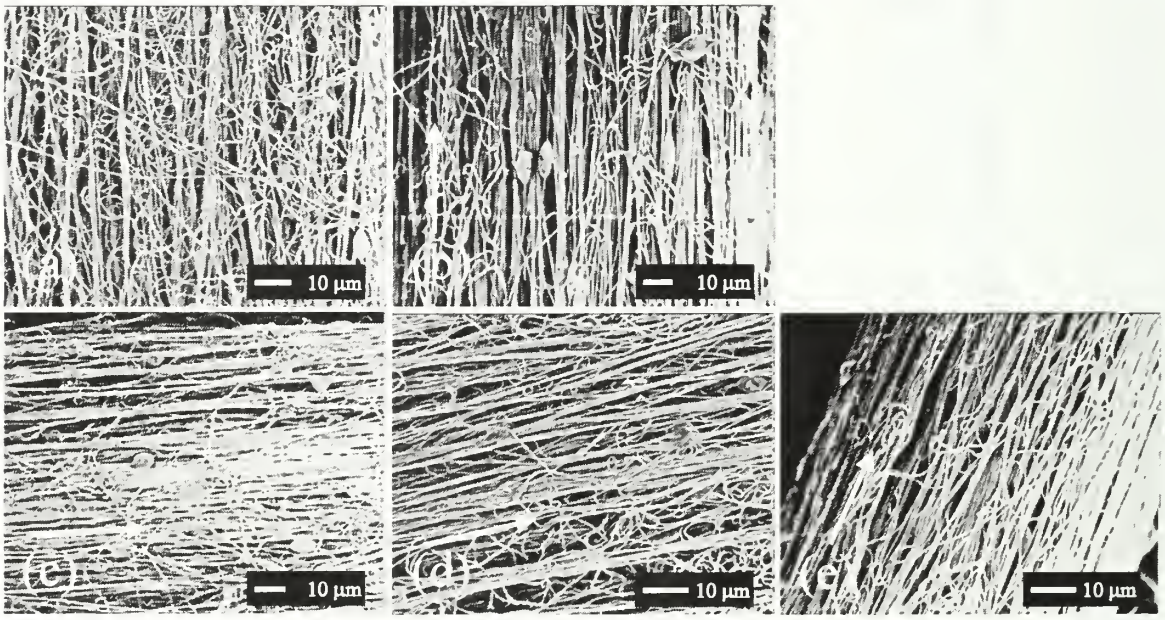

Figure 6.3: Field emission scanning electron microscopy images (FESEM) of the surface of continuously stretched, electrospun Polyacrylonitrile (PAN) yarn as a function of percent strain: (a) 0% (virgin yarn), (b) 23%, (c) 34%, (d) 38%, and (e) 50%. The superimposed arrows describe the direction of draw along the yarn axis

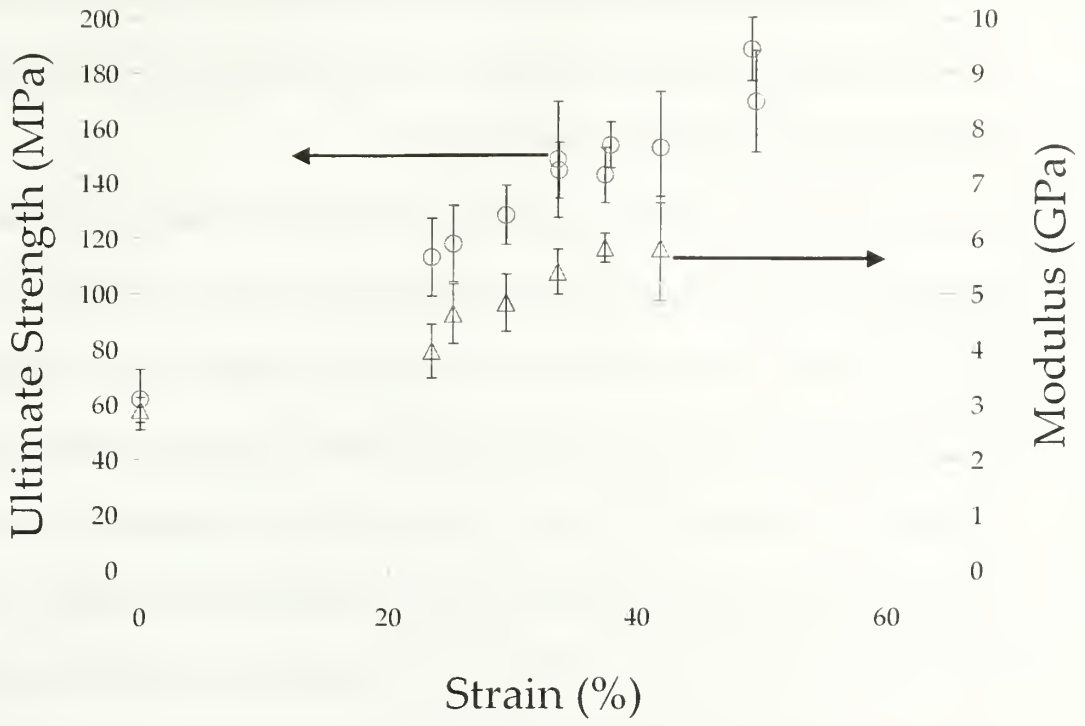

Figure 6.4: The ultimate strength (MPa) (●) versus modulus (GPa) (▲) as a function of strain (%) of continuous, electrospun Polyacrylonitrile (PAN) yarn drawn in boiling water with back tension (air pressure between 24-36psi). Draw ratio determined by weight

Table 6.4: Ultimate strength, modulus and strain at break of continuously drawn electrospun Polyacrylonitrile (PAN) yarn by continuous stretching

Draw (%)	Ultimate Strength (MPa)	Modulus (GPa)	Denier (g/9000m)	Ultimate Strength (g/denier)	Modulus (g/denier)	Strain (%)
0	62 ± 11	2.9 ± 0.3	28	0.6 ± 0.2	30 ± 3	18 ± 9
23	113 ± 14	3.9 ± 0.5	22	1.1 ± 0.1	38 ± 4	6.3 ± 1.4
29	128 ± 11	4.8 ± 0.5	20	1.2 ± 0.1	47 ± 5	7 ± 1.4
38	153 ± 8	5.5 ± 0.7	18	1.4 ± 0.2	50 ± 5	6.9 ± 1.1
50	170 ± 18	5.9 ± 0.8	14	1.6 ± 0.2	57 ± 8	5.8 ± 0.9

Regardless of the method of post treatment (stretching in batch or continuously), the strength of the yarn per percent draw is fixed; although, the modulus and ultimate strain are affected by the applied stretching method. The modulus of continuously

treated yarn is significantly greater than that of the batch treated yarn; the ultimate strain is half that of the batch treated yarn. The continuously post-treated yarns are stiffer than those post treated in batch (Table 6.3).

In commercial operations, carbon precursor fiber is drawn up to 14 times in steam at 100°C[8,9] prior to stabilization to generate the preferred orientation. It is only possible to stretch electrospun fiber 1.5 to 2 times their original length. The percent crystallinity of the virgin electrospun Polyacrylonitrile (PAN) yarn is compared to that of a laboratory prepared PAN fiber of similar composition; the percent crystallinity of the yarn and fiber is determined by wide angle X-ray diffraction (WAXD). A PAN precursor fiber with a diameter of 113μm, as measured by laser diffraction is prepared by dry-jet solution spinning in our laboratory from a 27.6wt% solution of PAN and DMF into a coagulation bath of 40:60 wt. H_20: DMF, as described in previously (Section 4.5). The X-ray diffraction (XD) pattern of the virgin yarn and fiber are collected using a Rigaku RU-H3R rotating anode x-ray diffractometer (Rigaku, Tokyo, Japan) equipped with a multiplayer focusing optic (Osmic Inc., type CMF23-46Cu8) and an evacuated Statton type scattering camera, as described previously (Section 4.4.6). Tricosane is used as a reference. The XD patterns exhibit two sharp diffraction peaks at $2\theta = 17°$ and 29° [10] superimposed on an amorphous background. The crystallinity of polymers is generally determined by separating the intensity contributions from the crystalline and the amorphous region of a diffractogram by subtracting that of a completely amorphous sample. Generally, it is not possible to successfully prepare a completely amorphous sample of PAN because it degrades before it melts; attempts to prepare a completely amorphous PAN sample from solution

by the method described by Matta et al.[11] failed. The empirical method developed by Hinrichsen[12] is used to determine the crystallinity of the electrospun PAN yarn and the dry jet solution spun PAN fiber (Table 6.5). The percent crystallinity of the electrospun yarn is less than that of the laboratory single fiber. Therefore, it is suggested that the inability to stretch the electrospun yarn to a greater extent is not due to high percent crystallinity within the yarn, but rather due to the inhomogeneity of the yarn. The results of batch processing show that the electrospun yarn may be stretched to a draw ratio of 2x, although this is not possible by the

Table 6.5: The percent crystallinity (%) of virgin, continuous, electrospun Polyacrylonitrile (PAN) yarn and of fiber prepared in the laboratory by dry-jet solution spinning into a coagulation bath of 40:60 DMF: H_2O without post treatment drawing

	Percent Crystallinity (%)
Continuous electrospun Polyacrylonitrile Yarn	67.13
Laboratory prepared single fiber	83.52

continuous post treatment method. The batch method stretches lengths (10cm) of multiple yarns simultaneously through a relatively stationary process (there is very little movement of the surroundings, i.e. water flow). As long as there are no severe defects, such as yarn diameter fluctuations, the fiber may be drawn to 100% strain. In the continuous stretching method, yarn with a length of upwards of several 10s of meters is stretched, or dragged, through moving water (which is being circulated through the tank by the heater), and wound onto a spindle. As the length of the yarn is increased the potential to come across segments of the yarn containing defects is increased; electrospun fibrous materials are notorious for being inhomogeneous. The continuous post treatment process is limited by the inhomogeneous nature of the yarn.

The post-treated yarn (drawn to 50% strain) is stabilized continuously in air. A stabilization process is developed, as described previously in Section 5.5. Attenuated total reflectance infrared spectroscopy (ATR IR) is used to monitor the progress of the cyclization and dehydrogenation reactions during the stabilization process (Table 6.6). Ratios of the bands describing the linear polyacrylonitrile copolymer and those referring the cyclized ladder structure of the stabilized material are compared (Table 6.7), as described previously (Section 5.4.3.1). Stabilization temperatures are determined by comparing these ratios to those of the commercial stabilized fiber (Table 6.8). The post treated yarn is stabilized at the following temperatures: 230°C, 250°C, and 260°C; the yarn is passed through a tube furnace preheated to each of the previous temperatures. The residence time in the furnace is 13min at each temperature.

When PAN is subjected to heat treatment, the polymer becomes colored and the intensity of the color depends upon the intensity and duration of the treatment. PAN yarn, stabilized according to the batch procedure described above, appears dark brown (Figure 6.5) similar to that observed of the previously described lengths of aligned electrospun yarn (Section 5.5). Additionally, the nanofiber morphology is maintained after stabilization; the yarns contain both fibers exhibiting cylindrical and 'beads-on-a-string' morphology, which is typical of electrospun fibers prepared from low viscosity solutions.

Table 6.6 Infrared absorbance of stabilized, electrospun Polyacrylonitrile (PAN) yarn with continuous post-treatment stretching under various conditions, reaction progress monitored by attenuated total reflectance infrared spectroscopy
(ATR IR)

														Ladder Structure	
	Post treatment								*C≡N*	*CH, CH_2*	*NC-C=*	*C=O aliphatic ketone*	*C=O conjugated ketone*	*C-N, C-C, NH*	*C=C-H*
Temp (°C)	220	230	240	250	260	270	290	cm^{-1}	2240	2940	2200	1725	1660	1595	810
	Polyacrylonitrile Fiber							Abs	0.11	0.01		0.11	1659 (DMF)		
Time (*min*)	13			13					0.088	0.088	0.007	0.034	0.069	0.05	0.1
	13			13		13			0.077	0.013	0.043	0.068	0.092	0.21	0.046
		13			13				0.086	0.009	0.047	0.07	0.094	0.18	0.030
		13			13	13			0.03	0.02	0.015	0.039	0.1	0.34	0.055
		13			13		13		0.01	0.006	0.008	0.023	0.074	0.21	0.041
		13			13			13	0.026	0.021	0.01	0.038	0.11	0.31	0.05

Table 6.7: Stabilized, electrospun Polyacrylonitrile (PAN) yarn after various high temperature post treatments monitored by attenuated total reflectance infrared spectroscopy (ATR IR). Accepted batch stabilization conditions are highlighted

	Post treatment								Ratio:				
Temp (°C)	**220**	**230**	**240**	**250**	**260**	**270**	**290**	**cm^{-1}**	***2240: 1595***	***1595: 2240***	***2940: 2200***	***2200: 2940***	***2940: 810***
Time	13		13					**Abs.**	1.77	1.13	13.2	0.076	0.88
(min)	13		13		13				0.37	0.6	0.3	3.31	0.28
		13		13					0.47	0.35	0.19	5.23	0.29
		13		13	13				0.096	1.69	1.36	0.73	0.38
		13		13		13			0.047	4.3	0.86	1.16	0.16
		13		13			13		0.085	1.94	1.89	0.53	0.42

Table 6.8: Commercially stabilized, Polyacrylonitrile fiber characterized by attenuated total reflectance infrared spectroscopy (ATR IR)

	C≡N	*CH, CH_2*	*NC-C=*	*C=O aliphatic ketone*	*C=O conjugated ketone*	*C-N, C-C, NH*	*C=C-H*	***Ratio:***				
cm^{-1}		**2940**	**2200**	**1725**	**1660**	**1595**	**810**	***2240: 1595***	***1595: 2240***	***2940: 2200***	***2200: 2940***	***2940: 810***
Abs	0.049	0.017	0.017	0.041	0.10	0.24	0.09	0.2	1.87	1.02	0.98	0.19

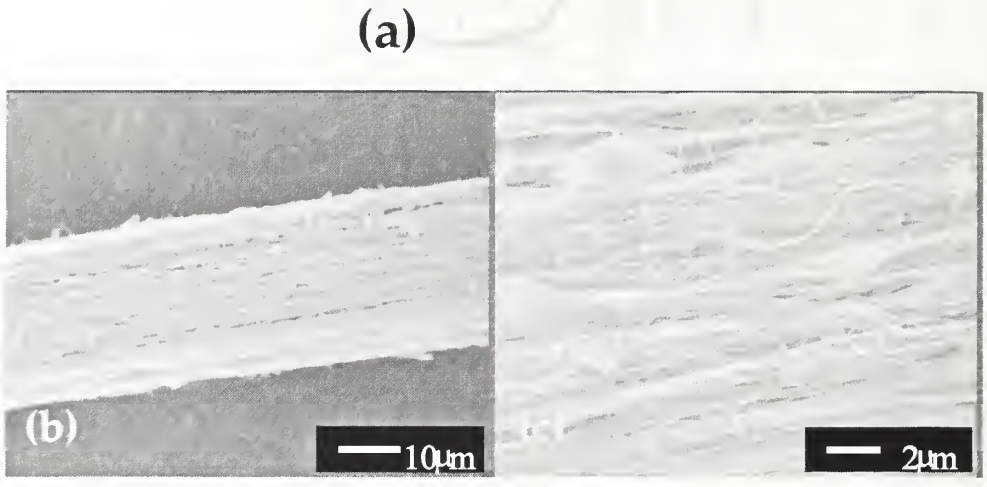

Figure 6.5: (a) Photograph and (b-c) field emission scanning electron microcopy (FESEM) images of electrospun Polyacrylonitrile (PAN) yarn (draw ratio of 1.5x) stabilized between 220°C and 260°C in air

The mechanical properties of the stabilized yarn are evaluated and compared to those of commercial stabilized fiber (Table 6.9). The ultimate strength of the stabilized yarn is 26% greater than that of the previously described lengths of aligned yarn (Table 5.7). The discrete lengths of aligned yarned, used previously to prepare carbon nanofiber yarn (Chapter 5), are held at constant length during stabilization while the present yarn is held under constant tension. The preferred orientation induced during the post treatment drawing is not lost during the continuous stabilization process, as it was previously during the batch process, rather it is maintained or improved. Therefore, it is not surprising that the mechanical properties of this yarn are greater than those of the lengths of yarn described earlier (Section 5.5). Additionally, the

commercial stabilized fiber is only 30% stronger than the stabilized yarn. The modulus of the stabilized yarn is greater than that of the commercial fiber; the electrospun yarn is stiffer than the commercial fiber prepared from the same precursor copolymer.

Table 6.9: Mechanical properties of stabilized, electrospun Polyacrylonitrile (PAN) yarn with an average denier of 11 and commercial stabilized, single fiber of denier 1.8. A density of 1.4g/ml is assumed

	Ultimate Strength (MPa)	Modulus (GPa)	Ultimate Strength (g/denier)	Modulus (g/denier)	Strain (%)
Stabilized, electrospun yarn	217 ± 30	8.7 ± 1.2	1.8 ± 0.2	71 ± 9	7.1 ± 2
Commercial stabilized single fiber	310 ± 45	7.4 ± 0.7	2.2 ± 0.3	54 ± 6.5	14 ± 2

After completion of the oxidation process, the yarn did not pass the flame test, as described previously (Section 5.5), and behaved similar to that of the aligned electrospun yarn described previously. The yarn shrank slightly and then glowed red when placed in the core of a flame. Although, the yarn only experienced partial stabilization, it is subjected to pyrolysis to a final temperature of 2000°C. The ratio of the integrated intensity of the disorder-induced (D) and the Raman-allowed (G) line $R = I_D/I_G$ is determined and compared to that of commercial carbon fiber prepared from the same copolymer precursor (Table 6.10). The value of R for the carbonized yarn and the commercial carbon fiber are the same, within the calculated error.

Table 6.10: The ratio *R* of electrospun Polyacrylonitrile (PAN) yarn carbonized to 2000°C in helium and commercial carbon fiber

	I_D/I_G of Stabilized, electrospun yarn
Carbonized, electrospun yarn	1.3
Commercial carbon fiber	1.13 ± 0.03

The wide angle X-ray diffraction (WAXD) pattern of the PAN based carbon nanofiber yarn is collected. A narrow peak at $2\theta = 24°$ and a broad peak at corresponding to the refection of the (002) layer of the graphite structure is observed, but a peak at $2\theta = 44°$ due to the (10) layer[13] is not observed (Figure 6.6) (presumably due to weak scattering). The lattice parameters of the carbonized yarn and the commercial stabilized yarn are determined (Table 6.11) and compared. Although, the carbonized yarn appears to exhibit the initial structural requirements to be termed 'carbon,' it is extremely delicate and brittle. It is not possible to evaluate the mechanical properties of the carbonized nanofiber yarn. The weakness of the resultant nanofiber yarn is due to incomplete stabilization and fusion of the nanofibers during high temperature pyrolysis (Figure 6.7). Incomplete oxidation of the fibers results in the degradation of the properties of the final carbonized yarn.

The post-treated, electrospun yarns are subjected to further stabilization, prior to high temperature carbonization. The partially stabilized yarns are wrapped around a Grafoil tube (held at constant length) and heated in a Fisher Scientific Isotemp Oven in air: to 250°C in 1h, held at 250°C for 2h, ramped to 280°C in 1h, and held at 280°C for 2h, as described previously (Section 5.5).The mechanical properties of the fully stabilized yarns are less than those measured for the same yarns prior to further oxidation (Table 6.9 and 6.12). It is expected that orientation within the nanofibers is lost during this further heating; the effect of constant tension versus fixed length during stabilization on the strength of theoxidized is observed. The denier of the yarn is observed to increase slightly with further heat treatment, suggesting that the density of the nanofibers and yarn increased.

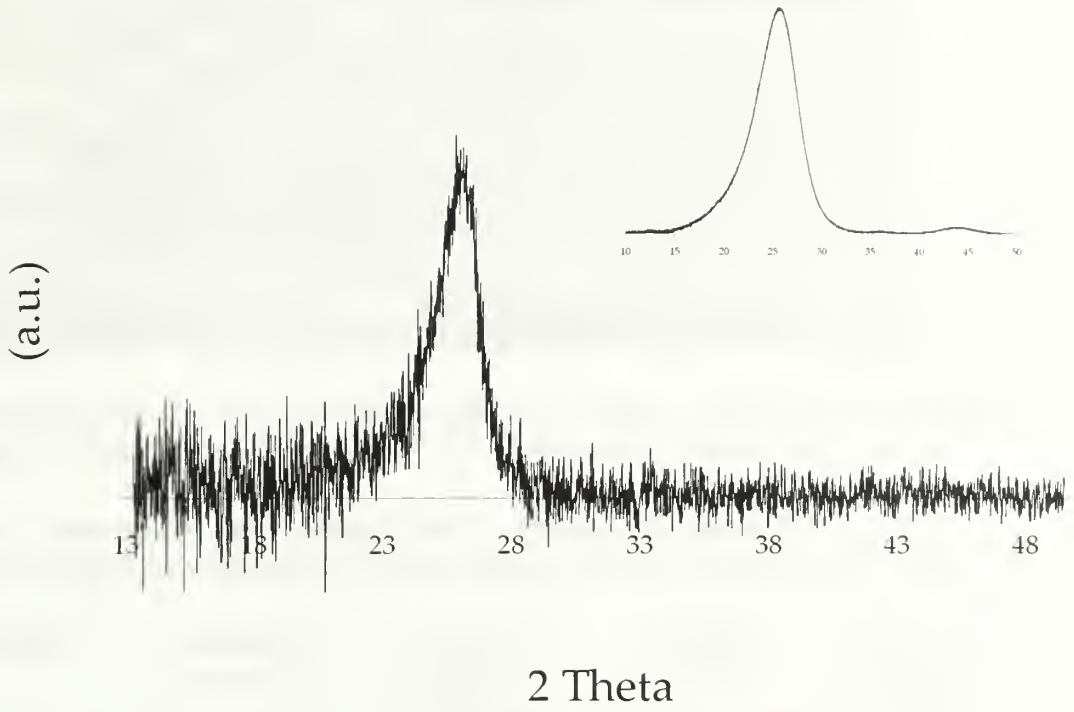

Figure 6.6: Wide angle X-ray diffraction (WAXD) of commercial carbon fiber (upper right) and that of electrospun Polyacrylonitrile (PAN) yarn carbonized to 2000°C (center) in helium

Table 6.11: Lattice parameters of electrospun Polyacrylonitrile (PAN) yarn carbonized to 2000°C in helium and commercial carbon fiber as determined by wide angle X-ray diffraction (WAXD)

	$d_{(002)}$ (nm)	L_c (Å)	No. of graphite sheets (L_c/d)	L_a (Å)
Carbonized, electrospun yarn	0.341	48	14	
Commercial carbon fiber	0.347	16.5	4.8	48.3

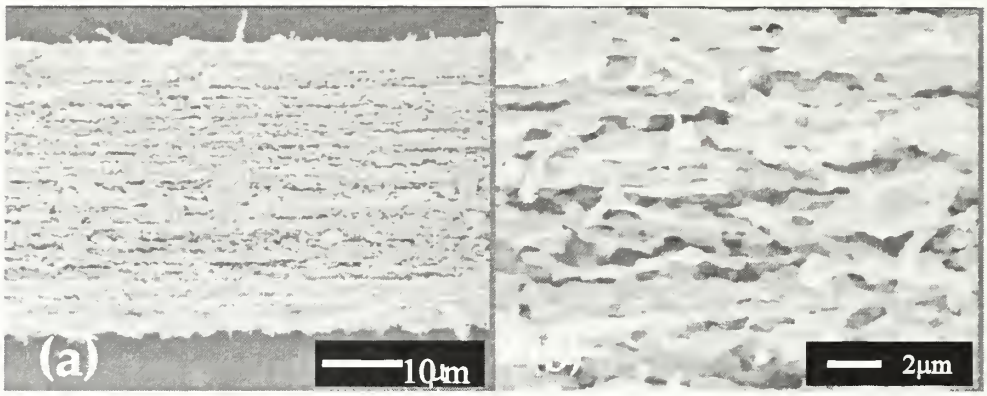

Figure 6.7: (a-b) Field emission scanning electron microscopy (FESEM) images of electrospun Polyacrylonitrile (PAN) yarn carbonized to 2000°C in helium

Table 6.12: Mechanical properties of electrospun, Polyacrylonitrile (PAN) yarn with an average denier of 13 stabilized to 280°C. A density of 1.4g/ml is assumed

Ultimate Strength (MPa)	Modulus (GPa)	Ultimate Strength (g/denier)	Modulus (g/denier)	Strain (%)
26 ± 1.7	4.13 ± 0.3	0.2	34 ± 1.6	$9.4 \times 10^{-5} \pm 7.8 \times 10^{-6}$

The stabilized yarn is pyrolyzed at 2000°C as described earlier. The resultant yarn is black; the fiber morphology is maintained after carbonization (Figure 6.8). The carbonized yarn is characterized by Raman scattering and wide angle X-ray diffraction (WAXD); the ratio of the integrated intensity of the disorder-induced (D) and the Raman- allowed (G) line $R = I_D / I_G$ increased with further oxidation. The average value of R suggests that the translational order within the nanofiber is equivalent to, if not greater than, that of the commercial carbon fiber prepared from the same precursor copolymer (Table 6.10 and 6.13). A narrow peak at $2\theta = 24°$ and a broad peak at $2\theta = 44°$ corresponding to the refection of the (002) and (10) layer[13] are observed (Figure 6.9). The lattice parameters of the carbonized yarn are determined (Table 6.14); the interplanar spacing suggests graphitic structure. The crystallite size in the c- and a-

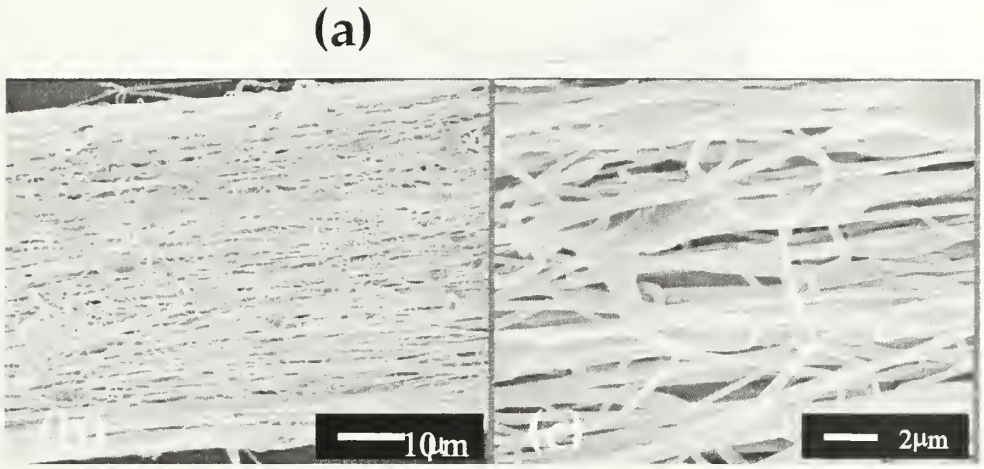

Figure 6.8: (a) Photograph and (b-c) Field emission scanning electron microscopy (FESEM) images of carbonized electrospun Polyacrylonitrile (PAN) yarn. Yarn underwent continuous post-treated, extended batch stabilization to 280°C, and finally batch carbonized to 2000°C

Table 6.13: The ratio *R* of carbonized electrospun Polyacrylonitrile (PAN) yarn determined by Raman scattering. Yarn underwent continuous post-treatement and extended batch stabilization to 280°C, prior to carbonization to 2000°C in helium

I_D/I_G of Stabilized, electrospun yarn
1.6 ± 0.01

direction is approximately twice that of the commercial carbon fiber (Table 6.11). The carbonized electrospun fiber is quite delicate; mounted samples with a minimal gauge length of 6mm were tested in tension. The ultimate strength of the carbonized nanofiber yarn is determined and compared to those of commercial carbon fiber (Table 6.15); the modulus cannot be compared due to the small test gauge length. The strength

of the carbon nanofiber yarn is approximately 5% of that of the commercial carbon fiber prepared from the same precursor copolymer. The poor properties are due to a loss of preferred orientation during the extended stabilization process and the poor orientaion of the nanofiber within the yarn.

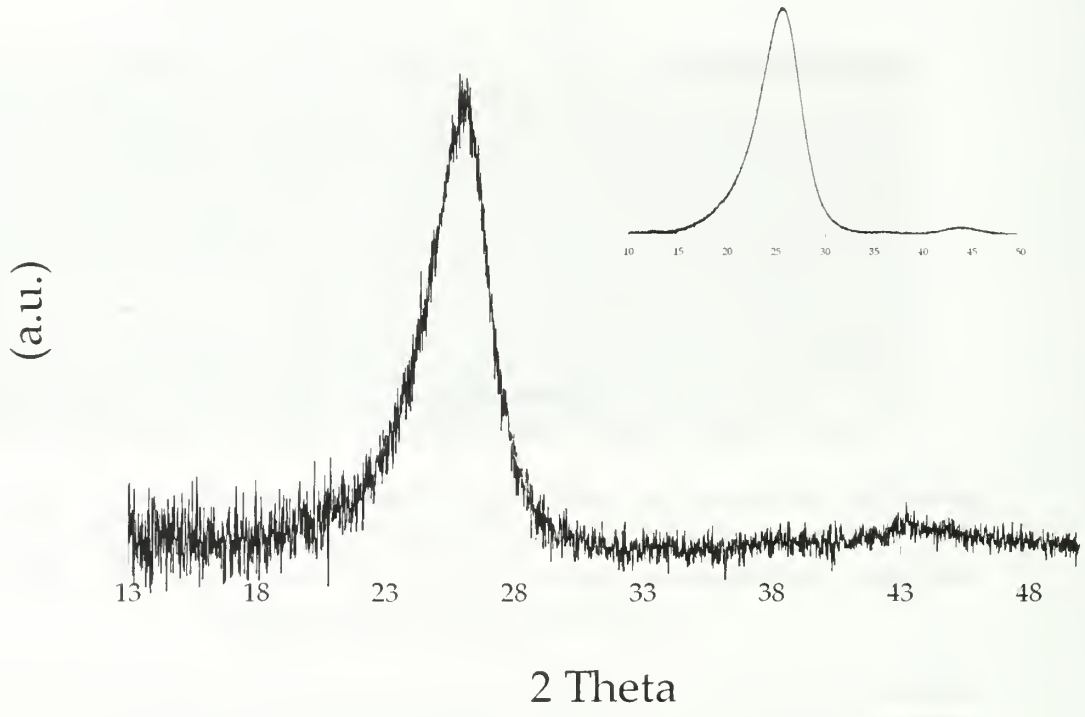

Figure 6.9: Wide angle X-ray diffraction (WAXD) of commercial carbon fiber (upper right) and that of carbonized electrospun Polyacrylonitrile (PAN) yarn (center). Yarn underwent continuous post-treatment and extended batch stabilization to 280°C prior to carbonization to 2000°C in helium

Table 6.14: Lattice parameters of carbonized electrospun Polyacrylonitrile (PAN) yarn determined by wide angle X-ray diffraction (WAXD). Yarn underwent continuous post-treatment and extended batch stabilization to 280°C prior to carbonization to 2000°C in helium

$d_{(002)}$ (nm)	L_c (Å)	No. of graphite sheets (L_c/d)	L_a (Å)
0.342	32	9.3	91

Table 6.15: Ultimate strength of carbonized, electrospun, Polyacrylonitrile (PAN) yarn and commercial carbon fiber with an average denier of 8.7 and 0.21, respectively. A density of 1.7g/ml is assumed

	Ultimate Strength (MPa)	Ultimate Strength (g/denier)
Carbonized, electrospun yarn	83 ± 11	0.6 ± 0.1
Commercial carbon fiber	1620 ± 200	15 ± 11

6.6 Conclusions

Extended lengths of electrospun Polyacrylonitrile (PAN) nanofiber yarns are successfully converted into carbon nanofiber yarns. The precursor yarn is continuously stretched above the materials' glass transition temperature, T_g, to 50% strain: the percent draw experienced by the yarn is limited by defects and inhomogeneities within the yarn. The preferred orientation is maintained and/or enhanced during continuous low temperature oxidation (stabilization); the yarn is held under constant tension. Unfortunately, the effectiveness of the stabilization is limited by the short residence time at each temperature setting and the resultant carbonized yarn is degraded. The resultant nanofibers fuse and degrade during the high temperature pyrolysis (carbonization). The effect of stabilization time and temperature on the resultant yarn is examined. A significant increase in exposure, or residence, time results in a more fully oxidized yarn. The resultant carbonized yarn exhibits typical 'graphitic structure' common to carbon fibers. The poor mechanical properties are a result of a loss of preferred orientation during the extended stabilization; the yarn is held at fixed length rather than under constant tension and orientation is lost with increased heating. The

properties of the resultant yarn are further limited by the inhomogeneities within the yarn and 'bead-on-a string,' globular morphology of the individual fibers.

6.5 References

(1) Donnet, J.B.; Bansal, R.C. Carbon Fibers. Marcel Dekker, Inc., New York (**1984**), Ch. 1.

(2) Haung, Z.M.; Zhang, Y.Z.; Kotaki, M.; Ramakrishna, S. *Compos. Sci. Technol.* **2003**, *63*, 2223.

(3) (a) Doshi, J.; Reneker, D.H. *J. Electrostat.* **1995**, *35*, 151. (b) Zussmann, E.; Theron, A.; Yarin, A.L. *Appl. Phys. Lett.* **2003**, *82*, 973. (c) Bournat, A. U.S. Patent 4,689,186 (**1987**). (d) Deitzel, J.M; Kleinmeyer, J.D.; Hirvonen, J.K.; Beck Tan, N.C. *Polymer* **2001**, *42*, 8163. (e) Fong, H.; Weidon, L.; Wang, C.S.; Vaia, R.A. *Polymer* **2002**, *43*, 775. (f) Dersche, L.T.; Schaper, A.K.; Greiner, A.; Wendorff, J.H. *J. Polym. Sci. Part A: Polym. Chem.* **2003**, *41*, 545.

(4) Fennessey, S.F.; Farris, R.J. *Polymer* **2004**, *45*, 4217.

(5) Ko, F.; Gogotsi, Y.; Ali, A.; Naguib, N.; Ye, H.; Yang, G.; Li, C.; Willis, P. *Adv. Mater.* **2003**, *15*, 1161.

(6) Smit, E.; Buttner, U.; Sanderson, R.D. *Polymer* **2005**, *46*, 2419.

(7) Kim, H.K.; Kim, K.W.; Lee, K.H.; Yoo, E.S.; Farris, R.J.; Fennessey, S.F. Polymer Preprints (American Chemical Society, Division of Polymer Chemistry) **2004**, *45*, 798.

(8) (a) Dorey, G. *Phys. Technol.* **1980**, *11*, 56. (b) Bajaj, P.; Sreekumar, T.V.; Sen, K. *J. Appl. Polym. Sci.* **2002**, *86*, 773.

(9) Damodaran, S.; Desai, P.; Abhiraman, A.S. *J. Text. Inst.* **1990**,*81*, 384.

(10) (a) Chari, S.S.; Bahl, O.P.; Mathur, R.B. *Fib. Sci. Tech.* **1981**, *15*, 153. (b) Warner, S.B.; Uhlmann, D.R.; Peebles, L.H. *J. Mat. Sci.* **1979**, *14*, 1893.

(11) Matta, V.K.; Mathur, R.B.; Bahl, O.P.; Nagpal, K.C. *Carbon* **1990**, *28*, 494.

(12) Hinrichsen, G. *J. Polymer. Sci.: Part C* **1972**, *38*, 303.

(13) Babu, V.S.; Seehra, M.S. *Carbon* **1996**, *34*, 1259.

CHAPTER 7

CONCLUSIONS

7.1 Conclusions

Electrospinning is an old technology; it has existed in the literature for more than 60 years as both an immature and the most interesting method to fabricate continuous nanofibers. To date, nanofibers from only a relatively small number of polymers have been prepared by electrospinning. The understanding of the electrospinning process in regards to property characterization of the nanofibers, particularly for application in nanocomposites, is very limited.

One of the most important applications of traditional (micro-size) fibers, especially engineering fibers,such as: carbon, glass, and Kevlar fiber, is in the reinforcement of composites[1]. Composites, prepared using these reinforcers, provide superior structural properties and the strength to weight ratios that generally are not achieved by other engineered monolithic materials alone. Eventually, nanofibers will find application in nanocomposites; the mechanical properties of nanofibers are anticipated to be greater than those of traditional fibers of the same material. Nanofiber reinforced composites may posess additional merits that cannot be shared by traditional micro-fiber composite; for example: as the fiber diameter of the reinforcer becomes smaller than the wavelength of visible light, transparent composites which do not scatter light can be prepared[2].

A majority of the work in the current literature on nanofiber composites is concerned with carbon nanofiber or nanotube reinforcement, although these fibers and

tubes are not obtained through the electrospinning technique. Polymer nanofibers made from electrospinning have not been extensively examined for use as composite reinforcement. A limited number of researchers have attempted to prepare nanocomposites reinforced with electrospun polymer nanofibers[2, 3]. Descriptions of the fabrication and structure-property relationships of such nanocomposites are not available in great quantities. In addition to improving the strength and stiffness of a matrix, electrospun fiber has been used to improve interlaminar toughness of high performance composite[4]; polymer nanofiber is inserted between laminas of a laminate to improve delamination resistance. Polymer composites reinforced with electrospun nanofibers have been developed mainly to provide some beneficial physical (i.e. optical and electrical) and chemical properties, in addition to improving the mechanical performance of the composite.

Due to the limited number of papers published in the open literature, the important issues relevant to nanocomposites reinforced with electrospun polymer nanofiber have not yet been considered, such as: interfacial bonding between a polymeric nanofiber and polymer matrix and how to modify the bonding, and modeling and simulation of the mechanical properties of nanofiber composites. The main barrier to the implementation of such work for nanofiber composites is that that mechanical behavior of a single polymer nanofiber is unknown. There are several reasons for the slow development in the area of nanocomposites reinforced with electrospun polymer nanofiber, including: a lack of uniaxial and continuous nanofiber in sufficient quantity. From composite theory and practice it is known that superior structural properties are achieved when fibers are arranged in pre-determined directions, as in unidirectional

laminae, multidirectional laminate, and woven or braided fabric reinforced composites. Generally, the use of nonwoven and randomly arranged fiber mat for reinforcement does not result in significant improvement in the mechanical properties of the composite. Continuous fiber bundles are necessary to prepare composites. Additionally, the polymeric nanofibers prepared by electrospinning and described in the literature are not suitable for reinforcement applications[5]. Although, in principal carbon nanofibers, which are achieved from post-processing of electrospun polymer precursor nanofiber[6], would be ideal for reinforcement applications, these fibers have not been obtained as a continuous yarn in large quantity until just now.

Future research should be focused on optimizing the production and processing of continuous carbon precursor nanofiber. Ideally, a homogeneous yarn could be electrospun and processed, based on the results described in this manuscript, to produce continuous tows of aligned carbon nanofiber yarn that could be used in the reinforcement of thin film nanocomposites. At which point, the interfacial adhesion between the nanofiber surface and the matrix and the use of nanofiber reinforced composites can be properly evaluated for structural applications.

7.2 References

(1) Chand, S. *J. Mater. Sci.* **2000**, *35*, 1303.

(2) Bergshoef, M.M.; Vancso, G.J. *Adv. Mater.* **1999**, *11*, 1362.

(3) Kim, J.S.; Reneker, D.H. *Polymer Composites* **1999**, *20*, 124.

(4) Dzenis, Y.A.; Reneker, D.H. U.S. Patent No. 626533 (**2001**).

(5) Huang, Z.M.; Zhang, Y.Z.; Kotaki, M.; Ramakrishna, S. *Composites Science and Technology* **2003**, *63*, 2223.

(6) (a) Chun, I.; Reneker, D.H.; Fang, X.Y.; Fong, H.; Deitzel, J.; Beck Tan, N. *SAMPE Proceedings* **1998**, *43*, 718. (b) Dzenis, Y.A.; Wen, Y.K. *Materials Research Society Symposium Proceedings* **2002**, *702*, 173. (c) Wang, Y.; Serrano, S.; Santiago-Aviles, J.J. *J. Mater. Sci. Lett.* **2002**, *21*, 1055.

APPENDIX

POLYACRYLONITRILE NANOFIBER MATS

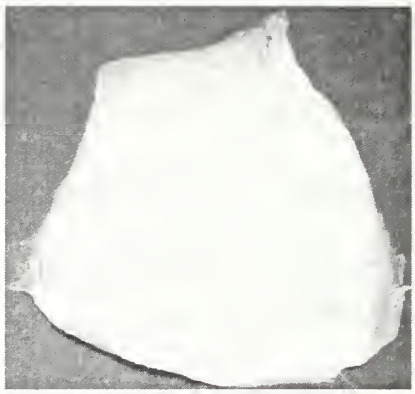

Figure A1.1: Photograph of Polyacrylonitrile (PAN) fibers electrospun from 15wt% PAN solution in dimethylformamide (DMF) at 16kV onto a stationary target

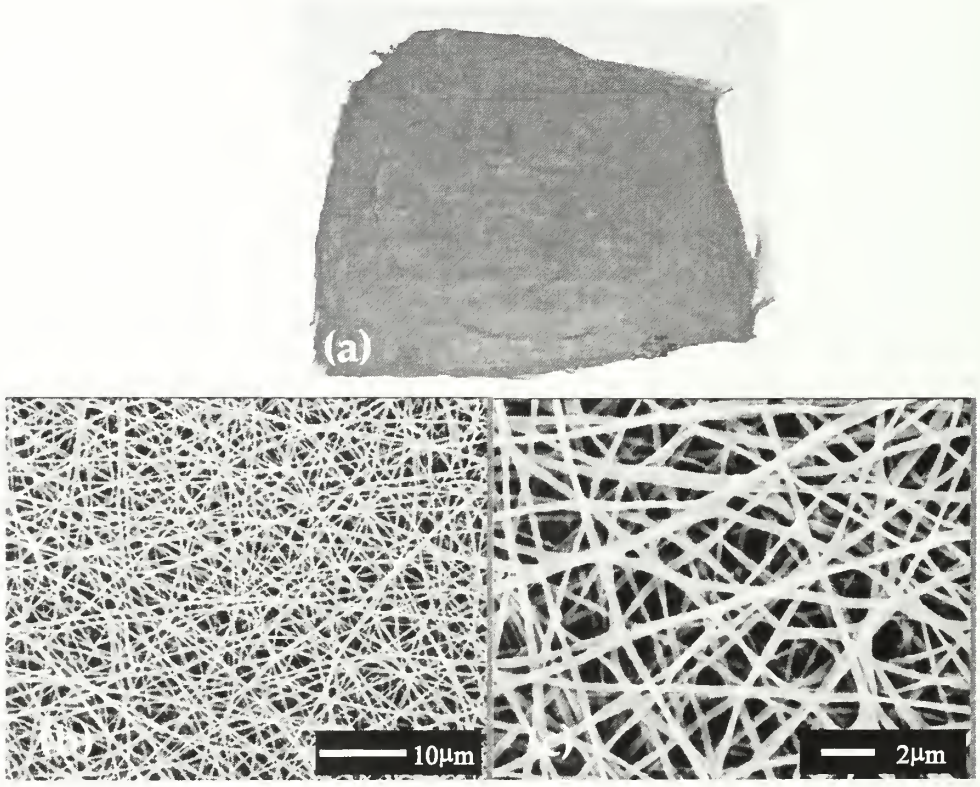

Figure A1.2: (a) Photograph and (b-c) field emission scanning electron microscopy (FESEM) images of Polyacrylonitrile (PAN) fibers stabilized between 220°C and 260°C, as described earlier (Section 5.5)

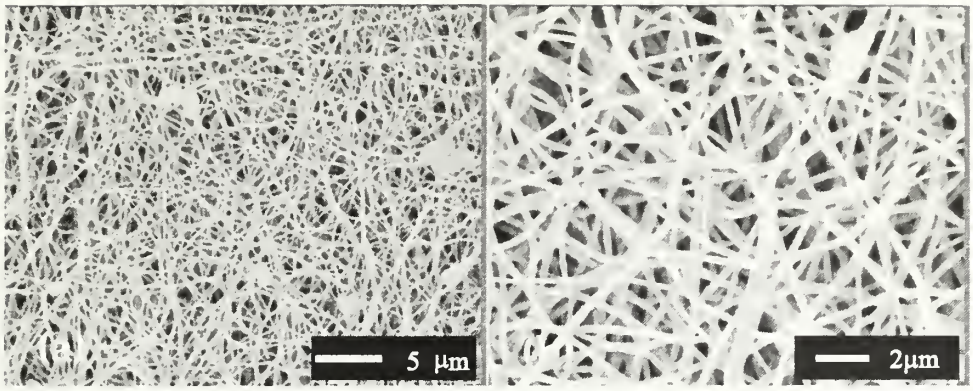

Figure A1.3: (a-c) Field emission scanning electron microscopy (FESEM) images of Polyacrylonitrile (PAN) fibers with extended stabilization to 280°C, as described earlier (Section 5.5 and 6.5)

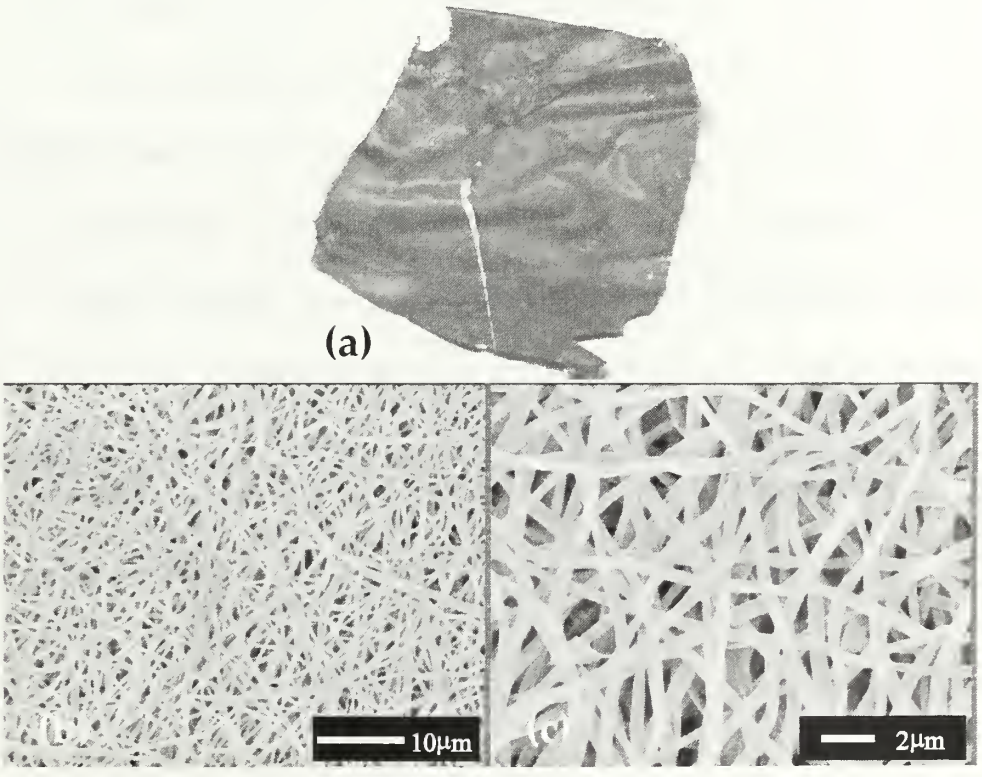

Figure A1.4: (a) Photograph and (b-c) field emission scanning electron microscopy (FESEM) images of Polyacrylonitrile (PAN) fibers carbonized to 2000°C in helium, as described previously (Section 5.5 and 6.4.5), after experiencing an extended stabilization to 280°C, as described earlier (Section 5.5 and 6.5)

BIBLIOGRAPHY

1. Allen, S.R. 'Mechanical and Morphological Correlations in Poly(p-phenylene benzobisthiazole Fibers.' Thesis, Unviersity of Massachusetts Amherst (**1983**), Ch. 3 and Appendix 1.1.

2. Babu, V.S.; Seehra, M.S. *Carbon* **1996**, *34*, 1259.

3. Bahl, O.; Mathur, R.; Kundra, K. *Fibre Sci. Tech.* **1981**, *15*, 147.

4. Bajaj, P.; Sreekumar, T.V.; Sen, K. *J. Appl. Polym. Sci.* **2002**, *86*, 773.

5. Bashir, Z. Acta Polymer **1996**, *47*, 125.

6. Bashir, Z.; Atureliya, S.; Church, S. *J. Mater. Sci.* **1993**, *28*, 2731.

7. Bashir, Z.; Church, S.; Waldron, D. *Polymer* **1994**, *35*, 967.

8. Bashir, Z.; Tipping A.; Church, S. *Polymer International* **1994**, *33*, 9.

9. Baumgarten, P.K. *J. of Colloid and Interface Sci.* **1971**, *36*, 71.

10. Bergshoef, M.M.; Vancso, G.J. *Adv. Mater.* **1999**, *11*, 1362.

11. Berry, J.P. U.S. Patent 5,024,789, Jun 18, 1991.

12. Bognitzki, M.; Hou, H.; Ishaque, M.; Frese, T.; Hellwig, M.; Schwarte, C.; Schaper, A.; Wendorff, J.H.; Greiner, A. *Adv. Mater.* **2000**.

13. Boland, E.D.; Wnek, G.E.; Simpson, D.G.; Pawlowski, K, J.; Bowlin, G.L. *J. Macromol. Sci. –Pure Appl. Chem.* **2001**, *A38*, 1231.

14. Bournat, A. U.S. Patent 4,689,186 (**1987**).

15. Brandrup, J. and E.H. Immergut. Polymer Handbook. 3rd Ed. New York, John Wiley & Sons Inc. **1989**, V/57.

16. Brandrup, J.; Immergut, E.H. and E.A. Grulke. Polymer Handbook. 4th Ed. New York, John Wiley & Sons Inc. **1999**, VII/11.

17. 'Carbon fibers electrical conductivity found to offer new uses.' *Composites News* **1998**, 3.

18. Casper, C.L.; Stephens, J.S.; Tassi, N.G.; Chase, D.B.; Rabolt, J.F. *Macromolecules.* **2004**, *37*, 573.

19. Chamot, E.; Mayson, C. Handbook of Chemical Microscopy Volume 1. New York, John Wiley & Sons 1938, Ch.10.
20. Chand, S. *J. Mater. Sci.* **2000**, *35*, 1303.

21. Chari, S.; Bahl, O.; Mathur, R. *Fibre Sci. Tech.* **1981**, *15*, 153.

22. Chen, K.; LeMaistre, C.W.; Wang, J.H.; Diefendorf, R.J. *Polymer Preprints. Division of Polymer Chemistry, American Chemical Society* **1981**, *22*, 212.

23. Christensen, R.M. Mechanics of Composite Materials. John Wiley & Sons, New York, 1979. Ch. 3.

24. Chu, B.; Hsiao, B.S.; Fang, D.; Okamoto, A. U.S. Patent Appl. No. 10/674,464, **2003**..

25. Chun, I. Dissertation. University of Akron, **1995**.

26. Chun, I.; Reneker, D.H.; Fang, X.Y.; Fong, H.; Deitzel, J.; Beck Tan, N. *SAMPE Proceedings* **1998**, *43*, 718. Chun, I.; Reneker, D.H.; Fong, H.; Fang, X.;

27. Deitzel, J.; Beck Tan, N.; Kearns, K. *Adv. Mater.* **1999**, *31*, 36.
Chung, D. Carbon Fiber Composites. Boston, Butterworth-Heinemann **1994**.

28. Chung, D.D. *Carbon* **2001**, *39*, 1119.

29. Connell, S.J.; Abusafieh, A. *SAMPE J.* **2002**, *38*, 46.

30. Cooley, J.F. U.S. Patent 692,631,**1902**.

31. Cazaplewski, D.; Kameoka, J.; Craighead, H.G. *J. Vac. Sci. Technol.* **2003**, *B21*, 2994.

32. Czaplewski, D.A.; Verbridge, S.S.; Kameoka, J.; Craighead, H.G. *Nano Lett.* **2004**, *4*, 437.

33. Dalton, S.; Heatley, F.; Budd, P. *Polymer* **1999**, *40*, 5531.

34. Dalton, P.D.; Klee, D.; Moller, M. *Polymer* **2005**, *45*, 611.

35. Damodaran, S.; Desai, P.; Abhiraman, A.S. *J. Text. Inst.* **1990**,*81*, 384.

36. Davidson, J.; Jung, H.; Hudson, S.; Percec, S. Polymer 2000, 41, 3357.

37. Deitzel, J.M.; Harris, K.D. and N.C. Beck Tan. *Polymer* **2000**, *42*, 261-272.

38. Deitzel, J.M.; Kleinmeyer, J.; Harris, D.; Beck Tan, N.C. *Polymer.* **2001**, *42*, 261.

39. Deitzel, J.M.; Kleinmeyer, J.D.; Hirvonene, J.K.; Beck Tan, N.C. *Polymer* **2001**, *42*, 8163.

40. Demier, M.M.; Yilgor, I.; Yilgor, E.; Erman, B. *Polymer.* **2002**, *43*, 3303.

41. Dersch, R.; Liu, T.; Schaper, A.K.; Greiner, A.; Wendorff, J.H. *J. Polym. Sci.: Part A* **2003**, *41*, 545.

42. Ding, B.; Kim, H.; Lee, S.; Lee, D.; Choi, K. *Fibers and Polymers* **2002**, *3*, 73.

43. Donnet, J.; Bansal, R.C. Carbon Fibers. Marcel Dekker, Inc., New York (1984), Ch. 1.

44. Dorey, G. *Phys. Technol.* **1980**, *11*, 56.

45. Doshi, J.; Reneker, D.H. *J. Electrostatics.* **1995**, *35*, 60.

46. Dresselhaus, M.S.; Dresselhaus, G.; Pimenta, M.A.; Eklund, P.C. "Raman Scattering in Carbon Materials." Pelletier, M.J. Ed. Analytical Applications of Raman Spectroscopy. Blackwell Science, Inc., Malden, MA (**1999**), Ch. 9.

47. Dror, Y.; Salalha, W.; Khalfin, R.L.; Cohen, Y.; Yarin, A.L.; Zussman, E. *Langmuir* **2003**, *19*, 7012.

48. Dorey, G. *Phys. Technol.* **1980**, *11*, 56.

49. Dzenis, Y.A.; Reneker, D.H. U.S. Patent No. 626533 (**2001**).

50. Dzenis, Y.A.; Wen, Y.K. *Materials Research Society Symposium Proceedings* **2002**, *702*, 173.

51. Feng, L.; Li, S.; Li, H.; Zhai, J.; Song, Y.; Jiang, L. *Angew. Chem. Int. Ed.* **2002**, *41*, 1221.

52. Fennessey, S.F.; Farris, R.J. *Polymer.* **2004**, *45*, 4217.

53. Fennessey, S.F.; Pedicini, A.; Farris, R.J. "Mechanical Behavior of Nonwoven Electrospun Fabrics and Yarns." Reneker, D.H.; Fong, H.F. American Chemical Society Symposium Series 918: Polymeric Nanofibers. American Chemical Society, Wahsington. (**2006**), Ch. 21.

54. Fitzer, E. *Carbon.* **1989**, *27*, 621.

55. Fitzer, E.; Frohs, W. *Chem. Eng. Technol.* **1990**, *13*, 41.

56. Fitzer, E.; Manocha, L.M. Carbon Reinforcements and Carbon/Carbon Composites. Springer-Verlag, New York (1998), Ch. 1.

57. Fong, H.; Chun, I.; Reneker, D.H. *Polymer* **1999**, *40*, 4585.

58. Fong, H.; Weidon, L.; Wang, C.S.; Vaia, R.A. *Polymer* **2002**, *43*, 775.

59. Formhals, A. U.S. Patent 1,975,504, **1934**.

60. Formhals, A. U.S. Patent 2,160,962, **1939**.

61. Formhals, A. U.S. Patent 2,187,306, **1940**.

62. Formhals, A. U.S. Patent 2,323,025, **1943**

63. Formhals, A. U.S. Patent 2,349,950, **1944**.

64. Fridrikh, S.V.; Yu, J.H.; Brenner, M.P.; Rutledge, G.C. *Phys. Rev. Lett.* **2003**, *90*, 144502-1.

65. Frigge, K.; Buchtemann, A.; Fink, H.P. *Acta Polymerics* **1991**, *42*, 322

66. Gibson, P.W.; Schreuder-Gibson, H.L., Rivin, D. *AIChE Journal* **1999**, *45*, 190.

67. Goodhew, P.J.; Clarke, A.J.; Bailey, J.E. *Mater. Sci. and Eng.* **1975**, *17*, 3.

68. Halpin, J.C. Revised Primer on Composite Materials: Analysis. Technomic Publishing Co., Pennsylvania, 1984, Ch. 6.

69. Halpin, J.C. and J.L. Kardos. *Polym. Eng. & Sci.* **16** (15), 344-352 (1976).

70. Huang, L.; MiMillan, R.D.; Apkarian, R.P.; Pourdeyhimi, B.; Conticello, B.P.; Chaikof, E.L. *Macromolecules.* **2000**, *33*, 2989.

71. Haung, L.; Nagapudi, K.; Apkarian, R.P.; Chaikof, E.L. *J. Biomater. Sci. Polymer Edn.* **2001**, *12*, 979.

72. Haung, Z.M.; Zhang, Y.Z.; Kotaki, M.; Ramakrishna, S. *Composites Science and Technology.* **2003**, *63*, 2223.

73. Hawthorne, H.M.; Baker, C.; Bentall, R.H.; Linger, K.R. *Nature* **1970**, *227*, 946.

74. Henrici-Olive, G.; Olive, S. 'The Chemistry of Carbon Fiber Formation from Polyacrylonitrile.' In: Advances in Polymer Science: Industrial Developments. Springer Verlag, Berlin (1983).

75. Hillig, W.B. *Proceedings of International Conference on Reinforced Materials and Composite Technologies.* Weisbaden, Germany (1988).

76. Hinrichsen, G. *J. Polymer. Sci.: Part C* **1972**, *38*, 303.

77. How, T.V. U.S. Patent 4,689,186, Aug 25, 1987.

78. Jain, M.K.; Balasubramanian, M.; Desai, P.; Abhiraman, A.S. *J. Mater. Sci.* **1987**, *22*, 301.

79. Jasse B.; Koenig, J. J. Macromol. Sci.- Rev. Macromol. Chem. 1979, C17, 61.

80. Jiang, H.; Fang, D.; Hsiao, B.S.; Chu, B.; Chen, W. *Biomacromolecules* **2004**, *5*, 326.

81. Jones, B.F.; Duncan, R.G. *J. Mater. Sci.* **1971**, *6*, 289.

82. Kameoka, J.; Craighead, H.G. *Appl. Phys. Lett.* **2003**, *83*, 371.

83. Kameoka, J.; Orth, R.; Yang, Y.; Czaplewski, D.; Mathers, R.; Coates, G.W.; Craighead, H.G. *Nanotechnology* **2003**, *14*, 1124.

84. Kang, Y.S.; Kim, H.K.; Ryu, Y.J.; Lee, D.R.; Park, S.J. *Polymer (Korea).* **2002**, *26*, 360.

85. Kardos, J. L. High Performance Polymers. Baer, E. and A. Moet, Eds. Hanser Publishers, New York (1991), Ch 6.

86. Kasatochkin, V.I.; Kargin V.A. *Doklady Phys.Chem.* **1970**, *191*, 303.

87. Katta, P.; Alessandro, M.; Ramsier, R.D.; Chase, G.G. *Nano. Lett.* **2004**, *11*, 2215.

88. Kenawy, E.; Abdel-Fattah, Y. R. *Macromol. Biosci* **2002**, *2*, 261.

89. Kim, C.; Park, S.H.; Cho, J.I.; Lee, D.Y.; Park, T.J.; Lee, W.J.; Yang, K.S. *J. Raman. Spectrosc.* **2004**, *35*, 928.

90. Kim, C.; Yang, K.S. *Appl. Phys. Lett.* **2003**, *83*, 1216.

91. Kim, H.K.; Kim, K.W.; Lee, K.H.; Yoo, E.S.; Farris, R.J.; Fennessey, S.F. Polymer Preprints (American Chemical Society, Division of Polymer Chemistry) **2004**, *45*, 798.

92. Kim, J. and D. H. Reneker. *Polym. Comp.* **1999**, *20*, 124.

93. Kim, K.; Yu, M.; Zong, X.; Chiu, J.; Fang, D.; Seo, Y.S.; Hsiao, B.S.; Chu, B.; Hadjiarqyrou, M. *Biomaterials* **2003**, *24*, 4977.

94. Khil, M.S.; Cha, D.I.; Kim, H.Y.; Kim, I.S.; Bhattarai, N. *J. Biomed. Res. B Appl. Biomater.* **2003**, *67*, 675.

95. Knight, D.S.; White, W.B. *J. Mater. Res.* **1989**, *4*, 385.

96. Ko, T. *Mater. Chem. & Phys.* **1994**, *38*, 289.

97. Ko, F.; Gogotsi, Y.; Ali, A.; Naguib, N.; Ye, H.; Yang, G.; Li, C.; Willis, P. *Adv. Mater.* **2003**, *15*, 1161.

98. Koombhongse, S.; Liu, W.; Reneker, D.H. *J. Polymer Sci.: Part B: Polymer Phys.* **2001**, *39*, 2598.

99. Kumar, S.; Doshi, H.; Srinivasarao, M.; Park, J.O.; Schiraldi, D.A. *Polymer* **2002**, *43*, 1701.

100. Larrondo, L. and R.S. Manley. *J. Polym. Sci.* **1981**, *19*, 921.

101. Lee, K.; Kim, H.; Ryu, Y.; Kim, K.; Choi, S. J. Polym. Sci.: Part B 2003, 41, 1256.

102. Lee, S.; Yoon, J.; Suh, M. *Macromol. Res.* **2002**, *10*, 282.

103. Lee, S.H.; Yoon, J.W.; Suh, M.H. *Macromol. Res.* **2002**, *10*, 282.

104. Lennhoff, J.D. U.S. Patent Appl. No. 10/967,627, **2004**.

105. Li, D.; Ouyang, G.; McCann, J.T.; Younan, X. *Nano Lett.* **2005**, *5*, 913.

106. Li, D.; Wang, Y.; Xia, Y. *Adv. Mater.* **2004**, *16*, 361.

107. Li, D.; Wang, Y.; Xia, Y. *Nano. Lett.* **2003**, *3*, 1167.

108. Li, D.; Xia, Y. *Nano Lett.* **2003**, *3*, 555.

109. Liu, G.J.; Ding, J.F.; Qia, L.J.; Guo, A.; Dymov, B.P.; Gleeson, J.T. *Chem.-A European J.* **1999**, *5*, 2740.

110. Liu, H.Q.; Hsieh, Y.L. *J. Polym. Sci.: Part B Polym. Phys.* **2002**, *40*, 2119.

111. Lubin, G. (Ed) Handbook of Composites. Van Nostrand Reinhold Co., New York (1982).

112. Ma, P.X.; Zhang, R. *J. Biomed. Mat. Res.* **1999**, *46*, 60.

113. MacDiarmid, A.G.; Jones, W.E.; Norris, I.D.; Gao, J.; Johnson, A.T.; Pinto, N.J.; Hone, J.; Han, B.; Ko, F.K.; Okuzaki, H.; Llaguno, M. *Synth. Met.* **2001**, *119*, 27.

114. Macky, W.A. *Proc. R. Soc. A* **1931**, *133*, 565.

115. Madhugiri, S.; Dalton, A.; Gutierrez, J.; Ferraris, J.P.; Dalkus, K.J. *J. Am. Chem. Soc.* **2003**, *125*, 14531.

116. Mallick, P.K. Fiber-reinforced Compostites: Materials, Manufacturing, and Design. 2nd Ed. Marcel Dekker, Inc., New York (1993).

117. Martin, C.R. *Chem. Mater.* **1996**, *8*, 1739.

118. Matta, V.K.; Mathur, R.B.; Bahl, O.P.; Nagpal, K.C. *Carbon* **1990**, *28*, 494.

119. Matthews, J.; Wnek, G.; Simpson, D.; Bowlin, G.. *Biomacromolecules* **2002**, *3*, 232.

120. McKee, D.W.; Mimeault, V.J. 'Surface Properties of Carbon Fibers.' In: Walker, P.L.; Thrower, P.A. Chemistry and Physics of Carbon.Vol. 8 Marcel Dekker, Inc., New York (1973), Ch. 2.

121. McKee, M.G.; Wilkes, G.L.; Colby, R.H.; Long, T.E. *Macromolecules.* **2004**, *37*, 1760.

122. Megelski, S.; Stephens, J.S.; Chase, D.B.; Rabolt, J.F. *Macromolecules* **2002**, *35*, 8456.

123. Mit-uppatham, C.; Supaphol, P.; Nithitanaku, M. Society of Plastics Engineers Annual Technical Conference (ANTEC). **2003**, 1685.

124. Mochida, I.; Yoon, S.H.; Takano, N.; Fortin, F.; Korai, Y.; Yokoawa, K. *Carbon* **1996**, *34*, 941.

125. Moncrieff, R.W. Man-Made Fibres, 6th Ed. John Wiley & Sons, New York (**1975**).126. Nolan, J.J. *Proc. R. Irish. Acad.* **1926**, *37A*, 28.

127. Otani, S.; Yokoyama, A.; Nukui, A. *Appl. Polymer Symposia.* **1969**, *9*, 325.

128. Ondarchuhu, T.; Joachim, C. *Europhys. Lett.* **1998**, *42*, 215.

129. Overberger, C.G.; Moore, J.A. *Adv. Polymer Sci.* **1970**, *7*, 113. Peebles, L.H. *J. Polym. Sci. Part A-1* **1967**, *5*, 2637.

130. Park, S.H.; Kim, C.; Choi, Y.O.; Yang, K.S. *Carbon* **2003**, *41*, 2653.

131. Park, S.H.; Kim, C.; Yang, K.S. *Synthetic Metals* **2004**, *143*, 175.

132. Pedicini, A.; Farris, R.J. *J. Polym. Sci.: Part A* **2004**, *42*, 752.

133. Peebles, L.H. *J. Polym. Sci. Part: A-1* **1967**, *5*, 2637.

134. Peebles, L.H.; Brandrup, J. *Makromol. Chem.* **1966**, *98*, 189.

135. Perry, A.J.; Ineichen, B. and B. Eliasson. *J. Mater. Sci.* **1974**, *9*, 1376.

136. Raleigh, Lord X. *London, Edinburgh, Dublin Philos. Mag.* **1882**, *44*, 184.

137. Reneker, D.H.; Fong, H. *J. Polym. Sci.: Part B Polym. Phys.* **1999**, *37*, 3488.

138. Reneker, D. H.; Yarin, A.L.; Fong, H. and S. Koombhongse. *J. Appl. Phys.* **2000**, *87*, 4531.

139. Ross, T.E. *Textile Res.* **1968**, *38*, 906.

140. Russel, W.B. *Z. Angew. Math. Phys.* **1973**, *24*, 581.

141. Schadler, L.S.; Giannaris, S.C. and P.M. Ajayan. *Appl. Phys. Lett.* **1998**, *73*, 3842.

142. Schreuder-Gibson, H.; Gibson, P.; Senecal, K.; Sennett, M.; Walker, J.; Yeomans, W.; Ziegler, D.; Tsai, P.P. *J. Adv. Mater.* **2002**, *34*, 44.

143. Schwartz, M.M. Composite Materials: Properties, Nondestructive Testing, and Repair. Prentice Hall Inc., New Jersey (1996), Ch 1.

144. Shimada, I.; Takahagi, T.; Fukuhara, M.; Morita, K.; Ishitani, A. *J. Polym. Sci. Part: A* **1986**, *24*, 1989.

145. Shin, Y. M; Hohman, M.M.; Brenner, M.P.; Rutledge, G.C. *Polymer* **2001**, *42*, 9955.

146. Shin, Y.M.; Hohman, M.M.; Brenner, M.P.; Rutledge, G.C. *Appl. Phys. Lett.* **2001**, *78*, 1149.

147. Shindo, A. *Yogyo-Kyokai-Shi* **1961**, *69*, 195.

148. Shkadov, V.Y.; Shutov, A.A. *Fluid Dyn. Res.* **2001**, *28*, 23.

149. Simons, H.L. U.S. Patent 3,280,229, **1966.**

150. Smit, E.; Buttner, U.; Sanderson, R.D. *Polymer* **2005**, *46*, 2419.

151. Spivak, A.F.; Dzenis, Y.A. *Appl. Phys. Lett.* **1998**, *73*, 3067

152. Sundaray, B.; Subramanian, V.; Natarajan, T. S.; Xiang, R.Z.; Chang, C.C.; Fann, W.S. *Appl. Phys. Lett.* **2004**, *84*, 1222.

153. Talley, C.P. *J. Appl. Phys.* **1959**, *30*, 1114.

154. Tang, M.M.; Bacon, R. *Carbon.* **1964**, *2*, 211.

155. Taylor, G.I. *Proc. R. Soc. Lond. A* **1969**, *313*, 453.

156. Theron, A.; Zussman, E.; Yarin, A.L. *Nanotechnology* **2001**, *12*, 384.

157. Tsai, J.S. *J. Mater. Sci. Lett.* **1994**, *13*, 1162.

158. Tsai, J.S. *J. Mater. Sci. Letters* **1996,** *15*, 835.

159. Tsai, J.S. *SAMPE Quarterly* **1993**, *Apr.*, 21.

160. Tuinstra, F.; Koenig, J.L. *J. Chem. Phys.* **1970**, *53*, 1126.

161. Uchida, T.; Shinoyama, I.; Ito, Y.; Kukuda, K. Proc. 10th Biennial Conf. On Carbon, Bethlehem, PA (**1971**), p. 31.

162. Vonnegut, B.; Neubauer, R.L. *J. Colloid Sci.* **1952**, *7*, 616.

163. Wang, P.H.; Yue, Z.R.; Li, R.Y.; Liu, J. *J. Appl. Polym. Sci.* **1995**, *56*, 289.

164. Wang, X.; Kim, Y.G.; Drew, C.; Ku, B.C.; Kumar, J.; Samuelson, L.A. *Nano Lett.* **2004**, *4*, 331.

165. Wang, Y.; Santiago-Aviles, J.; Furlan, R.; Ramos, I. *IEEE Transactions on Nanotechnology.* **2003**, *2*, 39.

166. Wang, Y.; Serrano, S.; Santiago-Aviles, J.J. *J. Mater. Sci. Lett.* **2002**, *21*, 1055.

167. Wang, Y.; Serrano, S.; Santiago-Aviles, J.J. *Synthetic Metals* **2002**, *138*, 423.

168. Warner, S.B.; Buer, A.; Ugbolue, S.C.; Rutledge, G.C.; Shin, M.Y. National Textile Center Annual Report No. 83-90, **1998**.

169. Warner, S.B.; Uhlmann, D.R.; Peebles, L.H. *J. Mat. Sci.* **1979**, *14*, 1893.

170. Watt, W.; Phillips, L.N.; Johnson, W. *Engineer (London)* **1966**, *221*, 815.

171. Wawnes, F.E. 'Boron Filaments.' In: Brautman, L.; Kersch, R. (Eds) Modern Composite Materials. Addison-Wesley, (1967).

172. Whitesides, G.M.; Grzybowski, B. *Science.* **2002**, *277*, 1971.

173. www.hexcelfibers.com

174. www.toyobo.co.jp

175. Xu, C.Y.; Inai, R.; Kotaki, M.; Ramakrishna, S. *Biomaterials* **2004**, *25*, 877.

176. Xue, T.J.; MeKinney, M.A.; Wilke, C.A. *Polym. Degrad. & Stab.* **1997**, *58*, 193.

177. Yang, K.S.; Edie, D.D.; Lim, D.Y.; Kim, Y.M.; Choi, Y.O. *Carbon.* **2003**, *41*, 2039.

178. Yang, Q.B.; Li, D.M.; Hong, Y.L.; Li, Z.Y.; Wang, C.; Qiu, S.L.; Wei, Y. *Synth. Met.* **2003**, *137*, 973.

179. Yarin, A.L.; Koombhongse, S.; Reneker, D.H. *J. Appl. Phys.* **2001,** *89*, 3018.

180. Zeleny, J. *Proc. Cambridge Philos. Soc.* **1915**, *18*, 17.

181. Zeleny, J. *Phys. Rev.* **1914**, *3*, 69.

182. Zeleny, J. *Phys. Rev.* **1917,** *10*, 1.

183. Zheng, J.; Xu, X.; Chen, X.; Liang, Q.; Bian, X.; Yang, L.; Jing, X. *J. Controlled Release* **2003**, *92*, 227.

184. Ziabicki, A. Fundamentals of fibre formation: the science of fiber spinning and drawing. Wiley & Sons, Inc., New York, **1976**.

185. Zbinden, R. Infared Spectroscopy of High Polymers. New York, Academic Press **1964**, Ch V.

186. Zong, X.; Kim, K.; Fang, D.; Ran, S.; Hsiao, B.S.; Chu, B. *Polymer* **2002**, 4403.

187. Zussman, E.; Theron, A.; Yarin, A.L. *Appl. Phys. Lett.* **2003**, *82*, 973.